MOCVD growth of InGaAs/GaAs QDs for long wavelength lasers and VCSELs

vorgelegt von
M.Sc. Ilia Kaiander
aus St.Petersburg, Russland

von der Fakultät II- Mathematik und Naturwissenschaften
der Technischen Universität Berlin
zur Erlangung des akademischen Grades

Doktor der Naturwissenschaften
Dr.rer.nat.

genehmigte Dissertation

Promotionsausschuss:

Vorsitzender:	Prof. Dr. H.J. Eichler
Berichter:	Prof. Dr. D. Bimberg
Berichter:	Priv. Doz. Dr. U. Pohl

Tag der wissenschaftliche Aussprache: 20. Dezember 2005

Berlin 2006
D83

Parts of this work were published in:

I. N. Kaiander, U.Pohl and D. Bimberg, *MOCVD of InGaAs/GaAs quantum dots using InGaP interlayers* 11th European workshop on Metalorganic Vapour Phase Epitaxy, Lausanne, Switzerland, 5-8 June, (2005)

I.N. Kaiander, F. Hopfer, T. Kettler, U.W. Pohl and D. Bimberg *Alternative precursor growth of quantum dot-based VCSELs and edge emitters for near infrared wavelengths*, J. Crystal Growth **272**, 154 (2004).

U.W. Pohl, K. Pötschke, I. Kaiander, J.-T. Zettler and D. Bimberg *Real-time control of quantum dot laser growth using reflectance anisotropy spectroscopy*, J. Crystal Growth **272**, 143 (2004).

I.N. Kaiander, R.L. Sellin, T. Kettler, N.N. Ledentsov, D. Bimberg, N.D. Zakharov and P. Werner *1.24 μm InGaAs/GaAs quantum dot laser grown by metalorganic chemical vapor deposition using tertiarybutylarsine*, Appl. Phys. Lett. **84**, 2992 (2004).

I. N. Kaiander, U.Pohl and D. Bimberg, *MOCVD growth of InGaAs quantum dots on GaAs substrates for 1.3 μm lasers using InGaP interlayer* DGKK Workshop, Freiburg im Breisgau, Germany, 9-10 December, (2004)

D. Ouyang, N.N. Ledentsov, S. Bognr, F. Hopfer, R.L. Sellin, I.N. Kaiander and D. Bimberg *Impact of the mesa etching profiles on the spectral hole burning effects in quantum dot lasers*, Semicond. Sci. Technol. **19**, L43 (2004).

I. N. Kaiander, T. Kettler, R. L. Sellin, N. N. Ledentsov and D. Bimberg, *Long Wavelength (>1.24 μm) InGaAs/GaAs quantum dot laser grown by alternative precursor MOCVD* InternationalSymposium Nanostructures: Physics and Technology, StPetersburg, Russia, June 2328, (2003) (post deadline)

C. Ribbat, R.L. Sellin, I. Kaiander, F. Hopfer, N.N. Ledentsov, D. Bimberg, A.R. Kovsh, V.M. Ustinov, A.E. Zhukov and M.V. Maximov *Complete suppression of filamentation and superior beam quality in quantum-dot lasers*, Appl. Phys. Lett. **82**, 952 (2003).

R.L. Sellin, I. Kaiander, D. Ouyang, T. Kettler, U.W. Pohl, D. Bimberg, N.D. Zakharov and P. Werner *Alternative-precursor metalorganic chemical vapor deposition of self-*

organized InGaAs/GaAs quantum dots and quantum-dot lasers, Appl. Phys. Lett. **82**, 841 (2003).

Zusammenfassung

In Rahmen dieser Arbeit wurden das Wachstum und die Eigenschaften von selbstorganisierten InGaAs Quantenpunkten (QP) auf GaAs Substraten untersucht. Das Ziel war die QP mit guter optischer Qualität herzustellen, um sie als aktives Medium für kanten- und oberflächenemitierende Laser nutzen zu können.

Die QP wurden mittels metallorganischer Gasphasenepitaxie (MOCVD) hergestellt. Der Einfluss von verschiedenen Wachstumsparametern, wie Wachstumstemperatur, V/III Verhältniss, Zusamensetzung u.a., auf optische und strukturelle Eigenschaften von QP wurde untersucht. Dabei wurde der Standard Arsen-Vorläufer Arsin (AsH_3) durch das weniger toxische Tertiärbutylarsin (TBAs) ersetzt. TBAs hat eine fast 200℃ niedrigere Zerlegungstemperatur als AsH_3. Das hat Vorteile für das Wachstum von QP, das normalerweise bei 500℃ stattfindet.

QP mit Emissionswellenlängen von 1100 nm bis 1400 nm und Dichten von 2-7$\times 10^{10}$ cm^{-2} sind hergestellt worden. Der Bereich der Emissionswellenlängen schließt den für Datenübertragung in Glasfasern wichtigen Bereich in der Nähe von 1.3 μm ein. Diese langwelligen InGaAs QP enthalten oft strukturelle Defekte, die durch starke elastische Verspannung verursacht werden. Diese Defekte mindern somit die Perfektion von Bauelementen. Es wurde ein spezielles Verfahren entwickelt um die Defekte zu eliminieren. Die QP werden bei dieser Methode mit einer dünnen Schicht abgedeckt und ausgeheilt. Das führt zum Abdampfen der Defekte. Es wurde gezeigt, dass ein derartiges in-situ Tempern von QP ihre optische Effizienz verbessert und sich positiv auf die Lasereigenschaften auswirkt.

Das Wachstum von QP wurde auch bei InGaAs Deposition auf InGaAs und InGaP untersucht. Eine InGaAs Unterschicht verursacht einen wesentlichen Anstieg der QP Dichte, aber auch die Reduktion der Größe der QP und entsprechend der Emissionswellenlänge. Eine InGaP Unterschicht verursacht den Übergang von einer monomodalen zu einer bimodalen Größeverteilung der QP mit sehr großem energetischem Abstand von etwa 150-200 meV zwischen unterschiedlichen QP-Ensembles.

Kantenemittierende Laser im langwelligen Bereich wurden im Rahmen dieser

Arbeit realisiert. Die relativ niedrige QP Dichte bei großen Wellenlängen ist für den relativ kleinen modalen Gewinn verantwortlich und erfordert den Einsatz von Mehrfachstapeln. Zehnfach gestapelte $In_{0.65}Ga_{0.35}As$ QP auf GaAs und InAs QP auf $In_{0.3}Ga_{0.7}As$ Unterschichten wurden als aktive Zone genutzt. Der Laser mit der längsten Wellenlange bei Raumtemperatur ist mit 1243 nm gemessen worden. Der maximale modal Gewin ist in Höhe von 2 cm^{-1} für InGaAs/GaAs QPe und 4 cm^{-1} für InAs/InGaAs QPe pro QP-Schicht gemessen worden. Dies entspricht dem Unterschied der QP Dichte.

Oberflächenemittierende Laser (VCSEL) wurden auf Basis von $In_{0.5}Ga_{0.5}As$ QP mit einer Emissionswellenlänge von 1.1 μm realisiert. Dazu wurden hoch effektive AlO_x/GaAs Bragg-Reflektoren genutzt. Die höchsten gemessenen Leistungen waren 1.36 mW im Multimode- und 0.68 mW im Monomodebetrieb bei konstantem Strom. Die Nutzung von kurzen Pulsen ermöglicht Ausgangsleistungen bis 6.26 mW beziehungsweise 3.3 mW.

Contents

Chapter 1

Introduction

Quantum dots attract during the last decade an increased attention of the researches in the whole world. Often called artificial atoms due to their atom-like discrete energy spectra, quantum dots (QDs) have unique properties potentially useful for such devices as lasers, transistors, memory devices, and single photon emitters.

The discovery of self-assembling of QDs opened a possibility of mass-production of QDs and gave an additional impact to their investigation. The self-assembling principle is based on the fact, that during epitaxy by some growth conditions planar growth changes to 3-dimensional growth, forming objects with quantum confinement in all three dimensions. Self-assembled growth provides quick and simultaneous production of a huge number of QDs, making possible a creation of devices based on QDs. Self-assembled growth of QDs occurs by a lattice mismatch between growing film and substrate, and was observed in different epitaxial systems such as III-V InAs/GaAs, InAs/InP, GaSb/GaAs, InP/GaP; IV-IV Ge/Si; II-VI CdSe/ZnSe, CdTe/ZnTe. Good review of properties of self-assembled QDs and devices based on them is given in books [1, 2].

Semiconductor lasers became one of the most important devices since its first realisation in the mid-1970s. They are widely used for data transfer and storage, such as DVD, and fibre-optic network, as well as a pump source for high power YAG lasers, and for many other applications. Lasers based on an array of QDs have potentially superior properties compared with by now dominating lasers based on quantum wells (QW). QD-based lasers with very low threshold current, high modulation speed and high power output were already demonstrated.

The wavelength of zero dispersion and the lowest absorption, in quartz optical fibres 1.3 and 1.55 μm respectively, are the most important windows for telecommunication. By now the lasers operating at these two wavelengths are based on InP substrate. Low

conduction band discontinuity of InGaAsP materials leads to relative poor thermal stability of laser operation, caused by electron escape. This phenomena are especially strong in lasers operating at 1.3 μm, since the confinement is smaller. Lasers based on GaAs substrates provide larger temperature stability due to larger conduction band discontinuity. Moreover, GaAs substrates provide a possibility to product monolithic vertical-cavity surface-emitting lasers (VCSEL) using highly effective AlO_x/GaAs Bragg reflectors.

InGaAs QDs on GaAs substrate open a possibility to obtain an emission wavelength over a very wide range from 0.95 μm up to 1.55 μm. Such long wavelengths could not be achieved using InGaAs QWs due to the formation of misfit dislocations caused by a larger misfit strain. The longest lasing wavelength in conventional laser structures to our knowledge is about 1.2 μm [3]. The lasing wavelength up to 1233 nm was achieved by using a strain compensation [4]. By now operation of lasers based on InGaAs/GaAs QDs with wavelength up to 1.35 μm is demonstrated, and up to 1.55 μm using an InGaAs metamorphic buffer on GaAs substrate. Using of InP substrates extends the wavelength up to 2 μm.

Almost simultaneously with QDs huge progress was achieved with diluted nitrides, namely InGaAsN on GaAs substrates, also providing emission wavelengths over a range between 1.2 and 1.5 μm. Lasing operation at room temperature with wavelengths up to 1.55 μm was demonstrated. However, despite a rapid improvement of laser properties, problems with short lifetime often occur, making them unusable for commercial applications. On the other hand, lasers based on QDs were claimed to have a very long operation lifetime.

Metal organic chemical vapor deposition (MOCVD) as well as molecular beam epitaxy (MBE) are currently the mostly used epitaxial methods for the production of III-V-based semiconductor devices. Commercial production is almost equally divided between these two techniques. First investigations of self-assembled QDs were performed using both MBE and MOCVD with similar success. Laser fabrication was obtained almost simultaneously in the mid-90ies using both growth methods. However, long wavelength lasing near 1.3 μm was first demonstrated using MBE grown lasers in 1998. First QD-based lasers grown by MOCVD and operating near 1.3 μm were demonstrated only in 2002.

This work is concentrated on an investigation of growth of self-assembled InGaAs QDs on GaAs substrates with the purpose of an achievement of laser operation at 1.3 μm. In opposite to standard MOCVD, where AsH_3 is used as arsenic precursor, the growth of QDs was performed using the alternative liquid precursor tertiarybutylarsine (TBAs). Structural and optical properties of QDs and an influence of different growth

parameters were investigated. Implementation of an array of QDs as an active zone of edge emitting and vertical-cavity surface emitting lasers and their characteristics are discussed.

1.1 Definition of a quantum dot

Semiconductor structures can be classified depending on the number of dimensions in which the charger carriers can freely move. Quantum confinement is defined when one or more dimensions become comparable with de-Broglie wavelength, which is $\lambda = h/p$, where p is the quasi-momentum of the particle. In case of quantum confined the energetic spectrum transforms from quasi-continuum to a discrete one.

Four confinement possibilities are depicted in figure 1.1 [1]. There is no confinement in bulk material, charge carriers have a quasi-continuum energy spectrum. One-dimensional confinement is provided in a quantum well (QW), the density of states becomes step-like. In a quantum dot the charge carriers are confinement in all three dimensions forming an atom-like energy spectrum consisting of separate levels.

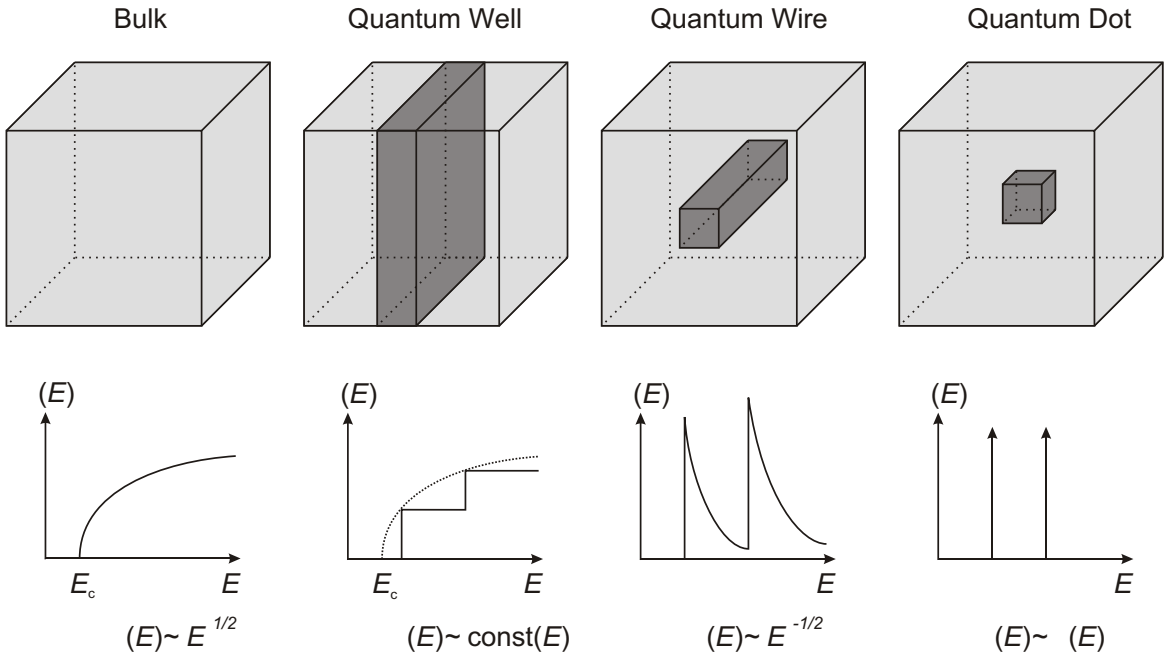

Figure 1.1: Semiconductor structures with different quantum confinement and correspondent density of states. Bulk material - no confinement, quantum well (QW) - 1D confinement, quantum wire - 2D confinement, quantum dot (QD) - 3D confinement.

The size, which is necessary in order to achieve 3D confinement, can be roughly estimated using an effective exciton Bohr radius. In semiconductors it is defined by:

$$a_B^* = \frac{m}{m^*}\epsilon a_B \tag{1.1}$$

where a_B^* is the effective Bohr radius in the semiconductor; m is the mass of free electron; m^* is the effective electron mass in the semiconductor; ϵ is the dielectric constant and a_B is the Bohr radius of the hydrogen atom, which is equal to 0.53Å. Depending on the semiconductor, a_B^* varies between 1 and 50 nm. Despite a very low size a QD still contains up to some thousands of atoms.

Usually QDs are formed by insertion of a material with narrow band gap into a wide gap matrix, for example InAs in GaAs. In this case if QD size exceeds some critical value bounded electron and hole levels appear inside the QD. If, however, the heterojunction has a typ-II alignment, for example GaSb in GaAs, only holes are confined in the QD. Growth of QD size provides an appearance of new energy levels and an increase of confinement energy of exciting states. Thus the size of a QD is limited from the top. In order to classify the object as a QD we assume that the separation energy between energy sublevels must be larger than the thermal energy

$$kT < E_2 - E_1 \tag{1.2}$$

since for many devices it is higly desirable to have only one level populated with carriers. So the lower the operation temperature the larger QD size can be [5].

The width of an energy transition in single QD, called homogeneous broadening, is defined by a carrier lifetime onto the level, was estimated to be in the range from 0.15 meV [6] up to 20 meV [7]. An array of real QDs has an inhomogeneous broadening of energy levels caused by a fluctuation of QD size. It is usually between 10 and 70 meV depending on fabrication method.

1.2 Self-organized growth of QDs

First QDs were fabricated in the middle 80's using lithography and etching. A structure with QW was taken as a starting point. Electron beam, focused ion beam, holographic lithography, and optical lithography were used to define the lateral dimensions and shape of QDs. After photoresist exposure, narrow columns were etched using photoresist as an etching mask. Thus, a confinement in all three dimensions was achieved. The QDs produced using such methods demonstrated discrete energy spectra, photoluminescence [8, 9] and electroluminescence was observed [10].

A fabrication of QDs using lithography and etching has a lot of disadvantages. Firstly, optical lithography has a small resolution. Therefore only QDs with relative large dimensions could be made, discrete spectra are observed only at low temperatures. Electron beam lithography has a very good resolution, but small productivity making a fabrication of large arrays very time-consuming. Secondly, the etch process damages the etching surface, causing an appearance of defects. The defects on the surface of QDs provide strong nonradiative recombinations in QDs.

A crucial moment in the history of QD investigation was a turnover from fabrication of QDs to implementation of self-organisation occuring in heteroepitaxial growth. It was found that by some conditions during growth of a layer on a planar substrate the growth mode transforms form planar 2-dimensional to a 3-dimensional mode. A patterning appearing during 3D growth can be used to fabricate quantum wires and QDs. A nonuniformity of a layer with a low band gap into a matrix with a large band gap can be interpreted as a QD.

Figure 1.2: Possible heteroepitaxy growth modes for heteroepitaxy: Frank-van der Merve (FM), Volmer-Weber (VW), and Stranski-Krastanow (SK).

We consider a heteroepitaxial growth, i.e. a layer of one material is deposited on a substrate of another material. Three growth modes depicted in figure 1.2 are possible. Planar film growth is called Frank-van der Merve growth mode. During Volmer-Weber growth 3D islands are formed on the substrate not covering it completly. In the Stranski-Krastanow mode the 3D islands grow on top of a thin film, called wetting layer. The wetting layer fully covers the substrate.

Which growth mode occurs depends on the surface energy and the difference of lattice constants between the substrate and the growing layer. The change of surface energy can be written as

$$\Delta\sigma = \sigma_{layer} + \sigma_{interface} - \sigma_{substrate} \ . \tag{1.3}$$

We say that the layer wets the substrate if $\Delta\sigma < 0$. In this case a growing film totally covers the substrate. If the film does not wet the substrate 3D islands grow on the substrate.

The lattice parameter of a growing layer can differ form the substrate. In this case an elastic energy accumulates during deposition of the film. If the film is thin enough the film accumulate tensile or compressive strain remaining planar. However, if the film thickness exceeds some critical value then either misfit dislocations or 3D islands appear. Both misfit dislocations and 3D islands reduce the elastic strain. A summary of growth modes is collected in the following table.

	Wetting	**Non-wetting**
lattice matching	FM	VW
lattice mismatching	FM, SK	VW

The evolution of a heteroepitaxial system is defined by the ratio of energy of dislocated interface and island formation. The energy of island formation can be written as a sum of surface and strain contribution [11],

$$\Delta E_{island} = \Delta E_{strain} + E_{facets} + E_{edges} - E_{WL} = \Delta E_{strain} + \Delta E_{surface} \tag{1.4}$$

where E_{facets} and E_{edges} are the energy of facets and of edges of formed island respectively, E_{WL} is the energy of the wetting layer area, which disappears due to island formation. The lattice constant inside the island is partly or fully relaxed to the value of unstrained material, so $\Delta E_{strain} < 0$. $\Delta E_{surface}$ is usually assumed to be positive, however Shchukin et al. [12] demonstrated that in some cases $\Delta E_{surface}$ could be negative due to renormalization of surface energy caused by strain relaxation. Therefore, island formation is favourable if the energy win exceeds that of dislocation formation.

The critical layer thickness for lattice-mismatch heteroepitaxy predicted by different theories: that of Matthews-Blakeslee (MB) [13] is based on the force balance, and that of People-Bean is based on energy balance [14]. There was a lot of work comparing experiment and theory. Many authors claimed that experimental values of critical layer thickness are significantly smaller than those predicted. Both theories do not take into account a growth temperature, which was found to have a strong impact on dislocation formation. Wang [15] modified the MB theory in order to consider the growth temperature and obtained a better agreement between experimental data and theoretical predictions.

Experimental investigations of depositions of InGaAs on GaAs demonstrated that by some growth conditions coherent, dislocation-free islands appear. It was found that the indium composition must exceed 30%, otherwise dislocations appear. Figure 1.3 shows a relation between critical layer thickness of dislocation formation and 3D growth [16].

Following equation 1.4, if $\Delta E_{surface}$ is positive then there is a thermodynamic driving force for island coalescence, so-called Ostwald ripening. Huge islands with zero density

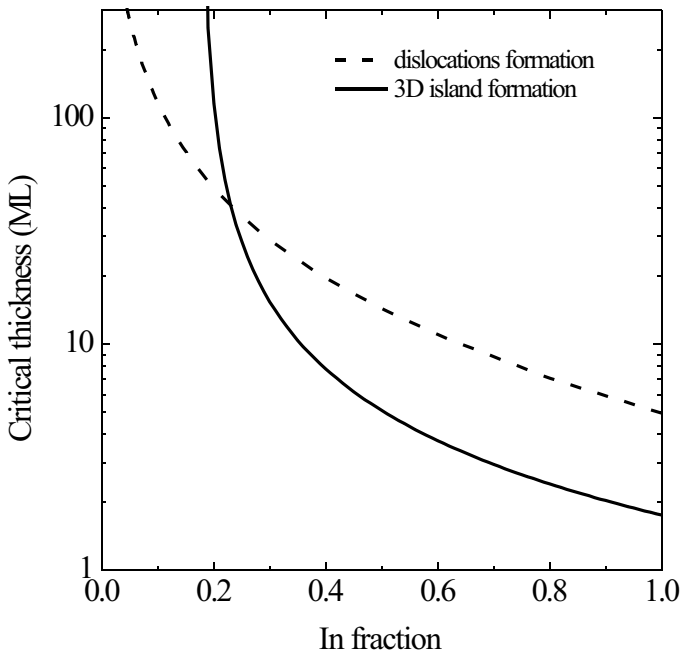

Figure 1.3: Critical layer thickness of misfit dislocation formation, calculated using Matthews-Blakeslee theory, and approximate experimental critical thickness of 2D-3D growth transition for the deposition of InGaAs on GaAs substrate. Taken from [16].

collecting all material must appear on the surface. Nevertheless, coherent islands were observed in many heteroepitaxial systems, such as InAs/GaAs, InP/GaAs [17], InSb and GaSb on GaAs [18], Ge/Si and many others. Shchukin et al. [12] developed a theory, which predicts an existence of equilibrium size of coherent islands by some growth parameters.

Daruka and Barabasi [19] calculated a phase diagram of heteroepitaxial growth depending on deposition thickness and lattice mismatch. They consider a simultaneous coexistence of coherent and ripening islands. The energy was assumed as a sum of contributions from wetting layer, coherent islands and ripening islands. The energy was minimized with respect to the amount of material in islands and WL. They achieved an equilibrium phase diagram, which is shown in figure 1.4. The model predicts 6 growth modes, depicted above and below the diagram. It can be seen that in some range of deposition thicknesses and strain only coherent islands exist.

Kinetic models assume the existence of thermodynamic driving force to ripening, but emphasize that the ripening can be slowed down by a progressively growing barrier for the attachment of new atoms to an island [20]. An attachment of adatoms is more

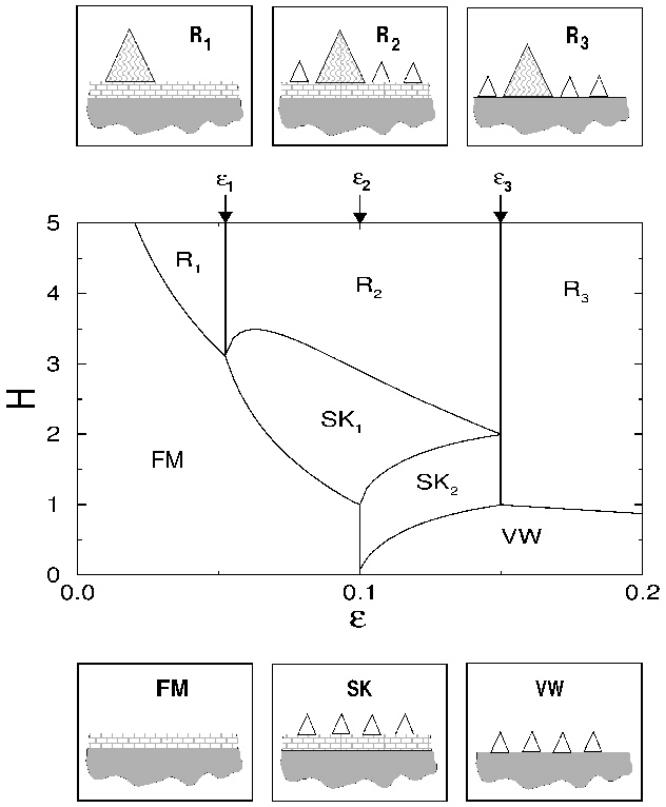

Figure 1.4: Equilibrium phase diagram as a function of the coverage H and misfit ϵ. The small panels on top and bottom illustrate the morphology of the surface in the six growth modes. Taken from [19].

favourable for small QDs, thus due to material exchange an array of QDs with equal size appears.

Ledentsov et al. [21] claimed that the growth of QDs is thermodynamically and not kinetically limited. InAs QDs were grown using MBE, it was shown that the QDs reach their equilibrium size after 10 seconds of growth interruption and do not grow further during long growth interruptions with duration of up to 2 min. The QDs demonstrate a reversible transformation caused by change of substrate temperature. Such behaviour, however, was observed only at low As pressure. Increase of As pressure by a factor of 3 induced an irreversible Ostwald ripening. Pötschke et al. investigated an impact of long growth interruptions onto properties of InAs QDs grown using MOCVD [22]. He discovered a monotonic growth of an average QD dimension and the appearance of a multimodal size distribution. The QDs in case of MOCVD were grown at larger As pressure, thus they are possibly close to the mode of Ostwald ripening.

The first observation of self-organized QD formation was made by Goldstein in

1985 [23]. He deposited a short period superlattice of InAs and GaAs, and cross-section TEM images showed a formation of stacked QDs. Active investigations of InGaAs QDs began in the mid-90ies, stimulated by a wish to extend the luminescence wavelength achieved on GaAs substrate towards longer wavelengths inaccessible using InGaAs QW.

1.3 Structural and optical properties of self-organized QDs

Optical and structural properties of self-assembled QDs were actively investigated during the last decade. A lot of different methods were implemented such as transmission electron microscopy (TEM), high resolution electron microscopy (HREM), scanning tunnelling microscopy (STM), atomic force microscopy (AFM), cathode luminescence (CL), and photoluminescence (PL).

First TEM investigations showed that the QDs have a pyramid-like form. Different other forms were observed later; among them are truncated pyramid, lens, and dashes. Determination of exact size and shape of QDs was found to be difficult using TEM, since strong strain disturbs a chemical contrast. Simulation of TEM images observed experimentally using different QD model forms, e.g. circle and square base, provides very similar images for these two different forms [24]. Nevertheless, TEM is useful to determine QD density and roughly estimate the QD size.

Many investigations were performed using STM. Some groups connected MBE growth chamber with a STM chamber, so that the sample can be transferred from a growth chamber to a microscope avoiding an exposure to air. Marquez et al. [25] observed InAs QDs with relative complex facet structure. The QDs had a lens-like shape bounded by (101), (111) and (137) facets. It should be mentioned that plan-view STM measurements require the samples to be cooled after QD deposition. This step usually takes some minutes. The shape and the density of QDs could be changed during cooling, since an atom surface migration is not suppressed what takes place if the QDs are covered with matrix material. The observed QD shape hence differs from the shape at growth temperature. Buried QDs do not depict the form of QDs during growth as well. It is assumed that the capping freezes the density, but it was found that depending on growth conditions the QDs could either partly dissolve during capping [26] or in opposite increase their size [27].

Cross-sectional STM was used to investigate the structure of buried InGaAs QDs in GaAs matrix. An inhomogeneous In distribution inside the QD was found [28]. Indium

atoms accumulate near the middle core and the apex of QDs, whereas the outside and base regions are Ga rich. The In distribution has a form of an inverted pyramid inside the QD.

Electronic structure of QDs was modelled using 8-band $k{\cdot}p$ method [29, 30] and a pseudopotential method [31,32]. Both calculations require a huge computational power. The electronic levels of a single QD predicted by these methods are in a good agreement with experiments. Unfortunately simulated results depend on some unknown factors, for example exact shape and size.

Photoluminescence investigations of QD arrays show a broad luminescence instead of predicted very narrow lines. The reason is an inhomogeneous broadening of energy levels caused by size fluctuations of QDs within the array. The inhomogeneous broadening of ground state emission of self-assembled QDs is typically about 30-60 meV. Using special growth techniques it can be reduced, for example a low growth rate can provide QDs with spectral halfwidths less than 20 meV [33]. Very low broadening of only 7.6 meV was reported for QDs grown on a prepatterned substrate [34]. However, luminescence measured from a single QD consists of very narrow lines corresponding to transitions between different sublevels and excitonic complexes. Grundman et al. reported about a luminescence linewidth less then 0.15 meV from a single QD [6]. The luminescence efficiency of coherent QDs was found to be very high, comparable with that of the best InGaAs QWs. A comparison of long wavelength InGaAsN QWs and InAs QDs emitting near 1.3 μm demonstrates a superiority of QDs from the point of view of stability of luminescence efficiency at different temperatures [35].

Carrier capture and relaxation between sublevels in the QD are important parameters for device performance. Optical gain, output power and frequency characteristics are all functions of capture and relaxation times. At the beginning of QD investigation there were some pessimistic statements that QD could not be used as an active material of lasers, because of slow relaxation between QD sublevels. In this case an inversion of population required for laser generation can not be reached. This effect was called bottleneck. Later it was discovered that the relaxation time between sublevels is much shorter than the radiative relaxation time of ground state transition 10-100 ps versus 0.5-1 ns respectively [36, 37]. Dominating relaxation mechanisms were found to be carrier-carrier interaction at low temperatures and phonon scattering near room temperature.

1.4 Lasers based on QDs

First, the advantages of lasers based on QDs were predicted by Arakawa and Sakaki in 1982 [38]. They assumed in their model an array of ideal QDs with single electron and hole level. The calculation shows that the threshold current of a laser based on QDs must be independent on temperature. An experiment with GaAs/AlGaAs QW laser placed in a strong magnetic field provided a confirmation of their theory. The electrons confined inside the QW in one direction become confined in the other two directions by forming circle orbits in the magnetic field (Landau levels). A significant increase of the threshold current stability was observed. The dependence of threshold current on temperature for semiconductor lasers can be in some temperature range described using the empirical equation

$$J_{thr} = J_0 e^{\frac{T}{T_0}} \tag{1.5}$$

where T_0 is the characteristic temperature. The higher T_0 the better the temperature stability of the threshold current. For lasers based on QDs T_0, according the prediction, should be infinity.

Another predicted advantage of QDs is a very high material gain. Asada et al. [39] calculated an optical gain for quantum objects with different degree of confinement. It was found that the maximal saturated gain of QDs is much larger than for any other structures, see figure 1.5. The threshold current of a laser based on QDs is expected to be also smaller than that of other structures. The advantage of modal gain is partly eliminated if we take into account the fact that the volume of QDs is significantly smaller than that of a QW or a quantum wire. For example by the density of $1{\times}10^{11}$ cm^{-2} and lateral dimensions $10{\times}10$ nm^2 the QDs occupy only one tenth of the volume of a QW with the same thickness.

Characteristics of first lasers based on self-assembled InGaAs QDs [40, 41] were far away from predictions. The threshold current density was very high ($\gtrsim$1 kA/cm^2), the temperature stability near room temperature was very low as well ($T_0 \lesssim 50$ K), lower than that of InP-based lasers. One of the main reasons was found to be low optical gain of QDs.

A condition of laser radiation generation is fulfilled when the optical gain is equal to the losses in the laser cavity

$$g = g_{material}\Gamma = \alpha \tag{1.6}$$

where g is the modal gain, $g_{material}$ is the material gain, Γ is the optical confinement factor, α is the optical losses. Optical losses can be presented as a sum of intrinsic

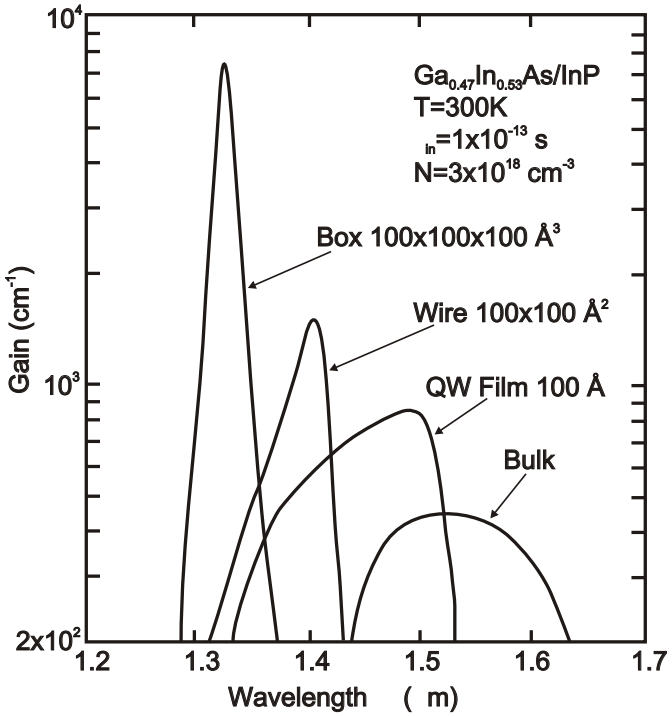

Figure 1.5: Theoretically calculated optical material gain for bulk material, QW, quantum wire, and QD. Taken from [39].

losses and loss due to light outcoupling

$$\alpha = \alpha_{internal} + \frac{1}{2L} \ln\left(\frac{1}{R_1 R_2}\right) \tag{1.7}$$

Here $\alpha_{internal}$ denotes the internal losses, the second term is the loss due to light outcoupling. L is the laser cavity length, R_1 and R_2 are the reflectivities of the resonator mirrors. The internal losses mostly originate from light scattering and absorption in the laser cavity. Internal losses of real laser devices can be estimate using the experimental dependence of the inverse external differential efficiency vs. cavity length

$$\eta_{diff} = \frac{\Delta P}{\Delta I \cdot h\nu_{lasing}} \frac{1}{\eta_{diff}} = \frac{1}{\eta_{internal}} \left(1 + \frac{2\alpha_{internal} L}{\ln\left(\frac{1}{R_1 R_2}\right)}\right) \tag{1.8}$$

where $\eta_{internal}$ is the internal quantum efficiency.

Despite larger material gain of QDs, the modal gain is relatively low, first due to the small volume ocupied by QDs, comparing with QW. The second reason is an inhomogeneous broadening of energy spectra, caused by size fluctuation. Since the QD spectrum is much wider than the cavity mode, only a part of QDs is involved into laser operation.

Modal gain of a real array of QDs considering inhomogeneous broadening was investigated in some theoretical work [42–46]. Following [43], the maximum modal gain for a transition between sublevels i and j of QD is

$$g_{ij}^{max} = \frac{\xi}{4}\left(\frac{2\pi\hbar c}{E_{ij}\sqrt{\epsilon_{ij}}}\right)^2 d_{ij}\frac{1}{\tau_{ij}^{QD}}\frac{\hbar}{\Delta\varepsilon_{inhom,ij}}\frac{\Gamma_{ij}}{a}N_S Z_L \tag{1.9}$$

where ξ is a numerical constant; E_{ij} is transition energy; ϵ_{ij} is dielectric constant; Γ_{ij} is the modal optical confinement factor along the transverse direction to the QD layer; d_{ij} is the degeneracy of the transition; $\Delta\varepsilon_{inhom,ij}$ is the inhomogeneous broadening of energy level due to QD size distribution; N_S is the surface density of QDs in a layer; Z_L is the number of QD layers. The reciprocal spontaneous radiative lifetime is

$$\frac{1}{\tau_{ij}^{QD}} = \frac{8}{3}\alpha\sqrt{\epsilon_{ij}}\frac{E_{ij}}{\hbar}\left(\frac{P}{\hbar c}\right)^2 I_{ij} \tag{1.10}$$

where P is Kane's parameter and I_{ij} is the overlap integral of the electron and hole wave functions. The overlap integral is a function of the size and shape of QDs, it depends also on the strain distribution inside the QD.

Using this equations we can make some key conclusions how to increase the modal gain of an array of QDs: first of all the number of QDs, means the density N_S and the number of QD layers Z_L, must be as large as possible, second, the inhomogeneous broadening $\Delta\varepsilon_{inhom,ij}$ must be reduced. Other parameters, such as radiative life time τ_{ij}^{QD} could not be really controlled.

Various experimental works gave the value for saturated modal gain of 3-4 cm^{-1} per one QD layer with a QD density of about 3-4$\times10^{10}$ cm^{-2}. This value is a few orders of magnitude smaller than for a QW. Kirstaedter et al. found the material gain of a single InGaAs QD as high as $6.8\cdot10^4$ cm^{-1} [47], larger than for an InGaAs QW. Such low modal gain requires an extremely high quality of the laser structure. Using equation (1.7) we can estimate the losses due to light outcoupling to be about 11 cm^{-1} for a GaAs waveguide with 1 mm length ($R_1 = R_2 = 0.33$). Therefore, long cavity, multiple stacking of QDs in the active zone, and/or high reflection coating of laser facets are needed in order to achieve laser operation.

An increase of QD layers in the active zone increases the maximal gain [48], but at the same time the threshold current [46, 49], since more QDs should be excited at the threshold. High reflection coating acts as an effective increase of cavity length, the output power, however, drops. Therefore, it is undesirable to make HR coating of the front mirror.

The first InGaAs/GaAs QD lasers had an emission wavelength near 1-1.1 μm. Despite the fact that a long wavelength luminescence up to 1.4 μm from QDs was

shown already in 1994-95 [50–52], it took some years until in 1998 the first QD laser emitting near 1.3 μm was demonstrated. First lasers suffered from low gain. Very long devices with cavity lengths up to 8 mm with high reflection coating were used in order to achieve lasing [53]. Huffaker et al. [54] demonstrated a laser emitting at 1.31 μm at room temperature with a threshold current density of 270 A/cm^2, based on $In_{0.5}Ga_{0.5}As$ QDs grown by separate deposition of In and Ga. Such a growth method provides large QDs with a low density. Zhukov et al. used InAs QDs overgrown with an InGaAs QW [55]. The wavelength was somewhat shorter, but the lasing occured without HR coating. Park et al. suggested to grow the InAs QDs on an InGaAs buffer and overgrow them with InGaAs (dots in a well - DWELL) [56]. Using HR coating of both facets a threshold current density as low as 19 A/cm^2 was achieved.

All first lasers emitting near 1.3 μm were grown using MBE. MOCVD seems to have more difficulties achieving long-wavelength lasing. First lasers emitting beyond 1.24 μm were demonstrated in 2003. Until now characteristics of long wavelength lasers grown using MOCVD remain behind those grown by MBE. This phenomenon was tried to be explained by a smaller overlap of electron-hole wave functions into QDs grown by MOCVD [57] causing lower optical gain. Published results on long wavelength QD laser achieved by different research groups are collected in table 1.1.

Table 1.1: Performance of long wavelength lasers based on InGaAs/GaAs QDs published by different research teams. All data are taken at room temperature.

QD type	Growth method	QD density (cm^{-2})	g_{max} per layer, cm^{-1}	J_{thr}, A/cm^2	λ, nm	Facets coating	Reference
InAs/InGaAs DWELL	MBE	$2.5{\cdot}10^{10}$	5.4	16	1246		[58]
InAs/InGaAs DWELL	MBE	$7.5{\cdot}10^{10}$	15.6		1230		[58]
InAs/InGaAs DWELL	MBE	$2{\cdot}10^{10}$		19	1330	HR/HR	[56]
InAs/InGaAs	MBE	$2\text{-}3{\cdot}10^{10}$	1	45	1310	HR/HR	[59]
InAs/InGaAs	MBE	$4{\cdot}10^{10}$	3	85	1260	NO	[55, 60]
InAs/InGaAs DWELL	MBE	$4.3{\cdot}10^{10}$		17	1305	HR/HR	[61]
InAs/InGaAs	MOCVD	$1.7{\cdot}10^{10}$		655	1245	HR/HR	[62]

InAs/InGaAs	MOCVD	$1.4{\cdot}10^{10}$	1.8	475	$1280_{(ES)}$	HR/HR	[63]
InAs/InGaAs DWELL	MOCVD	$5{\cdot}10^{10}$	2.6	550	1249	HR/HR	[64]
InGaAs	MOCVD	$4.3{\cdot}10^{10}$	5.5	55	1100	NO	this work
InGaAs/ InGaAs	MOCVD	$2{\cdot}10^{10}$	1.4	200	1243	NO	this work
InAs/InGaAs DWELL	MOCVD	$4{\cdot}10^{10}$	2.8	450	1240	NO	this work

Low T_0 near room temperature was a crucial problem of earlier QD lasers. It was attributed to escape of electrons and holes from the ground state due to thermal activation. An existence of many electron and hole levels in a QD favours this process [44]. At low temperature the threshold current is usually independent on temperature, but near room temperature and higher, the population of excited states becomes significant, increasing the current necessary to reach inversion. The non-radiative recombination in the waveguide also becomes important [65]. Shchekin et al. [66] demonstrated a rise of T_0 if the separation between ground and excited state is increased. It was found that the threshold current stability could be improved by placing the QDs in a matrix with larger band gap, such as AlGaAs [67,68]. A laser with T_0=385 K up to 50℃ was demonstrated [69]. Another useful method to improve T_0 was found to be p-doping of surrounding layers. Holes are more affected to thermal escape, since the separation of holes sublevels in QDs is much smaller than of electrons. The p-type doping increases the population of hole levels. $T_0=\infty$ up to an operation temperature of 350 K was observed in lasers with p-doped waveguide [70].

The dependence of threshold current on temperature has a feature specific for QDs. At low temperature it is either constant, $T_0=\infty$, or even negative, $T_0<0$ [71]. This effect arises due to a deviation of the carrier distribution in QDs from a Fermi distribution. At low temperatures the escape time from a QD is larger than the recombination time. So the carriers captured in the QDs do not thermalize, and the distribution is close to unity, all QDs are equally populated. At higher temperatures the carriers thermalize and have a Fermi-like distribution, larger QDs are more populated than the small ones. The transition from an uniform to a Fermi distribution take place between 150-250 K, depending on QDs. It was demonstrated that a negative T_0 can be eliminated if the inhomogeneous broadening is reduced [72].

Efficient capture of charge carriers into QDs and 3-dimensional localization was found to be very useful for laser implementation. In opposite to a QW, where electrons and holes can freely move along the QW, in QDs lateral migrations is strongly suppressed, thus the surface recombination rate is smaller than in a QW. It make possible to produce a lasers with a mesa etched through the active zone without a significant increase of threshold current [73].

1.5 Metalorganic vapor phase deposition

Metalorganic chemical vapor deposition (MOCVD), also often called metalorganic vapor phase epitaxy (MOVPE), was invented in the end of 1960s and since then became the most important growth method for optoelectronic devices. It was designed to produce thin epitaxial layers and can be used to grow almost any V-III and VI-II material. Different device types were demonstrated using MOCVD growth, such as lasers, light emitting diodes, transistors and so on. A good review on MOCVD is given in the book of Stringfellow [74].

The MOCVD setup is schematically shown in figure 1.6. Highly purified hydrogen is used as carrier gas. It is conducted through bubblers containing the precursors. The bubblers are made of stainless steel and filled with chemical agents of elements, which are necessary for the growth. The precursors are mostly organic-compounds and are liquids at room temperature. The bubblers are kept at constant temperature between -10 and 20℃ in thermostats. A gas pressure in the bubblers is also kept constant in the range from 500 to 2000 mbar depending on precursor and desirable flow.

The carrier gas saturated with precursor vapor is directed either to the reactor (Run line) or in a bypass line - Vent line. It makes possible to achieve abrupt switching between different materials, since the switching valve needs 0.1 second to change the flow, while the valve controlling flow (Mass Flow Control valve - MFC) needs some seconds. In earlier equipment design the gases are mixed before injection into the reactor. Now all growth machines are constructed in such a way that the precursors of different groups, in our case V and III, are conducted until reactor separately. The mixture occurs in the front part of the reactor. It was made in order to avoid gas phase prereactions between precursors. Moreover, separate injection was found to improve uniformity of growing layers. Reactor pressure is usually kept between 20 and 500 mbar, depending on growth material. Low reactor pressure provides larger gas velocity allowing to grow abrupt heterointerfaces. Prereaction rate is also smaller in low pressure MOCVD, since the reaction speed in gas phase is proportional to a partial

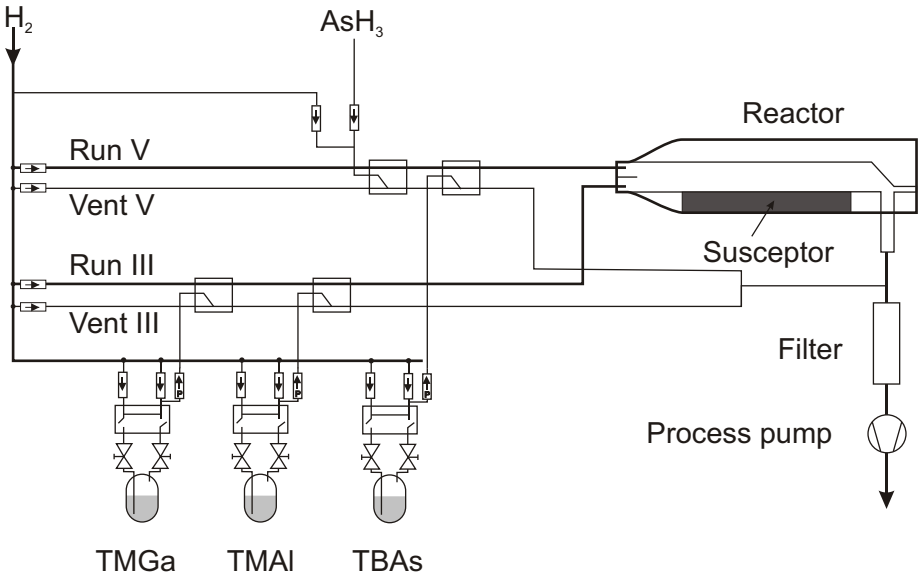

Figure 1.6: Schematic view of MOCVD equipment.

pressure of each reagent.

The growth occurs on a substrate placed on a carbon susceptor. In all modern reactors the substrate is placed on a thin carbon plates, which rotate in order to increase the uniformity. The susceptor is heated using either infrared (IR) or radio frequency (RF) waves. The growth temperature can be varied from 450℃ for antimony-containing materials up to 1200℃ for nitrides. Precursor molecules decompose on the heated substrate producing different species; some of them can incorporate into the growing crystal. The decomposition way of precursors strongly depends on growth temperature. At low temperature the decomposition of many molecules takes place directly on the surface. First they are adsorbed and than decompose. Sometimes reactions take place only if two precursors are present together on the surface, what is used for atomic layer epitaxy. At higher temperatures more reactions occur above the substrate in the gas phase. In opposite to MBE the growth using MOCVD is more complicated. The growth rate is not constant, like in MBE, but strongly temperature-dependent. At low temperature it grows with increase of temperature, so-called kinetically limited growth. At moderate temperatures the growth rate is almost independent on temperature - mass transport limited mode. At high temperatures the growth rate drops due to re-evaporation of material from the surface.

Most samples used in this work were grown on an Aixtron AIX200/4 machine. It has a horizontal quartz-glass reactor with graphite susceptor and gas-foil rotation of

the substrate plate. The susceptor is heated by an infrared heater. Substrates with 2", 3" and 4" diameter can be used. All experiments were performed using 2" substrates. The layer thickness non-uniformity over a 3" substrate was found to be better than 3%, what to our opinion is insufficient especially for devices such as VCSELs. At the same time the non-uniformity is only 1% over a 2" substrate except 3 mm border. A relatively small length to width aspect ratio for this reactor type can explain such poor uniformity over a large substrate. The samples discussed in section 2.7 were grown on an AIX200 machine with RF heating. It is a previous version of the AIX200/4 has a narrower reactor, growth can be performed on 2" substrates only.

Trimethylgallium (TMGa), triethylgallium (TEGa), trimethylaluminum (TMAl), and trimethylindium (TMIn) were used as group III precursors. All of them except TMIn are liquid at room temperature. TMIn is solid and is placed in the bubbler in form of a fine powder. All precursors have the best available quality with lowest contamination level - optograde. Thanks to a strong demand on high pure precursor their quality has steadily increased. We observe this on an example of TMAl precursor. During this work one used TMAl was replaced with another one having also optograde purity, but an intrinsic contamination with carbon was found to be almost one order of magnitude lower than with the old precursor.

For conventional MOCVD the gaseous precursor arsine (AsH_3) is used as an arsenic source. Arsine decomposes only partly at typical temperatures used for QD growth (470-530℃), thus a high V/III ratio should be used. The arsenic partial pressure has a huge impact on properties of QDs, therefore it should be precisely controlled during growth. Since the decomposition ratio of arsine strongly changes near 500℃, it is almost impossible to distinguish the impact of arsine partial pressure and growth temperature on the QD properties, because the V/III ratio changes simultaneously with temperature.

A lot of different chemicals were tested to substitute arsine. Most of them are compounds of As with organic molecules. The decomposition temperature was found to be lower than that of arsine, but many of them provide high level of intrinsic carbon doping. Epitaxial layers with good properties were demonstrated using tertiarybutylarsine (TBAs). TBAs has an almost 200℃ lower decomposition temperature than arsine. The decomposition efficiency of TBAs and arsine is shown in figure 1.7 taken from [75]. It can be seen that arsine fully decomposes only above 650℃, whereas TBAs above 450℃. Thus it can be assumed that TBAs is totaly decomposed by growth of QDs, and the growth temperature and the arsenic partial pressure can be tuned independently.

Now the growth using TBAs is good investigated. The layers grown using TBAs are not worse than grown using AsH_3, sometimes they have even better quality. It

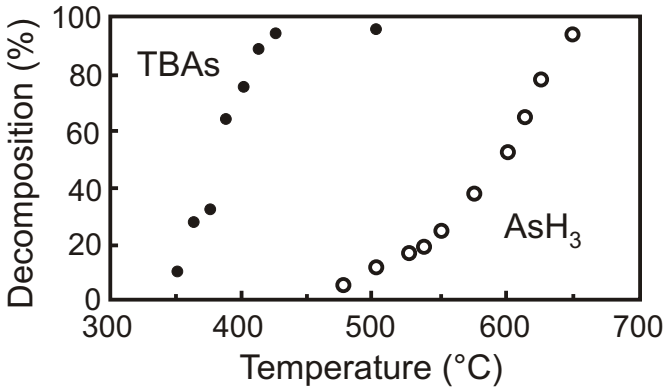

Figure 1.7: Temperature dependence of decomposition efficiency of TBAs and AsH_3, taken from [75].

was found that AlGaAs grown using TBAs has lower levels of oxygen and carbon contamination [76,77]. High performance lasers emitting near 1.2 μm based on InGaAs QWs were demonstrated using TBAs [78]. The imiting factor of TBAs spreading is a high price, but it is partly compensated by the possibility to use lower V/III ratio achieving the same layer quality. Successful device growth using TBAs in large scale production reactors was demonstrated [79].

TBAs is much preferable than arsine when the safety is taken into account. Use of arsine demands a lot of precautions, since it is extremely toxic and is stored under high pressure. TBAs, in opposite, is liquid at room temperature with a vapor pressure of only 150 mbar. The mortality concentration in the air is about ten times lower than that of arsine. All this makes the daily work with TBAs less dangerous.

Decomposition of arsine occurs by detachment of atomic hydrogen. TBAs decompose mostly via monolithic fusion when AsH_2 cut off from the TBAs molecule. By this reaction less atomic hydrogen is produced as during arsine cracking. Atomic hydrogen has a slight etching effect on the surface. The indium composition of InGaAs layers was found to be dependent on the kind of arsenic precursor [80]. AsH_3 produces the largest amount of atomic hydrogen among the As precursors and provides a lower In composition than TBAs in InGaAs layer. Despite the difference is only a few percents, it means that atomic hydrogen could noticeably change the growth. Thus the kind of As precursor has an impact on surface energy defining the QD growth.

Diethyltellurium (DETe) and carbon thetrabromide (CBr_4) were used as n- and p-type doping precursors respectively. DETe replaces standard gaseous precursor silane (SiH_4). Carbon as p-type dopant is actively used during last ten years. It has a huge benefit over other p-type precursors such as Zn and Sn, since its diffusion in crystal is

extremely low and very high doping levels up to 10^{20} cm^{-3} can be achieved.

Chapter 2

Growth of InGaAs/GaAs QDs

Self-assembled QDs are very complicated in fabrication. A lot of issues should be taken into account. Properties of an array of QDs can be controlled only indirectly by changing growth parameters, which have different impact on growth. The main target of this work was to achieve long wavelength luminescence from InGaAs QDs on GaAs substrate and fabrication of edge-emitting and vertical-emitting lasers. All investigations were made from this position. In this chapter main results concerning growth methods, optical and structural properties of QDs are discussed. Devices based on QDs are described in the chapters 4 - edge emitting lasers, and 5 - vertical emitting lasers (VCSEL).

2.1 Characterisation methods

The main characterisation method of QDs in this work was photoluminescence (PL). Emission spectra of QDs can be quickly measured, ground, excited states transition and wetting layer position can be estimated. Since no sample preparation is needed it allows a rapid feedback to epitaxy.

The typical layer scheme of a PL sample is shown in figure 2.1, on the left side a growth temperature typical for each layer is shown. All samples for PL investigation were grown on undoped exactly oriented (001) GaAs substrates. The accuracy of orientation is $\pm 0.1^{\circ}$. Before growth, the substrate is annealed in the reactor at about 730℃ during 5 minutes under TBAs flow. An oxide layer and most of contaminations are evaporated during this step. Afterwards a 300 nm thick GaAs buffer layer is deposited at 650℃. The buffer makes the surface flat and hinders a diffusion of rest contamination from the substrate towards an active zone. After the GaAs buffer a 50 nm thick $Al_{0.6}Ga_{0.4}As$ and a 100 nm thick GaAs are grown. The deposition of QDs takes

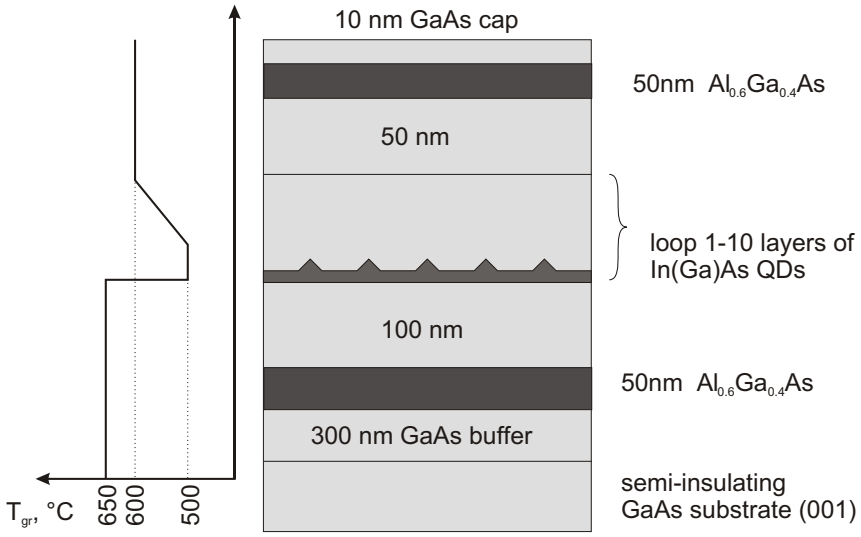

Figure 2.1: Structure of a sample for PL investigation. The diagram on the left shows the typical temperatures used for the growth.

place in the temperature range from 470 up to 530℃. After GaAs growth at 650℃ the growth is interrupted and the substrate temperature is decreased. When the temperature reaches the given value the substrate is kept another 2 minutes without growth in order to be sure that the substrate temperature is stable and uniform. After QD deposition the temperature is increased up to 600℃ to grow the rest of the structure. QD growth will be discussed in details later. QDs are covered with 50 nm thick GaAs and 50 nm thick $Al_{0.6}Ga_{0.4}As$. At the end the structure is capped with a thin GaAs cap layer, which prevents the AlGaAs from oxidation. The AlGaAs barriers confine charge carriers in a vicinity of QDs and prevent them from migration to the surface where rapid non-radiative recombination occurs.

For PL measurements the samples are excited with an argon Ar^+ ion laser with a wavelength of 514.5 nm. The luminescence is detected using a monochromator and a cooled Ge diode. A standard lock-in method is used to improve the signal to noise ratio. The laser power on the sample can be varied so that the effective excitation density is changed from 5 W/cm^2 up to 5 kW/cm^2. At low excitation density the number of electron-hole pairs is not enough to fill all QDs, thus only the luminescence from the ground state is visible, except for the case of QDs with a low density($<10^9$ cm^{-2}). If the excitation density is increased the number of excited electron-hole pairs becomes larger than can recombine via ground state, so the excited transitions become visible in the PL spectra. At highest laser power the luminescence of QDs is saturated and the

emission of the WL dominates in the spectrum. By direct comparison of PL spectra at low excitation besides the estimation of luminescence wavelength, a comparison of structural quality can be made. The spectra at high excitation give roughly a QD density. This comparison is not exactly and can be used only as a first approximation. As an example room temperature PL spectra of InAs QDs measured under different excitation powers are depicted in figure 2.2. An obvious rise of contribution of excited states can be seen as the excitation density grows.

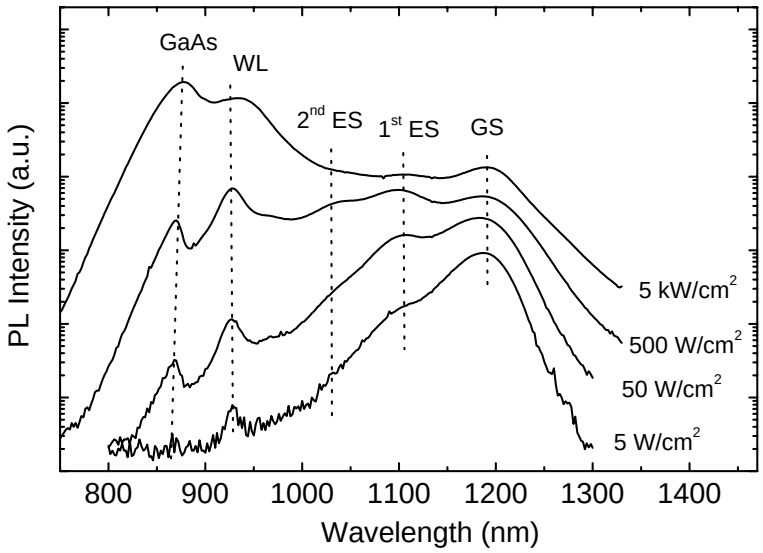

Figure 2.2: Room temperature PL of InAs QDs at different excitation densities.

PL samples with single QD layers were also used for plan-view TEM investigations to determine the QD density. The TEM images used in this work were made in Max-Plank Institut in Halle by P. Werner and N. Zakharov. Standard methods of sample preparation were used. The samples are thinned using first a mechanical polishing and then an ion milling.

Atomic force microscopy (AFM) and optical phase-contrast microscopy (Nomarski microscope) were used to control surface morphology especially the interfaces in devices. AFM can control the surface area of up to 100×100 μm^2 with a lateral resolution of about 10nm [1]. The vertical resolution is up to 1Å, allowing to see a single monatomic step. We do not use AFM to control QD growth, despite a big amount of publications where it was done. We discovered that in our case the QDs dissolve during cooling of the sample if they are not capped with GaAs or InGaAs. The optical phase-contrast

[1]Lateral resolution depends on measured area. The smaller scanned area is the better resolution.

microscope is constructed in such a way that it makes visible even small surface roughness. It has a much smaller lateral resolution than AFM but can control an area from 50×50 μm^2 up to some millimetres. It was also used to control the roughness of structures.

Growth rate calibration was performed using ex-situ optical reflectometry and high-resolution X-ray diffractometry (XRD). The growth rates of thick AlAs and GaAs were estimated using a structure consisting of 6 pairs of AlAs/GaAs with a thickness of about 70 nm. Reflection spectra were measured and simulated giving the growth rates of AlAs and GaAs. Indium-containing layers could not be grown thick enough for optical measurement due to dislocation formation. Therefore a superlattice containing thinn layers of InGaAs sandwiched between GaAs were grown. XRD rocking curves were measured and simulated. The indium concentration in the InGaAs was chosen to be about 15-25% in order to achieve dislocation-free growth mode. The composition of InGaAs in the solid was found to be a linear function of the In and Ga ratio in the gas phase for an In content up to 40%. So the growth rate was linearly extrapolated to higher In contents. Such a method gives the InAs growth rate to an accuracy of about $\pm5\%$.

2.2 Influence of growth parameters on properties of a QD array

QD growth is a self-organisation process. Final result can be controlled by changing conditions at which the process take place. There are many parameters describing the growing system: temperature, deposition thickness, growth rate, V/III ratio and others. In case of MOCVD some specific parameters are added: the kind of precursors, reactor pressure, the kind of carrier gas. All these parameters have different impact on the properties of QDs.

Most QD samples presented here were grown using the following procedure. As the substrate temperature is stabilized the material of QDs is deposited. Afterwards a growth interruption (GRI) is implemented. During GRI all sources are switched off including arsenic. The duration of the GRI is typically 0.5-1 minute. After GRI the QDs are overgrown with either GaAs or InGaAs. All sources, namely In, Ga, and As, are switched on simultaneously. First 5 nm of GaAs is grown at the same temperature as the QDs in order to avoid an intermixing of QDs, then the temperature is ramped up to 600℃. GaAs grown at low temperature, such as 500℃, has relative poor crystalline quality, and shows a high rate of non-radiative recombination. Therefore

it is preferable to grow GaAs at low temperature as thin as possible. However an increase of temperature without capping QDs or with cap layer thinner than 5-7 nm causes a strong blue-shift of the QD emission wavelength. The impact of overgrowth temperature on QD properties will be discussed in section 2.4 and 4.2.

Leonard et al. [81] investigated the evolution of an InAs QD array grown using MBE when the deposition thickness is changed. It was found that there are no QDs at all if the deposited layer thickness is less than some critical thickness. The density of QDs jumps to 10^9 cm^{-2} if the deposition thickness exceeds the critical thickness. The QD density grows by further increase of the deposition thickness but has a tendency to saturate at some level. It was found that the QDs size and luminescence wavelength, respectively, grow until the deposition thickness reaches about 3-3.5 ML [82,83]. Afterwards, the QDs reach critical dimensions and dislocations appear. Dislocated QDs grow more rapidly than coherent ones, they attract all supplied material and even force the migration of the material from already formed QDs, causing a reduction of dimensions of coherent islands. This can be easely observed in PL spectra, since the luminescence wavelength of QDs shows a blue-shift. TEM images also demonstrated a growing number of large clusters and a decrease of QD size.

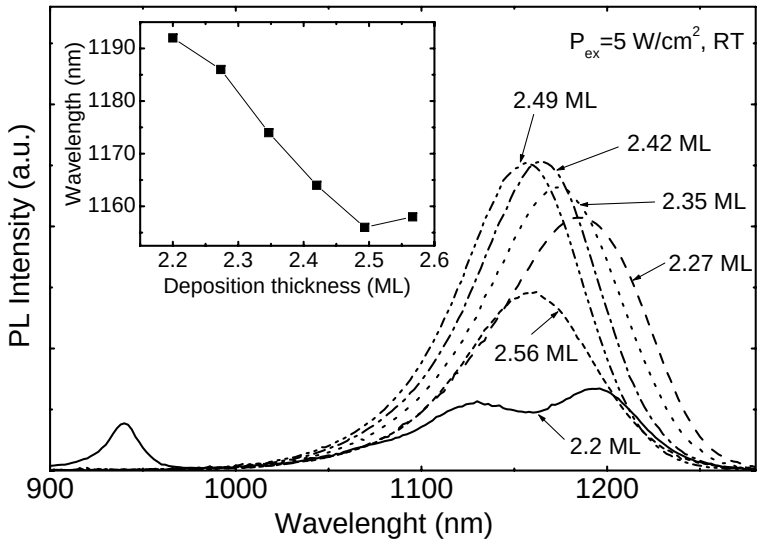

Figure 2.3: Room-temperature PL spectra of $In_{0.7}Ga_{0.3}As$/GaAs QDs grown at 500℃. The deposition thickness is varied as shown in the figure. The inset shows the dependence of peak wavelength vs. deposition thickness.

Figure 2.3 shows room-temperature PL spectra of $In_{0.7}Ga_{0.3}As$ grown at 500℃ using our MOCVD. The deposition thickness was varied from 2 ML (not shown in the figure)

up to 2.56 ML. The sample with 2 ML does not contain QDs, only an emission from a QW can be observed in PL spectra. The critical layer thickness is 2.2 ML. The QD density rises with increase of deposition thickness, which can be seen by growth of the luminescence intensity. If the thickness exceeds 2.5 ML the luminescence rapidly decreases. This is an evidence of dislocated cluster formation. The figure shows a typical evolution of a QD array, observed for all QDs independent on composition and growth temperature. Thus we observe some crucial differences between our MOCVD-grown QDs and results reported in the literature for MBE-grown QDs. The main differences are collected in the following table

MBE growth	**our MOCVD growth**
QD size increase with increasing deposition thickness	QD size decrease with increasing deposition thickness
Coherently QD formed in the range 1-2 critical thicknesses	Coherently QD formed in the range 1-1.3 critical thicknesses

The growth interruption after QD deposition was found to be crucial for QD formation. We found out that the QDs are not formed if the GRI is omitted. Many other research groups growing QDs use very low growth rates 0.1-0.01 ML/sec, giving adatoms enough time to migrate and form QDs during deposition. We used growth rate of about 0.4 ML/s, the QDs are deposited during 5-10 seconds. The growth rate can be used to tune the properties of QDs. Low growth rates lead to larger QDs with a low density. We found that in our case low growth rates makes the luminescence efficiency worse, possibly due to incorporation of contaminations. The optimal growth rate was found to be 0.4 ML/sec. A kinetic model of QD formation predicts a rise of QD density and decrease of their size by increasing the growth rate or/and decrease the growth temperature [84–86]. Tatebayashi et al. used very low growth rates in MOCVD of up to 0.01 ML/sec and achieved long wavelength luminescence with very narrow spectral halfwidth [87]. By high growth rate the GRI substitute long deposition time. The QDs were found to ripen during GRI, an increase of GRI duration leads to larger QDs with a smaller density [22]. It seems that we observe Ostwald ripening of QDs. Min et al. [88] reported also about Ostwald ripening of QDs grown using MOCVD . The ripening takes place during GRI, but can be hindered by using slightly missoriented substrates.

The growth interruption was found to have a minor negative impact on the luminescence efficiency of an InGaAs QW, but increases the luminescence efficiency of QDs. The optimal GRI duration was found to be between 30 seconds and 1 minute, for longer

durations the luminescence intensity drops. It is important to make the GRI without arsenic stabilization, as usually done during arsenide growth. Evaporation of material of a growing crystal near 500℃, including arsenic, is neglibly small. Thus even longer growth interruptions without surface stabilization could be made at this temperature. The presence of a TBAs flow during GRI causes the degradation of QD luminescence.

Since the main task of this work is a fabrication of laser devices based on QDs, the main attention was concentrated to achieve a QD array with maximal density and good quality. QDs with a deposition thickness closely below the occurence of dislocated clusters fulfill these criteria. QDs with such deposition thickness will be called further QDs with optimally deposited thickness. The behaviour of size and density of our QDs makes the fabrication of long wavelength QDs suitable for laser much more difficult than using MBE growth method. The narrow range of deposition thicknesses used for QD growth demands a prescise control of growth.

The critical layer thickness is a function of the lattice mismatch, namely the $In_xGa_{1-x}As$ composition. Our experimental data are shown in figure 2.4. The critical layer thickness in this case is the thickness of a deposited layer at which the QDs are first observed. Following the expectations the critical layer thickness decreases by rise of the In content.

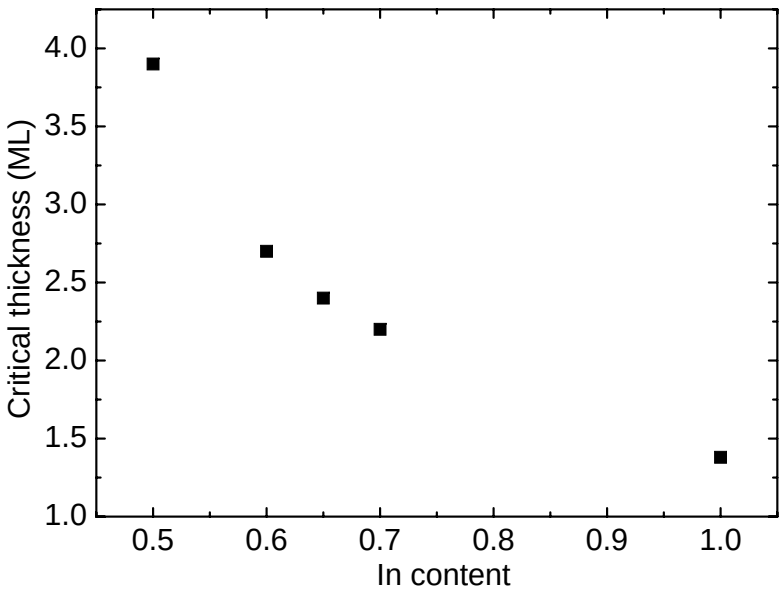

Figure 2.4: The dependence of critical layer thickness of QD formation for $In_xGa_{1-x}As$ layer on GaAs. The growth temperature is 500℃, the deposition rate is 0.4 ML/s.

Indium composition has not only influence on the critical layer thickness, but also on the properties of a QD array. Figure 2.5 shows the PL spectra of QDs with different In composition grown at 500℃. The deposition thickness is optimal for each QD type. The density of InGaAs QDs with different composition as well as their dimensions are listed in the table 2.1. It can be clearly seen that the QD density and dimensions reduce with increasing of In contents. However the exciton confinement is larger for QDs with higher In content. The shape of QDs transforms from flat pyramid-like for InGaAs QDs to lens-like for InAs QDs. Remarkably, TEM investigations demonstrate a presence of dislocated clusters in structures with InAs QDs. Figure 2.6 shows plan-view TEM images of 1×1 μm of samples with $In_{0.65}Ga_{0.35}As$ and InAs QDs. The sample with InAs QDs besides coherent islands contains a large dislocated cluster, their density was estimated to be 3-6×10^6 cm^{-2}. Such defects were not observed in samples with a single layer of $In_{0.65}Ga_{0.35}As$ QDs.

Our value of the critical layer thickness of InAs QDs is somewhat smaller than 1.7 ML what is usually reported. Nevertheless, there are some publications where an even smaller critical layer thickness is claimed, namely 1.2-1.25 ML [89, 90].

Table 2.1: Characteristics of $In_xGa_{1-x}As$/GaAs QDs grown at 500℃.

QDs type	**Critical thickness, ML**	**Optimal thickness, ML**	**Density, cm^{-2}**	**Lateral size, nm**	**Vertical size, nm**
$In_{0.5}Ga_{0.5}As$	3.9	4.3	$4{\cdot}10^{10}$	25	5
$In_{0.65}Ga_{0.35}As$	2.4	2.7	$2{\cdot}10^{10}$	20	4.5
InAs	1.4	1.48	$6{\cdot}10^{9}$	14	3

The width of PL spectra displays the inhomogeneous broadening of the ground state transition, caused by size fluctuation. In our case the width at half maxima varied from 55 up to 70 meV, corresponding to size fluctuations of about 5%. This value is a little higher than usually reported for self-assembled QDs 30-40 meV, possibly due to the relatively large deposition rate.

The growth temperature has a significant impact on QD properties. The influence of the temperature on QD properties was in detail studied for MBE grown QDs by Ledentsov et al. [21]. The QD density was found to be a linear function of the reciprocal temperature. The exciton localisation energy becomes larger at lower temperatures whereas the lateral size becomes smaller. This contradiction is explained by the fact

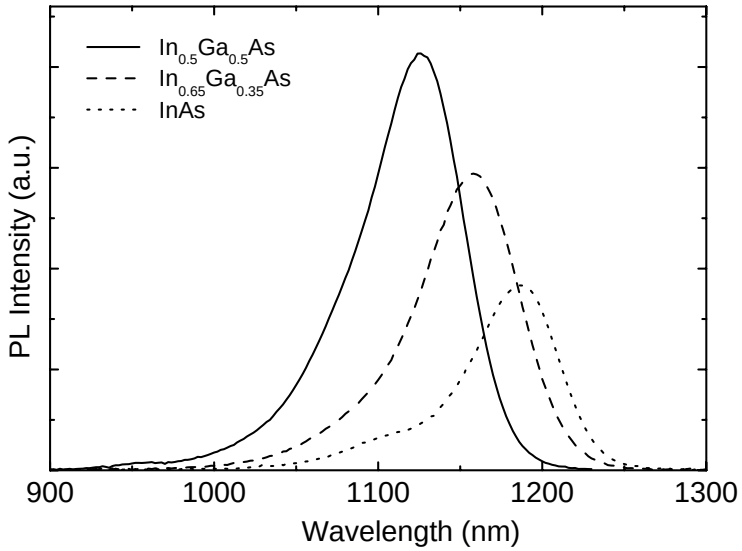

Figure 2.5: Room-temperature PL spectra of $In_xGa_{1-x}As$ QDs with different In composition (shown in the figure), grown at 500℃. The deposition thickness is optimal for each QD type, and corresponds to maximal QD density (see page 27).

that the height of QDs grow with reduction of the temperature. At high temperatures the QDs are very flat with an aspect ratio of height to base length of about 0.2, at low temperature this aspect ratio grows up to almost 1. Flat QDs have smaller localisation than high QDs [32]. We found that the growth temperature has only a minor influence on the luminescence wavelength of QDs. PL spectra of $In_{0.65}Ga_{0.35}As$ QDs grown at different temperatures are shown in figure 2.7. The QD density is larger at low temperature, but the luminescence efficiency drops very quickly with reduction of growth temperature. The best quality is achieved at 500℃.

The surface free energy depends on arsenic pressure [91] and consequently the QD formation is affected by the V/III ratio during growth and growth interruption. The impact of arsenic pressure was investigated for MBE [92] as well as for MOCVD growth [93]. In case of MBE coherent islands can be observed only in the range of an arsenic pressure of $1\text{-}3\cdot10^{-6}$ torr, at lower pressure planar surface and at higher pressure an Ostwald ripening was observed. We found that the best QDs are grown with low V/III ratio. Figure 2.8 shows PL spectra of $In_{0.65}Ga_{0.35}As$ QDs grown with a V/III ratio varied from 1.5 to 10. The QDs grown with high As pressure have larger luminescence wavelengths and lower efficiency. The density of QDs was found to reduce with an increase of the V/III ratio. It is 2×10^{10} cm^{-2} at V/III=1.5 and 1×10^{10} cm^{-2} at V/III=10.

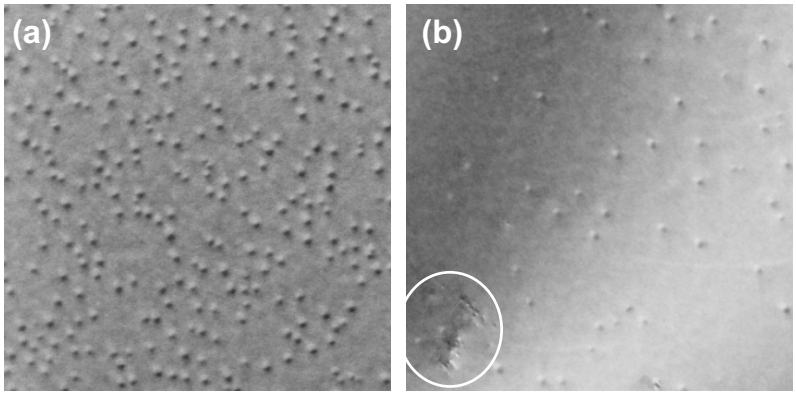

Figure 2.6: Plan-view TEM images of (a) 2.7 ML $In_{0.65}Ga_{0.35}As$ QDs, (b) 1.48 ML InAs QDs, grown at 500℃. Each image covers an area of 1×1 μm^2. The white oval in image (b) marks a dislocated cluster.

Leon et al. [93] reported for MOCVD grown QDs, that low As pressure results in an array of high density coherent QDs, while by increase the As pressure the density of huge dislocated islands grows. It was also found that larger As partial pressure delays the QD formation, increasing the critical layer thickness. The saturated density of QDs was found to be smaller, similar to our results. It was reported many times that a reduction of growth rate leads to the formation of larger QDs with a low density [94,95]. Probably this happens due to an effective increase of the V/III ratio. In our experiments was found that the growth of QDs was not defined by partial pressure of As but mostly by the ratio of the partial pressures of group V and group III sources. So the change of growth rate over some region keeping V/III constant does not change the luminescence wavelength. On the other hand changing the growth rate keeping As partial pressure constant, means a change of V/III ratio and, changes the luminescence wavelength.

In order to better understand the electronic structure of the QDs, photoluminescence excitation (PLE) spectra were measured. In opposite to PL, when the excitation energy is fixed and detection energy is scanned, in PLE the detection energy is fixed whereas the excitation energy is changed. The measurements were performed at 7 K using a halogen lamp as excitation source. Two kinds of QDs were compared, namely InAs and $In_{0.65}Ga_{0.35}As$. PLE spectra are plotted in figure 2.9, PL spectra are shown as well (dashed curve). Vertical lines on the PL spectra mark the detection energy. A significant difference of the electronic structure between InAs and $In_{0.65}Ga_{0.35}As$ QDs can be observed. The spectra of $In_{0.65}Ga_{0.35}As$ QDs have well pronounced ground and excited state transitions with an energetic gap between ground state and first excited state equal to 69 meV. On the other hand, the spectra of InAs QDs do not

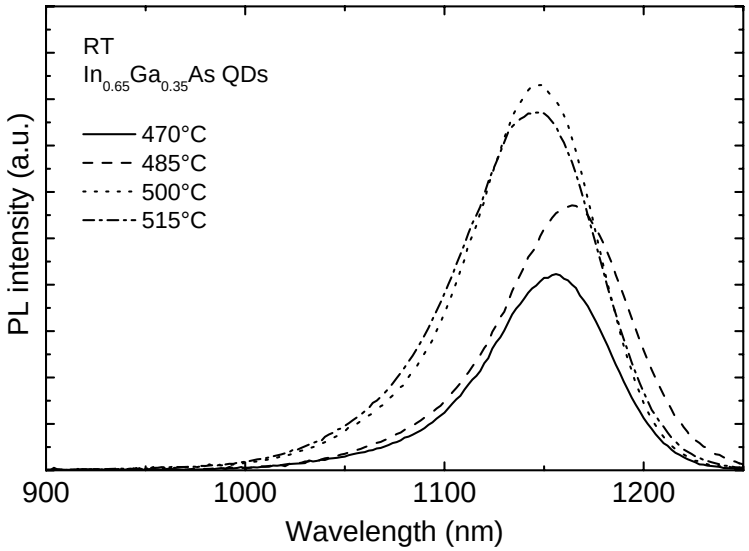

Figure 2.7: Room temperature PL spectra of $In_{0.65}Ga_{0.35}As$ QDs deposited at different temperatures (shown in the figure).

show clearly excited transitions. At the same time the ground state transition have some kind of a short wavelength shoulder. This can be either an excited transition or a ground transition of QDs with another size. It is more probable that InAs QDs have a bimodal size distribution. In this case the broad excited state transitions can be explained by an overlap of two peaks with small separation. It seems that in our case the size difference is not large, the energy difference is less than 30 meV. In addition the simulation performed using 8-band $k{\cdot}p$ method predicts a separation between ground state and first excited state of such QDs of about 60-70 meV. The bimodal size distribution of InAs QDs was reported earlier [96, 97]. What growth parameters really induce the formation of bimodal QDs is unknown, Mirin et al. [98] reported that the bimodal distribution of just nucleated QDs becomes unimodal if the deposition thickness increases. The use of small additions of antimony can change the size distribution to multimodal [99]. The InGaAs QDs in opposite to InAs seem to have an unimodal size distribution. It makes them more attractive for laser application.

2.2.1 Submonolayer multiple stacked QDs

An alternative method of InGaAs QD growth is a deposition of a superlattice consisting of thin layers of binary InAs and GaAs instead of an InGaAs ternary alloy. The thicknesses of both layers are kept near one monolayer. Such a growth method, called digital alloy, is often implemented in MBE in order to achieve a stepless transition from

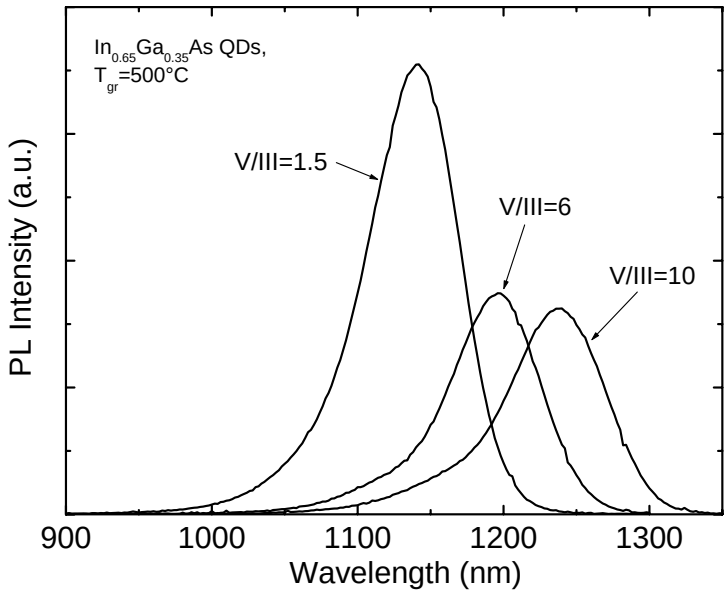

Figure 2.8: Room temperature PL spectra of $In_{0.65}Ga_{0.35}As$ QDs grown at 500℃ with different V/III ratio (shown in the image).

one composition to another, since it is impossible in MBE to quickly change the source flow. Usually a digital alloy has the same properties as a ternary alloy.

It was found that the digital alloy can also be used to grow QDs. Such QDs often were called submonolayer QDs. Most of the QDs grown using digital alloys were fabricated using the MBE growth method. Short wavelength submonolayer QDs emitting near 0.94-0.95 μm were successfully used as the active zone of a laser [100, 101], and demonstrated a large gain and high output power. The density of these QDs can reach more than 1×10^{11} cm^{-2}.

Some groups use an alternating supply of group V and III sources. Such a growth method is called migration enhanced epitaxy. It is assumed that a high mobility of In and Ga adatoms provides the formation of larger QDs. A high mobility originates from the fact that the bonding energy of In-In or Ga-Ga is much lower than that of In-As or Ga-As. Thus the hopping probability and as a consequence the diffusion length are larger. Huffaker et al. [102] reported about QDs with high efficient luminescence, emitting near 1.3 μm. $In_{0.5}Ga_{0.5}As$ in form of an InAs/GaAs SL was deposited, the As was supplied during a 5 second pause between In and Ga deposition. It was reported that the efficiency of long wavelength QDs grown using submonolayer depositions is comparable with QDs deposited using standard methods [103]. The density of submonolayer QDs was found to be smaller comparing with QDs grown using standard methods,

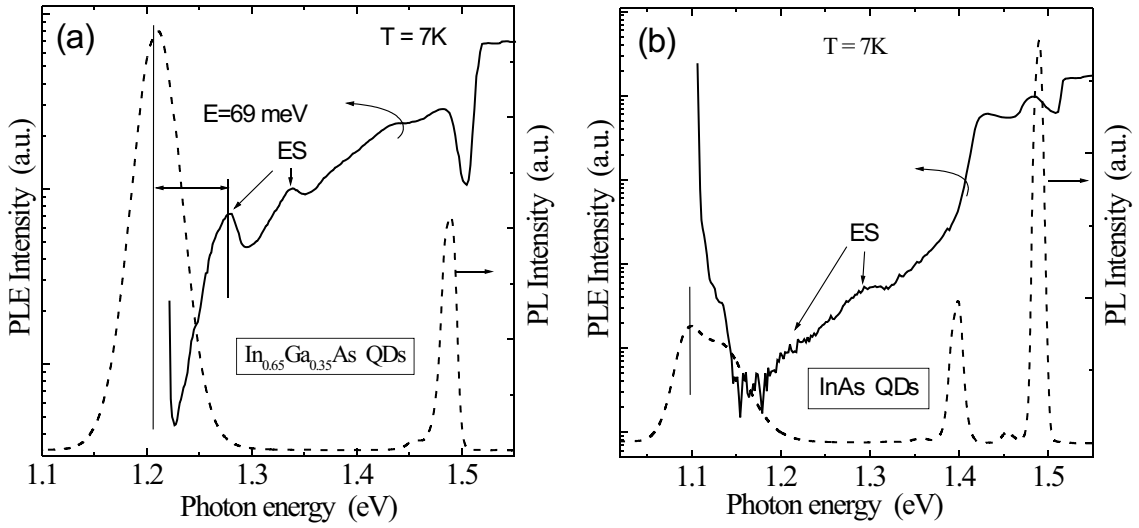

Figure 2.9: PLE spectra (solid curve) and PL spectra (dashed curve) of (a) $In_{0.65}Ga_{0.35}As$ QDs, and (b) InAs QDs. The measurements were performed at 7 K. Vertical lines crossing PL spectra display the detection energies of PLE. The vertical axis is logarithmic for PLE and linear for PL.

whereas the size is larger providing a longer luminescence wavelength. Luminescence even up to 1.4 μm was demonstrated [104], however the luminescence efficiency of such QDs was very low.

We tried to grow QDs using submonolayer deposition. The deposition was performed similar to the standard method. The growth temperature was chosen to be 500℃. The deposition rates of InAs and GaAs were kept at about 0.3 ML/sec, the TBAs partial pressure was kept at 0.5 Pa, and was identical for InAs and GaAs. The TBAs supply was constant during the whole deposition.

PL spectra of submonolayer deposited QDs are shown in figure 2.10. Figure 2.10(a) depicts samples with a fixed number of SL pairs, where the InAs thickness was kept constant at 2.5Å(0.8 ML) and the GaAs thickness was varied, causing the change of average In composition. The sample with 5×(2.5Å InAs/6Å GaAs), yelding in average 4.25 nm $In_{0.29}Ga_{0.71}As$, looks like a QW. The FWHM is 27 meV. If the In composition reaches 38% (5×(2.5Å InAs/4Å GaAs)), a long wavelength luminescence from QDs appears besides the luminescence from a QW. According to the PL intensity the QD density however is relative small. If the In composition increases once more, 41% (5×(2.5Å InAs/3.5Å GaAs)), the luminescence strongly drops, possibly caused by dislocation appearance.

The sample with 5×(2.5Å InAs/4Å GaAs) has a very good luminescence perfor-

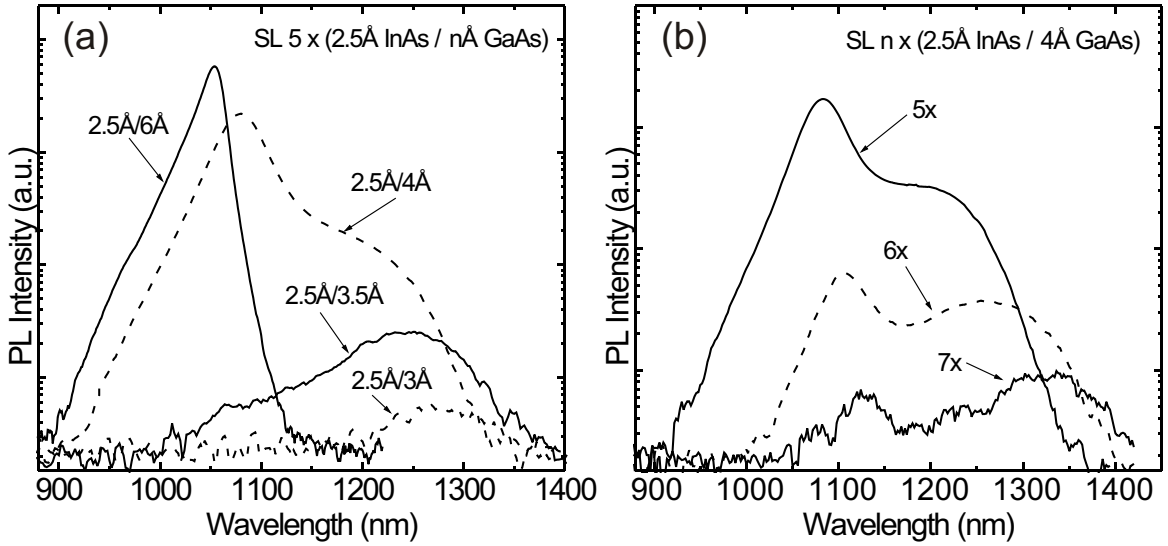

Figure 2.10: PL spectra of submonolayer InGaAs QDs. The QDs were grown as InAs/GaAs superlattice at 500℃. (a) SL with 5 periods of InAs/GaAs where the InAs thickness is 2.5Å, the GaAs thickness is varied, (b) SL with varied number of periods consisting of 2.5Å InAs/4Å GaAs.

mance, comparable with that of a QW and coherent QDs. We tried to increase the QD density by applying more stacking. The spectra are plotted in figure 2.10(b). The peak wavelength shifts towards 1.3 μm by increasing of the stacking number. It can be seen, however, that even a single additional InAs/GaAs layer causes a drastical reduction of the luminescence efficiency by more than one order of magnitude.

It should be mentioned that we found the growth of submonolayer QDs very sensitive to growth rate variations from run to run, making the reproducibility difficult. For example the samples 5×(2.5Å InAs/4Å GaAs) depicted in figures 2.10(a) and 2.10(b) were grown using the same growth procedure with an interval of a few days. The luminescence intensity of QDs near 1.2 μm differ by a factor of 2, what is much larger than for standard grown QDs where the deviations are usually within a few percent.

2.3 Overgrowth of QDs by an InGaAs layer.

The QDs presented in the previous section have a luminescence between 1.1 and 1.2 μm, what is far away from the target wavelength 1.3 μm. Using special growth parameters it is possible to tune the wavelength up to 1.3 μm and even further [105], but the optical quality and surface density become low. There are no publications to our knowledge

about lasers produced using such QDs.

The easiest way to increase the luminescence wavelength of QDs is to overgrow them with an InGaAs layer [87]. Figure 2.11 shows room temperature spectra of $In_{0.65}Ga_{0.35}As$ and InAs QDs overgrown with a 5 nm thick $In_xGa_{1-x}As$ QW. The In composition in the QW was varied from 10% up to 30%. A red-shift of the luminescence can be seen. The spectra of $In_{0.65}Ga_{0.35}As$ do not change their form, but just move to longer wavelengths, while the InAs QDs demonstrate a strong transformation of spectra form.

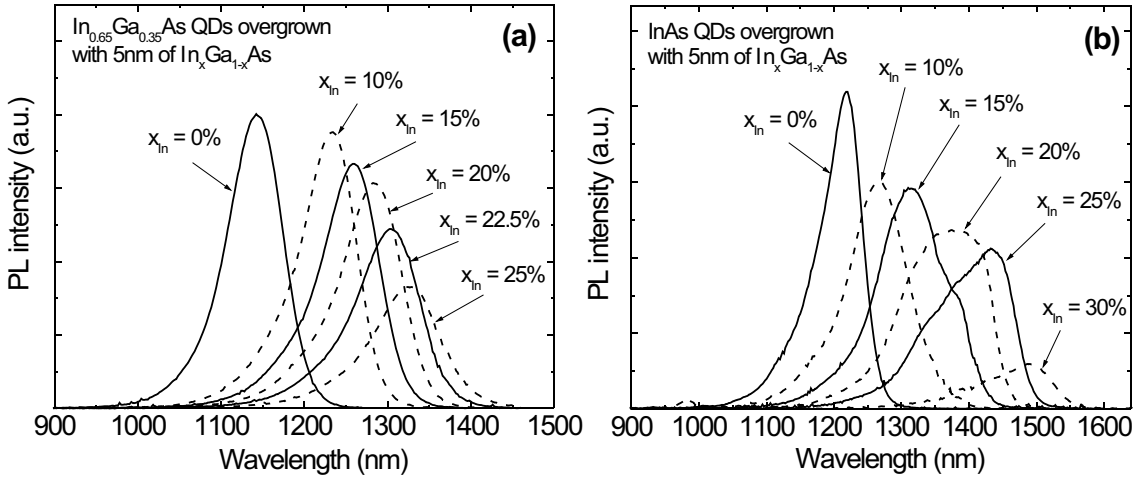

Figure 2.11: Room temperature PL spectra of (a) $In_{0.65}Ga_{0.35}As$ QDs and (b) InAs QDs, both overgrown with 5 nm of $In_xGa_{1-x}As$. The In composition of the QW is shown in the figure.

A summary the dependences of wavelength and integral PL intensity vs. In composition of the QW is plotted in figure 2.12. An obvious conclusion can be made using these data. The higher the In concentration in the QDs, the stronger the red-shift at a given QW composition. The reduction of luminescence is smaller for the InAs QDs. In order to explain these results processes occuring during overgrowth should be understood.

InGaAs QDs in GaAs matrix are compressively strained along all three axes, and have a lattice constant close to GaAs. A compressive strain is known to increase the band gap of semiconductors. Thus the band gap is larger than it would be without compression. An isomorphically grown InGaAs QW on a GaAs substrate is biaxially strained. This means that the lattice constant of the QW in the substrate plane is equal to that of the substrate, while in growth direction it is stretched. If we now overgrow the QDs with an InGaAs QW the strain along growth direction is reduced.

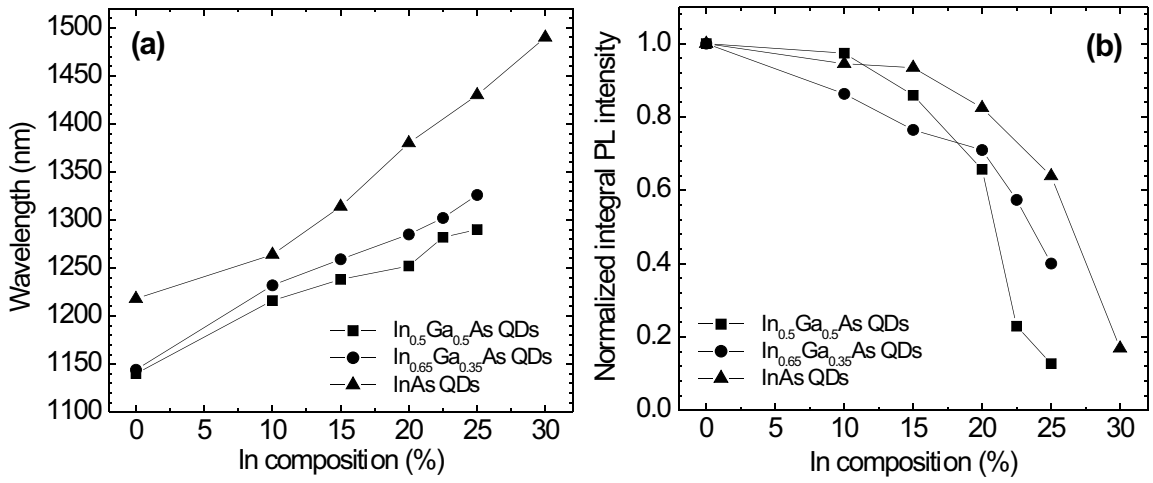

Figure 2.12: The dependence of (a) peak wavelength, and (b) integral PL intensity at room temperature of different $In_xGa_{1-x}As$ QDs overgrown with 5 nm of $In_xGa_{1-x}As$.

It provides a smaller band gap of the QD material and as a consequence a larger electron and hole localization in the QD [106]. The surrounding barrier height becomes also smaller, but according to simulations this contribution in total red-shift is smaller than from a reduction by hydrostatic strain. High resolution TEM investigations show that the lattice constant near the apex of the InAs QDs not caped with GaAs is close to the lattice constant of InAs [107]. The luminescence wavelength of uncapped QDs was found to be much longer than that of QDs caped with GaAs, despite the potential barrier between InAs and vacuum, which is much large than between InAs and GaAs [108].

The influence of strain and barrier height can be distinguished by substituting the matrix with a material having another band gap but the same lattice constant. We made this experiment by overgrowing QDs not with GaAs but with $In_{0.48}Ga_{0.52}P$. $In_{0.48}Ga_{0.52}P$ has the same lattice constant as GaAs, as verified using XRD, but the band gap is 1.92 eV at room temperature, being 0.5 eV larger than that of GaAs (1.42 eV). The spectra of $In_{0.5}Ga_{0.5}As$ QDs overgrown with GaAs and with $In_{0.48}Ga_{0.52}P$ are shown in figure 2.13. There is no wavelength difference between the emission of the two samples. On the other hand there are a lot of publications claiming a blue-shift of luminescence of InAs QDs grown in an AlGaAs matrix, which has a band gap also being larger than that of GaAs. However, it should be mentioned that the presence of phosphor or aluminium in a close vicinity of QDs could affect their growth.

Figure 2.14 shows the dependence of the luminescence wavelength of the QD ground

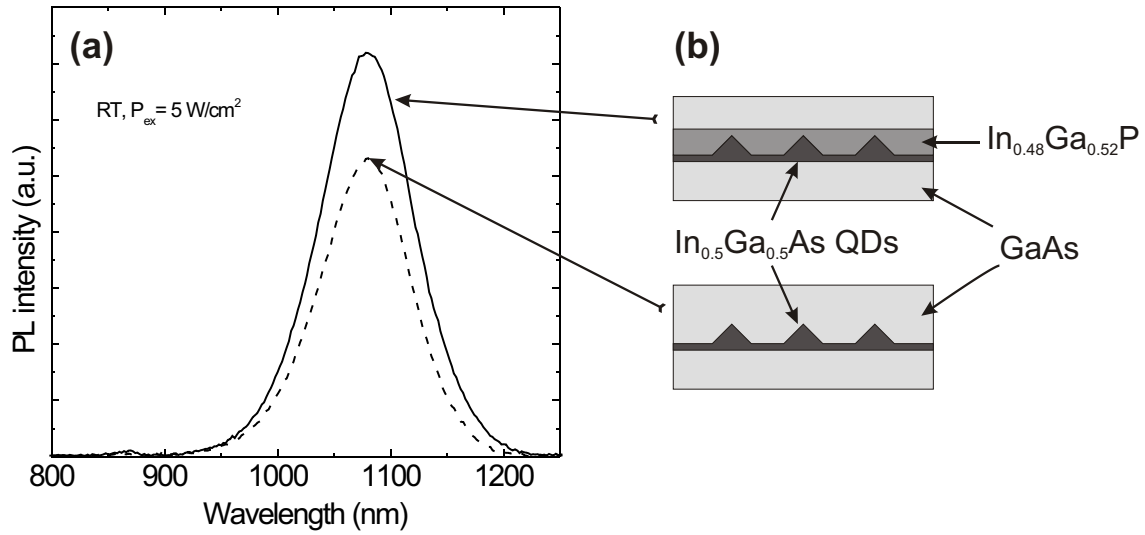

Figure 2.13: Room temperature PL spectra of $In_{0.5}Ga_{0.5}As$ QDs overgrown with either GaAs or with 45Å of $In_{0.48}Ga_{0.52}P$ (a). (b) - View of the samples. $In_{0.048}Ga_{0.52}P$ has the same lattice constant as GaAs.

state transition and the WL wavelength on the thickness of the QW. $In_{0.65}Ga_{0.35}As$ QDs were overgrown with an $In_{0.2}Ga_{0.8}As$ QW. The thickness of the QW was varied from 0 nm (overgrown with GaAs) up to 9 nm. The QW wavelength increases with increased thickness, whereas the QD wavelength reaches its maximum at a QW thickness of 6 nm and then remains constant. The height of the QDs according to TEM images is about 4 nm. This means that the wave function is fully localized into the QD, and the barriers, which are 1-2 nm from the QDs, do not influence the QD transition energy.

Reduction of strain is not the only one effect, taking place by overgrowth with InGaAs. The inhomogeneous stress originating from QDs induces a spinodal decomposition of the InGaAs QW, called activated alloy phase separation (AAPS) [27]. It is well known that some alloys tend to decompose into two or more phases, so called spinodal decomposition. A theory of spinodal decomposition was first developed for metal alloys and aftewards expanded onto semiconductor alloys. A thermodynamic theory assumes that the system is closed and do not exchange material with the environment. It was predicted a miscibility gap, a region of temperatures and compositions where the growth of homogeneous alloy is impossible. It is characterised by so-called "critical temperature" T_c, beyond which the decomposition is not observed. The critical temperature is

$$T_c = \frac{\Omega}{2k_B} - \frac{B_0}{4k_B} = T_c^0 - \frac{B_0}{4k_B} \tag{2.1}$$

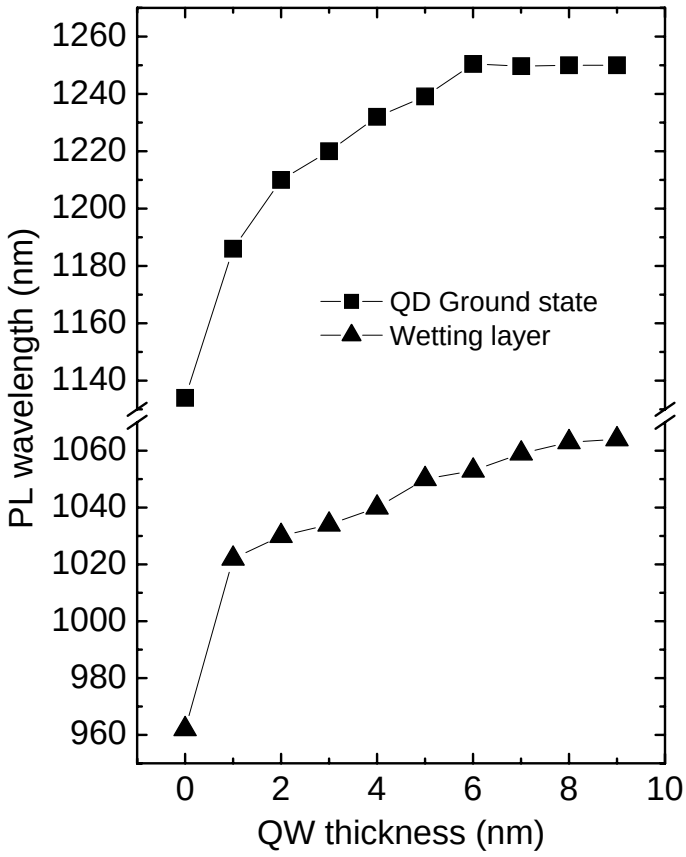

Figure 2.14: Dependence of the emission wavelength at RT of QD's ground state and WL vs. the thickness of QW. The QDs are $In_{0.65}Ga_{0.35}As$ overgrown with the $In_{0.2}Ga_{0.8}As$ QW.

where Ω is the interaction parameter of alloy formation, B_0 is the elastic energy arising due to the difference of lattice constants of alloy components, k_B is Boltzmann constant. It can be seen that the strain stabilises the alloy and prevents the decomposition. T_c was predicted to be negative for many ternary and quaternary V/III alloys. However thermodynamic equilibrium assumes the absence of material exchange, what can be realised practically by annealing the sample or strongly reducing the growth rate, so that the system is in quasi-equilibrium. It was developed a kinetic theory of spinodal decomposition assuming a steady arrival of the material on the surface [11, page 296]. It was found that in this case the strain favours the decomposition. The critical temperature in this case is

$$T_c^{kin} = T_c^0 + \frac{c_{12}}{c_{11} + c_{12}} \frac{B_0}{4k_B} \tag{2.2}$$

where c_{11} and c_{12} are the elastic modules. The schematic image of spinodal decomposition during growth is shown in figure 2.15(a). A small fluctuation of alloy composition causes domains with different local lattice constants, so the incorporation of the atoms with larger size is preferable in the domains with larger lattice constants and vice versa. In that way the domains with different compositions grow further.

The schematic image of AAPS on QDs is shown in figure 2.15(b). During overgrowth of QDs with InGaAs (fig.2.15(b), step 2), indium atoms preferably migrate towards the QDs and incorporate in the vicinity of QDs, since the lattice constant near the apex of QDs is larger than that of WL. Therefore the incorporation of large In atoms is energetically favourable. Hence In reach regions near the QDs are formed and the effective dimensions of the QDs increase (fig.2.15(b), step 3). Using high resolution TEM the spinodal decomposition during QD overgrowth was experimentally observed [27]. The dimensions of QDs overgrown with InGaAs was found to be larger than of QDs overgrown with GaAs.

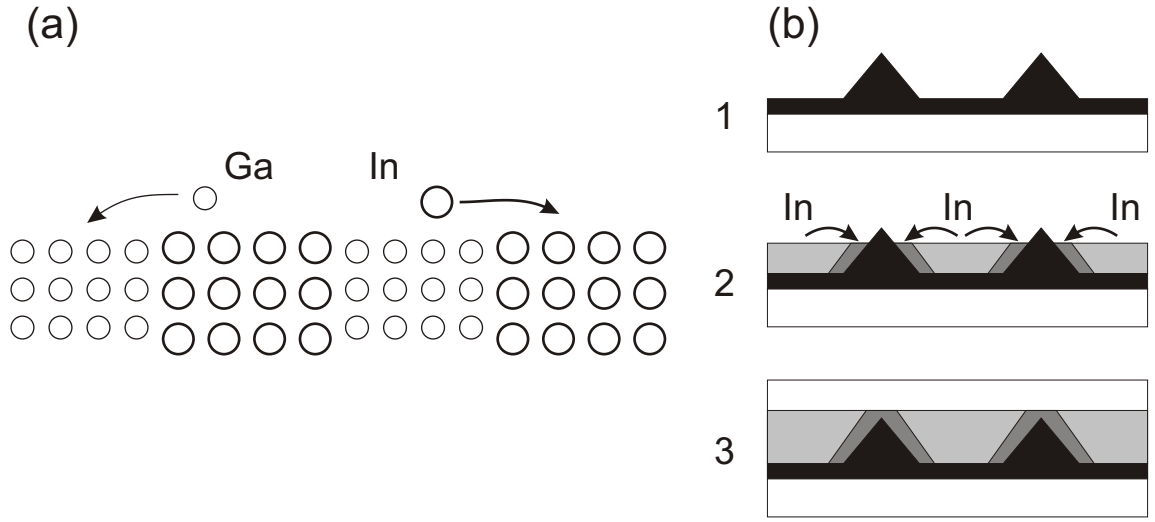

Figure 2.15: (a) Scheme of spinodal decomposition of InGaAs during growth caused by fluctuation of the composition. (b) Activated alloy phase separation of an InGaAs layer on InGaAs QDs. InGaAs QDs (1) favour the migration of In atoms towards the QDs and incorporation in their vicinity (2). Indium-rich regions appears around the QDs (3).

We do not make an investigation of overgrown QDs using high resolution TEM, but an evidence of AAPS in our case can be obtained comparing the evolution of the emission wavelength of QDs with simulations. The simulations were made by A. Schliwa. The 8 band $k \cdot p$ method was used, the details of calculations can be found

in [29, 30]. InAs QDs with a shape of a truncated pyramid were taken. The base length is 19 nm, the height is 3.4 nm, the side facets are (111) surfaces. The QDs were overgrown with 4.3 nm of $In_xGa_{1-x}As$, where x was varied from 0 up to 0.4. The 8 band $k \cdot p$ method provides a very good agreement with experiments if right data about the dimension and composition are supplied for simulation. The simulated and experimental data are plotted in figure 2.16. Experimental points are measured at 10 K from InAs QDs depicted in figures 2.11 and 2.12. The QDs are overgrown with 5 nm of $In_xGa_{1-x}As$, which is a little thicker than simulated, but the difference must by minor, cf. fig 2.14. The dimension of the real QDs overgrown with GaAs is 14 × 3 nm. It can be seen that at small In composition x the wavelength of real QDs is much shorter than simulated, what is due to smaller sizes. The increase of wavelength with growing x, however, is much stronger. This can be explained by an increase of the size due to spinodal decomposition of the InGaAs QW.

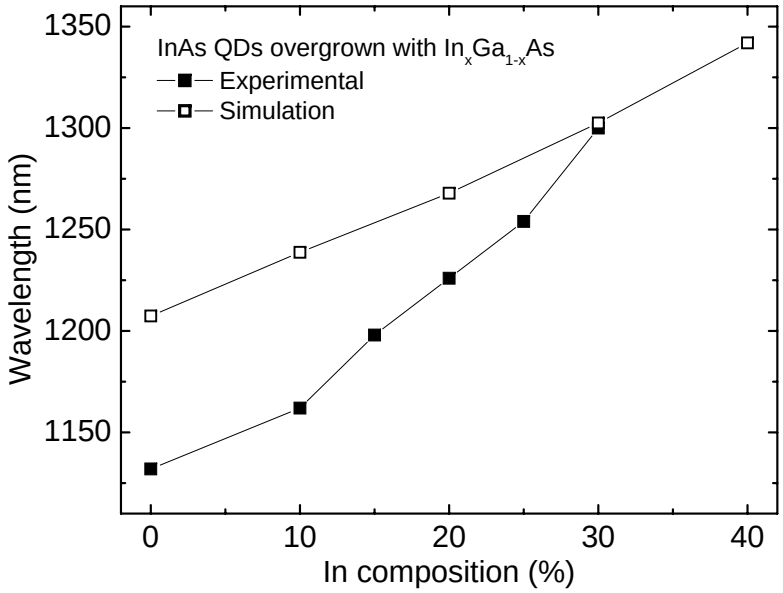

Figure 2.16: Comparison of the ground state transition wavelength of InAs QDs overgrown with InGaAs obtained experimentally and by simulation. Solid squares - InAs QDs deposited at 500℃ overgrown with 5 nm of $In_xGa_{1-x}As$. The PL was measured at 10 K. Open squares - simulation using 8 band $k \cdot p$ method. The QDs are InAs having the shape of a truncated pyramid with dimensions 19×3.4 nm (base length×height). The QDs are covered with 4.3 nm of $In_xGa_{1-x}As$. Material parameters correspond to 0 K.

A strong spectra transformation of the InAs QDs overgrown with an InGaAs QW

depicted in figure 2.11 may be also explained from the position of the AAPS. As discussed earlier the InAs QDs have a bimodal size distribution. The QDs of the two groups have a little different size and shape. During overgrowth they act as centres for decomposition of the InGaAs alloy. Since the size is different it influences the decomposition efficiency, for example QDs with a larger aspect ratio grow more quickly. It can be seen that between an In concentration of 15% and 25% the shoulder in the spectra shifts from the long wavelength side to the short wavelength side.

It was reported for MBE-grown QDs that use of InAlGaAs instead of InGaAs for QD overgrowth additionally increases the QD size and the splitting [18, 109] between energy sublayers within single QD. A large splitting is very important for temperature stability of lasers based on QDs. Due to the high reactivity of Al strong requirements for low contamination levels are necessary. In case of MBE very high vacuum with low concentration of water vapour and oxygen is required. In case of MOCVD high purity precursors as well as a high growth temperature are required in order to achieve low oxygen contamination. The growth temperature is usually near 600-700℃, what is not suitable for QD growth. Our experiments show that the presence of even small amounts of Al in the vicinity of QDs drastically reduces the luminescence efficiency. The same observation was made by Park et al. [110] who grew the QDs on AlAs and did not observe any luminescence. A thin insertion of GaAs between AlAs and QDs improves the luminescence, which was still much weaker in comparison with the QDs without Al.

The samples described earlier were grown with constant In composition in the QW. The most published QDs were grown in the same manner. The In composition, however, could be changed giving an additional parameter. We compare the growth methods with constant In concentration and with linearly varied. $In_{0.65}Ga_{0.35}As$ QDs were covered with either 4 nm $In_{0.19}Ga_{0.81}As$ (sample 2) or with a QW of the same thickness where the In composition linearly drops from 37% to 1%, giving an average value of 19% (sample 3). The total amount of indium in both structures is the same. Cross-section TEM images and room temperature PL spectra are shown in figure 2.17. The luminescence wavelength of the sample with graded In composition (1310 nm) is also much larger in comparison to the sample with constant In contents (1220 nm). The dimensions of the QDs in the sample 3 are obviously larger than in sample 2. Plan-view TEM images (not shown here) provide within a statistical error the same QD density of 2×10^{10} cm^{-2}. Thus the increase of QD size was induced by In migration from the InGaAs QW. The spinodal decomposition is more preferable for the alloy with a composition close to 50%.

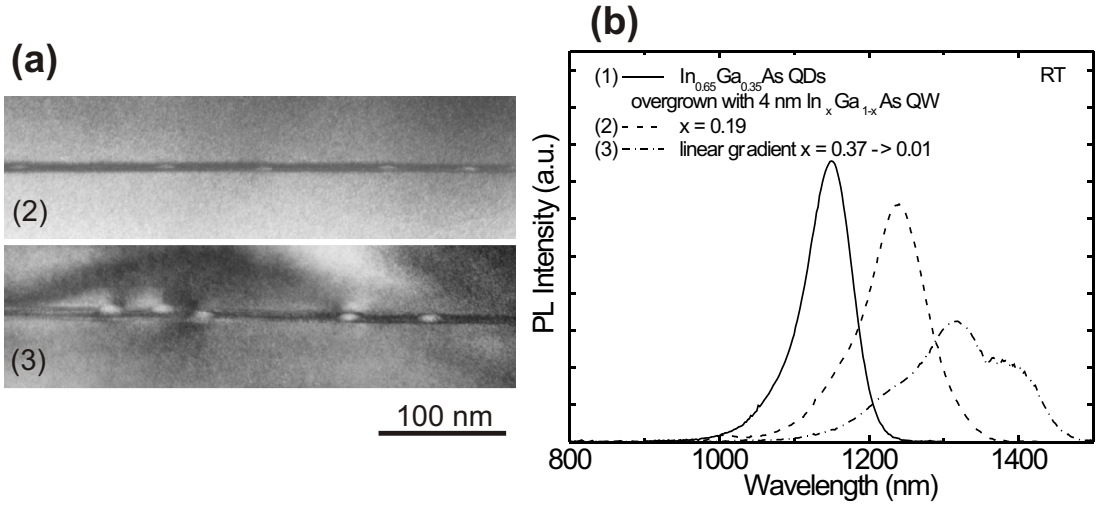

Figure 2.17: Cross-section TEM image (a) and room temperature PL (b) of $In_{0.65}Ga_{0.35}As$ QDs. Sample (1) is the reference QDs capped with GaAs. Samples (2) and (3) contain identical QDs as (1) overgrown with InGaAs. In sample (2) the InGaAs QW is 4 nm thick and the In composition is 19%. In sample (3) the thickness of the QW is also 4 nm, but the In composition is linearly reduced from 37% to 1% so that the average In concentration is the same as in the sample (2).

2.3.1 QDs overgrown by a short period InAs/GaAs superlattice

The QDs can be overgrown not only by a ternary InGaAs layer, but also by a short period submonolayer InAs/GaAs superlattice, fig. 2.18(b). The similar SL was used to form QDs and described in section 2.2.1. The inhomogeneous strain field originating from already formed QDs affects the growth of the SL. InAs and GaAs are deposited separately, so In atoms have more possibilities to diffuse on the surface since the bond energy of In-In is less than that of In-Ga. It is supposed that the In would collect near existing QDs and form the second layer of QDs.

Figure 2.18(a) depicts the room temperature PL spectra of $In_{0.65}Ga_{0.35}As$ QDs overgrown by a SL with 4 periods of 2Å InAs/8Å GaAs and by 4 nm thick ternary $In_{0.2}Ga_{0.8}As$ alloy. The average In composition and thickness of the SL and InGaAs layer are the same. The luminescence wavelength of both samples is the same, however the spectra halfwidth of QDs overgrown by a SL is smaller than of QDs overgrown by an InGaAs layer: 63 meV against 80 meV.

By growth of QDs using a SL the transition from 2D to 3D growth takes place when

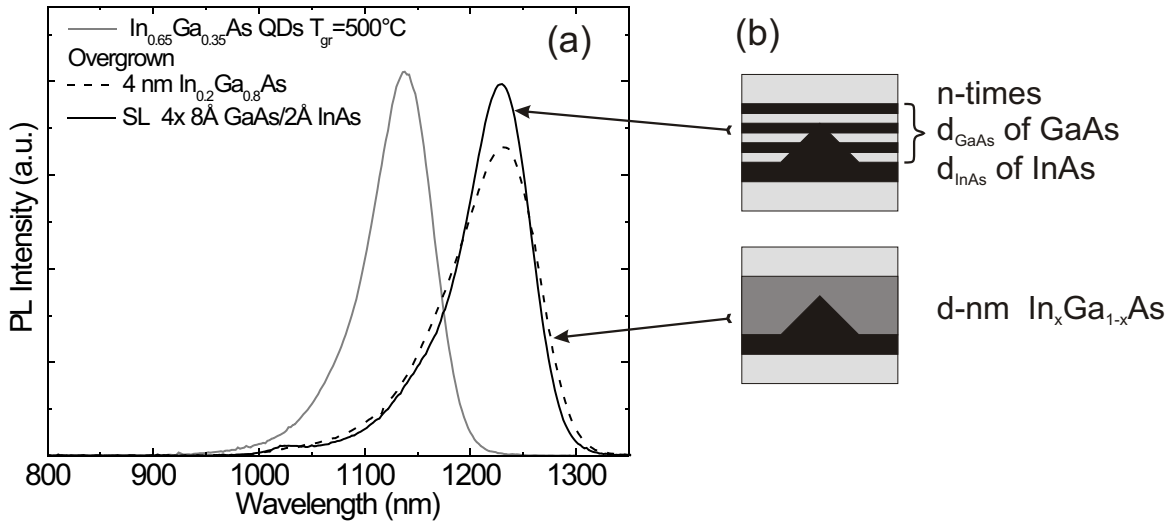

Figure 2.18: (a) Room temperature PL spectra of $In_{0.65}Ga_{0.35}As$ QDs deposited at 500℃ and overgrown by either 4 nm of $In_{0.2}Ga_{0.8}As$ or an InAs/GaAs superlattice with 4 periods of 8Å GaAs/2Å InAs. (b) scetch showing the overgrowth with a short period SL and a ternary alloy.

the average In composition is about 38%, and the luminescence efficiency strongly reduces after QDs formation (see section 2.2.1). For overgrowth of the QDs the In composition was varied between 20% and 33% so that it is always undercritical. Figure 2.19 shows the PL spectra of $In_{0.65}Ga_{0.35}As$ QDs overgrown with different InAs/GaAs SLs. The SL composition and thickness were varied by changing either the InAs thickness fig.2.19(a), or the GaAs thickness fig.2.19(b). It can be seen that the luminescence efficiency strongly reduces with increase of the average In composition, indicating defect formation.

The emission wavelength of samples with different numbers of SL periods is depicted in figure 2.20. The luminescence peak shifts monotonically with increase of the number of SL pairs. It looks similar to the evolution of luminescence wavelength of QDs overgrown by an InGaAs layer with different thickness, cf. fig. 2.14. Comparing the emission wavelength of QDs overgrown with SL and ternary alloy, see figures 2.12 and 2.14, we can conclude that the SL acts similar to a ternary alloy. No additional alloy decomposition or QD formation is observed.

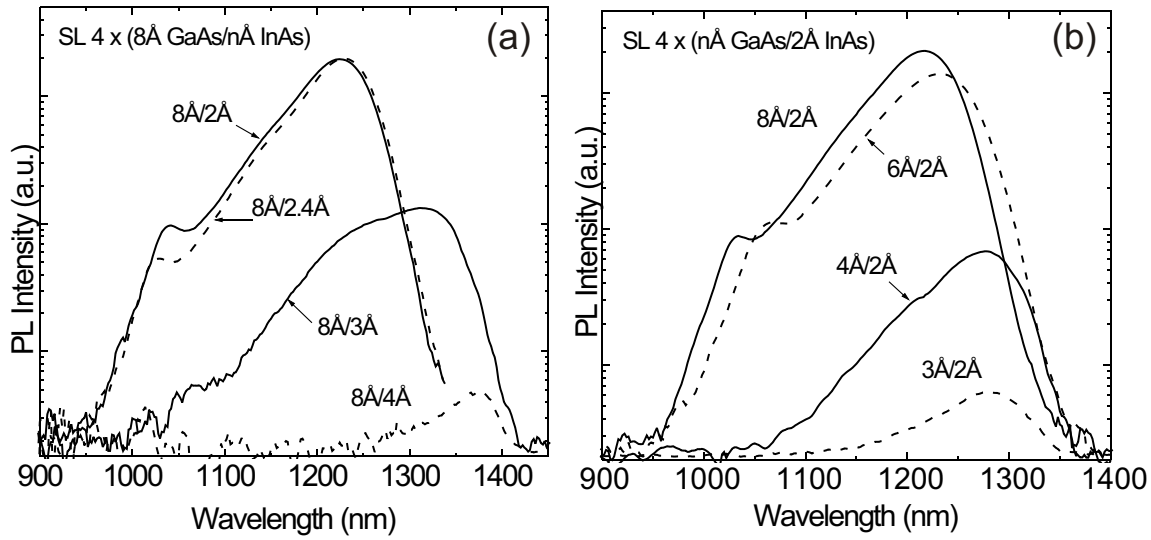

Figure 2.19: Room temperature PL spectra of $In_{0.65}Ga_{0.35}As$ QDs overgrown by an InAs/GaAs superlattice with 4 periods, the thickness of each GaAs and InAs layer is shown in the picture. (a) The GaAs thickness is fixed at 8Å and the InAs thickness is varied, (b) the InAs thickness is fixed at 2Å, the GaAs thickness is varied.

2.4 Defect reduction techniques

Long wavelength luminescence of QDs were demonstrated by many research groups, but only a few of them could demonstrate a laser operation near 1.3 μm. A defect-free active zone is necessary for laser realisation. During heteroepitaxy different kind of defects can appear in a structure. In order to improve the quality of the QD array a defect reduction should be applied.

Defect reduction is widely used for lasers based on QWs especially for long wavelength InGaAsN QWs as well as for InGaAs. Rapid thermal annealing (RTA) is usualy used. In this method, after finishing of growth, the sample is heated up to 700-800℃ for a relative short time of 0.5-1 minute. High temperature treatment increases the diffusion of defects and causes their annihilation. The luminescence efficiency of an InGaAsN QW may increase by 1-2 orders of magnitude as well as laser performance is improved [111, 112]. However this method can not be implemented for QD-based lasers. High temperature stimulates In-Ga intermixing, a strong blue-shift of emitting wavelength is observed if the temperature exceeds 600℃ [113]. Thus an annealing at low temperature ∼600℃ for a long duration, usually some minutes, was suggested. It was shown that such annealing procedures lead to the removal of plastically relaxed

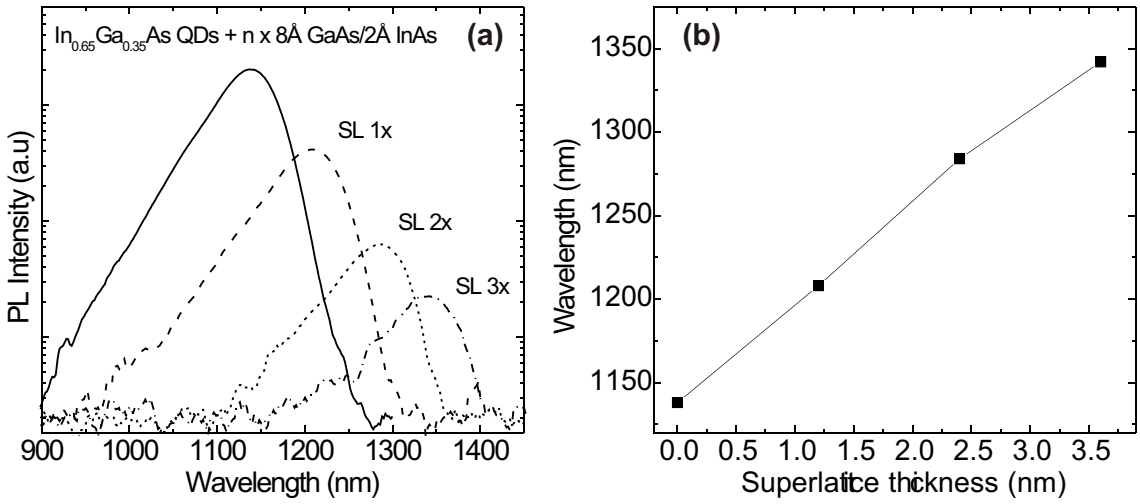

Figure 2.20: (a) Room temperature PL spectra of $In_{0.65}Ga_{0.35}As$ QDs overgrown by a 4Å InAs/8Å GaAs superlattice with a period number varied from 0 to 3. (b) Dependence of the peak wavelength on the SL period number.

defect clusters in both MBE [114] and MOCVD [115] but also to a reduction of point defects in cluster-free MOCVD-grown QD sheets [116].

The idea of a defect reduction method is shematicaly shown in figure 2.21. During conventional growth, described earlier, large dislocated clusters can form in the structure (Fig.2.21(a)). They disturb the optical quality of a QD array and act as non-radiative recombination centers. In order to eliminate them the growth procedure is changed. After QDs are deposited and overgrown with an InGaAs QW, a thin GaAs layer is deposited. The thickness of this GaAs cap is optimized in such a way that it covers coherent QDs but does not cover the dislocated QDs (Fig.2.21(b) step 1). Usually its thickness is about 2-4 nm. Then the growth is interrupted, and the temperature is increased (Fig.2.21(b) step 2). The temperature should be high enough to provide the evaporation of clusters but not too high, otherwise a strong intermixing takes place. In our case the optimal temperature for annealing was found to be 575-600℃. Afterwards the growth of GaAs continues (Fig.2.21(b) step 3). As a result the structure is free of clusters.

Figure 2.22 shows PL spectra of the $In_{0.65}Ga_{0.35}As$ QDs overgrown with a 5 nm thick $In_{0.2}Ga_{0.8}As$ QW and subjected to defect reduction. The spectra of the sample without annealing are shown as well. The overgrowth with a film leads to a decrease of the PL intensity, indicating the creation of non-radiative recombination centres. However, the PL intensity increases upon in-situ annealing and almost reaches the PL intensity of

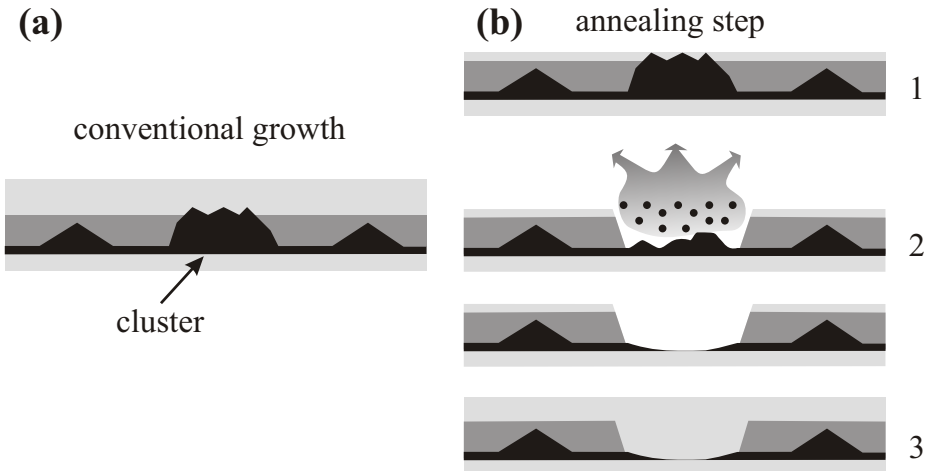

Figure 2.21: Schematic image of the defect reduction method. (a) conventional growth, (b) defect reduction using annealing of QDs under thin cap layer.

the reference sample without QW. The inhomogeneous broadening of the PL emission is reduced from 72 meV to 64 meV after annealing, indicating a slight narrowing of the QD size distribution. Due to in-situ annealing, the peak emission wavelength shifts by about 30 nm to the shorter wavelengths. This blue-shift is attributed to In-Ga intermixing, leading to changes in the electronic properties of the QDs [117]. The strength of intermixing during annealing is most likely due to the proximity of the QDs to the surface, which facilitates the In-Ga site exchange.

Large relaxed clusters are present in the sample without annealing and can be seen in plan-view TEM images shown in figure 2.23(a). White arrows mark the clusters. Their area density is estimated to be about 2×10^8 cm^{-2}. The sample grown with in-situ annealing does not exhibit such clusters. However, large crater-like objects are visible, as marked with arrows in figure 2.23(b). Within the limit of error, the area density of these objects is the same as the cluster density. The craters may be the traces of the evaporated clusters. This assumption is confirmed by the cross-sectional TEM image in Fig.2.23(c) which shows a lateral interruption of the In-containing layer whose width is in the same order as the lateral extension of the crater-like objects in Fig.2.23(b).

An efficient method to assess the luminescence efficiency of the samples is to compare the temperature dependence of the integral PL. The recombination current in photoexcited sample is equal to the generation rate of electron-hole pairs due to laser excitation,

$$J = An + Bn^2 + Cn^3 \tag{2.3}$$

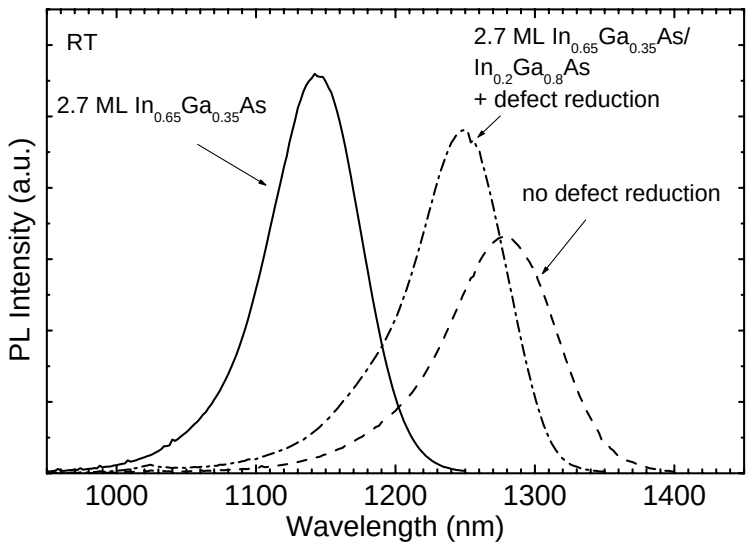

Figure 2.22: Room temperature PL of 2.7 ML $In_{0.65}Ga_{0.35}As$ QDs overgrown with 5 nm $In_{0.2}Ga_{0.8}As$ with and without in-situ annealing. As a reference the sample without QW is given.

where n is a carrier density, A is a coefficient of non-radiative recombination, B is a radiative recombination coefficient, C is the Auger recombination coefficient. The first term of equation (2.3) is non-radiative recombination, the second is radiative recombination, and the third is Auger recombination. Non-radiative recombination is proportional to the defect density and can be written as

$$A = \frac{N}{\tau_{def}} \tag{2.4}$$

where N is the defect density, τ_{def} is the recombination time constant. From this equation we conclude that the more QD layers we have the larger non-radiative recombination rates occur in the structure. The non-radiative recombination is strongly suppressed at low temperature, but increases with increase of the temperature. The largest contribution of non-radiative recombination in the total current is obtained when the carrier density is low, in case of PL this means a low excitation power.

Figure 2.24 shows the plot of integral PL intensity vs. temperature in the range from 10 to 480 K. The samples with a single layer and a triple stack of QDs without annealing are compared with a three-fold stacked sample with in-situ annealing. Three regions can be distinguished in this plot. From 10 K to 160 K the luminescence intensity is constant. The intensities of tree-fold stacked QD samples with and without annealing are equal and 2.5 times larger than that of the single layer. Thus we can conclude

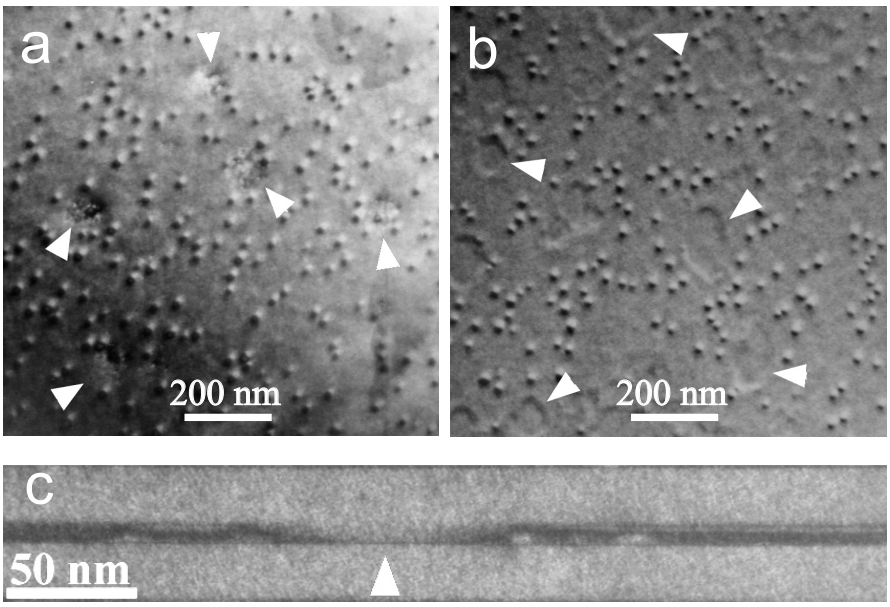

Figure 2.23: Plan-view TEM images of the sample with 2.7 ML $In_{0.65}Ga_{0.35}As$ QDs overgrown with 5 nm $In_{0.2}Ga_{0.8}As$ - (a). (b) - the same QDs subjected to in-situ annealing at 600℃. Each plan-view image displays an area of 1×1 μm^2. (c) Cross-section dark-field TEM image of the sample with annealing.

that a non-radiative recombination is fully suppressed below 160 K. In the region from 160 K up to 260 K the luminescence slightly reduces, but no difference can be seen. If the temperature, however, exceeds 260 K the luminescence rapidly drops with a specific slope for each sample. The luminescence of triply stacked sample reduces much more rapid than that of the single layer, since the number of defects is larger. However the sample with triply stacked QDs and in-situ annealing demonstrate the best performance with the smallest PL change between low and high temperatures. We can conclude that the defect density in the sample with three layers subjected to in-situ annealing is lower than in a single layer without annealing. Thus the PL provides an evidence of the positive impact of defect reduction on the optical properties of QDs. The defect reduction was found to be crucial for successful realisation of long wavelength lasers based on QDs, discussed in more detail in chapter 4.

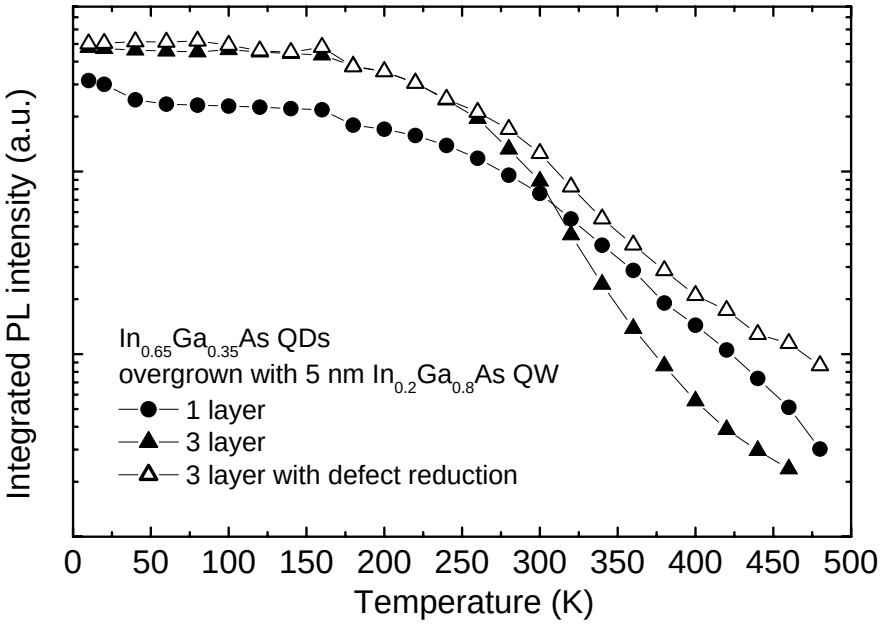

Figure 2.24: Dependence of the integral PL intensity of QDs vs. temperature. Compared single and triply stacked 2.7 ML $In_{0.65}Ga_{0.35}As$ QDs overgrown with 5 nm $In_{0.2}Ga_{0.8}As$ and triply stacked QDs subjected to in-situ annealing. The excitation density is 5 W/cm^2.

2.5 Growth of multiple stacked QDs

Growth of multiple stacked QDs is an important technique to modify the properties of QDs. As was mentioned above, that the modal gain of QDs is very low in comparison to a QW. Multiply stacked QDs have a larger overlap with the optical mode and a higher density of states, hence a larger optical gain could be obtained. The QDs in opposite to QWs provide an inhomogeneous strain field in the structure, what makes multiple stacking of QDs more complex to realise than multiple stacking of QWs.

Different scenarios of multiply stacked growth are shown in figure 2.25. Generally if the stacking period d is large the QDs of each layer grow independently and do not feel any influence from neighbouring stacks. In this case no correlation can be observed. The nucleation sites are randomly distributed in each layer. However, if the period becomes small, the nucleation is affected by the inhomogeneous strain field of the previous layer, and a correlated growth takes place. The QD distribution can be correlated in the vertical direction fig.2.25(b) when QDs of the upper layer nucleate exactly above QDs of underlying QDs or anticorrelated fig.2.25(c) when QDs nucleate between QDs. Theoretical work simulating the growth of closely stacked QDs predict

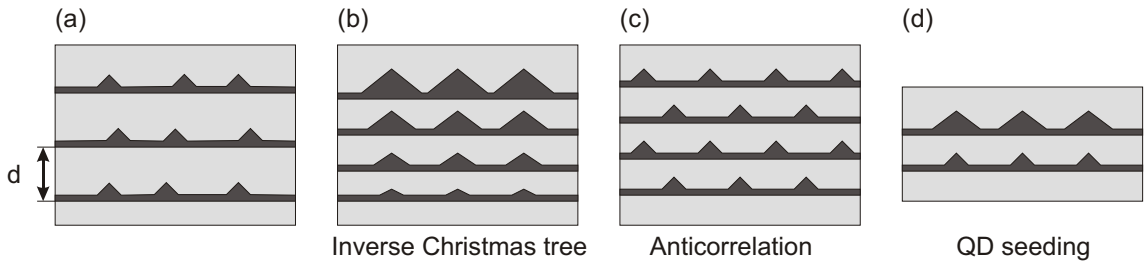

Figure 2.25: Different growth modes of stacked QDs. (a) - general scheme of stacking, d- stacking period, (b) - "Inverse Christmas tree" growth mode, (c) - Anticorrelation of QDs, (d) - QD seeding.

anticorrelation only if the anisotropy of the elastic modulus of the matrix is taken onto account.

It was predicted that the strain field of multiple stacking QDs improves the size distribution [118] in multiple stacked samples, since a material redistribution induced by the strain field occurs. However, a lot of experimental work with closely stacked QDs demonstrated a reduction of uniformity. The QD dimensions were not equal in different stacks. Usually it was observed, that the size of the QDs grows from layer to layer forming a so-called inverse Christmas tree [119, 120], fig. 2.25(b). This phenomenon was attributed to In segregation. Although the similar amount of InAs is deposited in each layer, segregating In increases the effective deposited thickness of InAs, causing the rise of QD size. Such structures often contain dislocations appearing in overdimensioned QDs.

Different authors reported different spacer thicknesses when correlated growth is observed. Xie et al. [121] observed full correlation if the spacer was thinner than 15 nm, and partly correlation until the thickness reaches 25 nm. On the other hand Heinrichsdorff [122] reported correlated growth only for spacer thinner than 10 nm.

Until recent times only correlated ordering was observed, it was explained by the fact that the anisotropy of the elastic modules in III-V semiconductors is relative small in compare to II-VI materials, where anticorrelation is often observed. Wang et al. [123] published results on experimentally observed anticorrelated growth of InGaAs/GaAs QDs. According to predictions the transition from correlation to anticorrelation happens when the spacer thickness was varied. At some spacer thickness clear anticorrelated growth was observed. The size distribution in this case was much better, no size increasing of QDs in upper layers was observed.

In order to achieve larger modal gain necessary for laser operation a multiple stack of QDs in the active zone is used. The modal gain is proportional to an overlap of

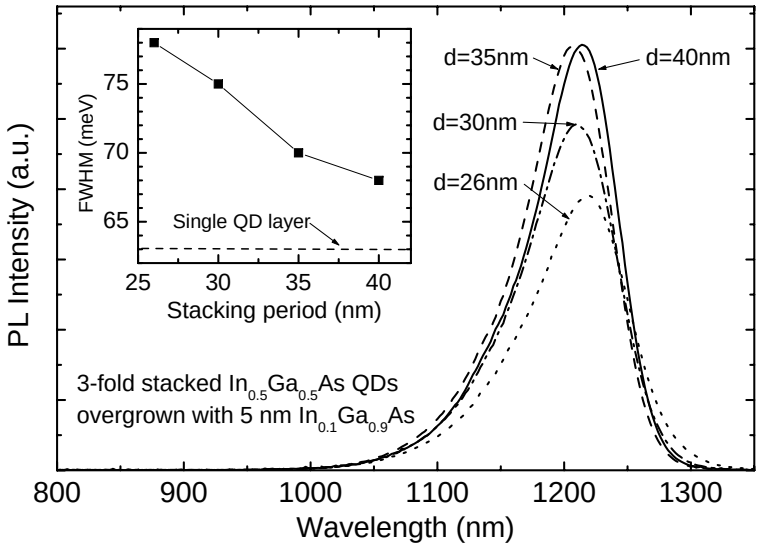

Figure 2.26: Room temperature PL of 3-fold stacked $In_{0.5}Ga_{0.5}As$ QDs overgrown with 5 nm of $In_{0.1}Ga_{0.9}As$. The stacking period is shown in the figure. The halfwidth of PL spectra is plotted in the inset.

the active volume with the optical mode. Thus the QD layer should be placed as close as possible to the wave maxima, usually in the middle of the waveguide. The QDs, however, could not be stacked arbitrarily close each to other due to reasons described earlier. It is desirable that QDs in each layer are uniform. Some authors reported a non-uniformity of multiply stacked QDs [62], the size and density varied between layers. Usually uniform QDs can be achieved if the spacer thickness is about 30-40 nm and more. Shchekin [124], however, claims that a spacer of 80 nm is needed in order to reach uniform growth.

According to our investigations the spacer thickness has to be at least 35-40 nm thick in order to avoid correlated growth. PL spectra of 3-fold stacked $In_{0.5}Ga_{0.5}As$ QDs with different spacers are plotted in figure 2.26. All three QD layers were grown identically. The QD material was deposited at 500℃, after growth interruption a GaAs spacer layer was grown. Its thickness was varied from 26 to 40 nm. The best luminescence efficiency is reached when the spacer thickness is 35 nm and more. Cross-section TEM images do not show any vertical correlation. The halfwidth of the PL spectra decreases with increase of the spacer thickness, showing that more uniform QDs grow, but even for 40 nm thick spacer layers it is still larger than that of a single layer.

In long wavelength lasers up to ten layers of QDs overgrown with InGaAs QWs were used. Additional compressive strain arising from the QWs requires the spacer layers

to be 40-45 nm thick in order to reduce the average strain. The in-situ annealing was found to have a positive impact on the multiple stacking of QDs. A cross-section TEM image of ten-fold stacked $In_{0.65}Ga_{0.35}As$ overgrown with 5 nm of $In_{0.2}Ga_{0.8}As$ QDs used in laser as active medium is shown in figure 2.27. The spacer thickness is 40 nm. The halfwidth is 70 meV what is a little more than 65 meV of a single layer.

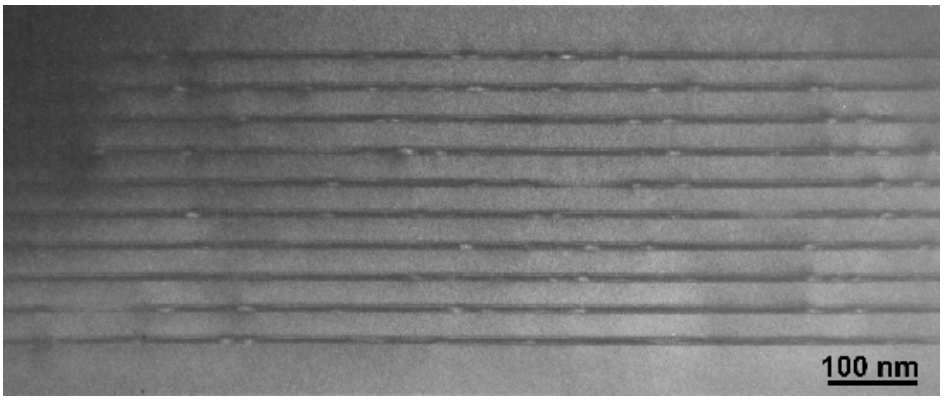

Figure 2.27: Cross-section TEM image of an active zone of a laser based on 10-fold stacked $In_{0.65}Ga_{0.35}As$ QDs overgrown with 5 nm $In_{0.2}Ga_{0.8}As$ and subjected to in-situ annealing.

2.5.1 Seeding of quantum dots

The correlated growth can be used to achieve some specific properties of QDs, since the QDs of the second layer could be much bigger than the QDs in the first layer having the same density, so-called seeding fig. 2.25(d).

Mukhametzhanov et al. [125] and Maximov et al. [126] suggested to use closely stacked QDs for an independent variation of QD properties such as dimension and density. In this method the elastic strain of the first QD layer defines the density of the second layer, which can be now varied to tune the size without changing the density. Mukhametzhanov used in the seed layer 1.74 ML InAs QDs with a density of about 3.7×10^{10} cm^{-2}, and in the second layer of QDs 3 ML InAs, grown on GaAs have a density of 9×10^{10} cm^{-2}, grown above seed layer they have the density 4.8×10^{10} cm^{-2} and larger size. Maximov et al. used InAlAs QDs with a huge density of 2×10^{11} cm^{-2}, which were overgrown with InGaAs QDs, having normally a density 5×10^{10} cm^{-2}. A laser realised using such QDs demonstrated improved performance and high modal gain [127].

It was shown in section 2.2 that long wavelength QDs, for example InAs QDs have a relative low density unsuitable for laser implementation, whereas a high density array

can be easily grown using InGaAs QDs, but the luminescence wavelength is about 1.1 μm, and can not be shifted much towards 1.3 μm. So a seeding becomes a very attractive opportunity to increase the density of long wavelength QDs, using short wavelength emitting QDs as a seed layer.

As a seed layer we used $In_{0.65}Ga_{0.35}As$ QDs on InGaAs template, the details of growth are described in section 2.6. The surface density is about 4×10^{10} cm^{-2}. The second layer was chosen to be $In_{0.65}Ga_{0.35}As$ QDs grown with a higher V/III=6 ratio and having a density of 10^{10} cm^{-2} without seed layer. The layers were separated by a 6 nm thick GaAs spacer. The deposition thickness of the second QD layer was varied from 1.9 ML (undercritical) to 2.51 ML. It was found that the critical layer thickness of the QDs in the second layer drops with a reduction of the spacer thickness. PL spectra and cross-section TEM of closely stacked QDs are shown in figure 2.28. The PL spectra show that the density of the QDs in the second layer saturates at a level close to though the QDs have without seeding layer (spectra are not shown). Further increase of deposition thickness causes luminescence degradation. The cross-section TEM images fig. 2.28(c) show that all QDs of the upper layer grow exactly above the QDs of the first layer, but their density is about 4 times smaller. Ovals in figure 2.28(c) depict double correlated QDs, whereas crosses depict the position where the QDs exist only in the first layer. Thus in our growth experiment seeding neither increased the density nor the size of the QDs in the second layer. The nucleation position is completely defined by the strain field of the first layer. The density and size, in opposite, are controlled by growth parameters. The additional strain from the seed layer gives only minor contributions to QD formation.

2.6 Growth of QDs using an InGaAs underlayer

Quantum dots with a high density are necessary for laser. There are a few methods how to increase the density of a QD array. On of them, namely the seeding described in the previous section did not provide any success at our growth conditions. An array of QDs with extremely high density up to 5×10^{11} cm^{-2} was demonstrated by growth directly on AlAs [110]. However the luminescence could not be measured due to high non-radiative recombination caused by AlAs. A thin insertion between AlAs and InAs QDs, and hydrogen passivation improve the luminescence [128], but it is still much less in comparison to the QDs grown on GaAs without Al. An efficient method to increase the QD density was found to grow the QDs on a thin InGaAs layer deposited on GaAs, what is schematically depicted in figure 2.29. The use of InGaAs templates

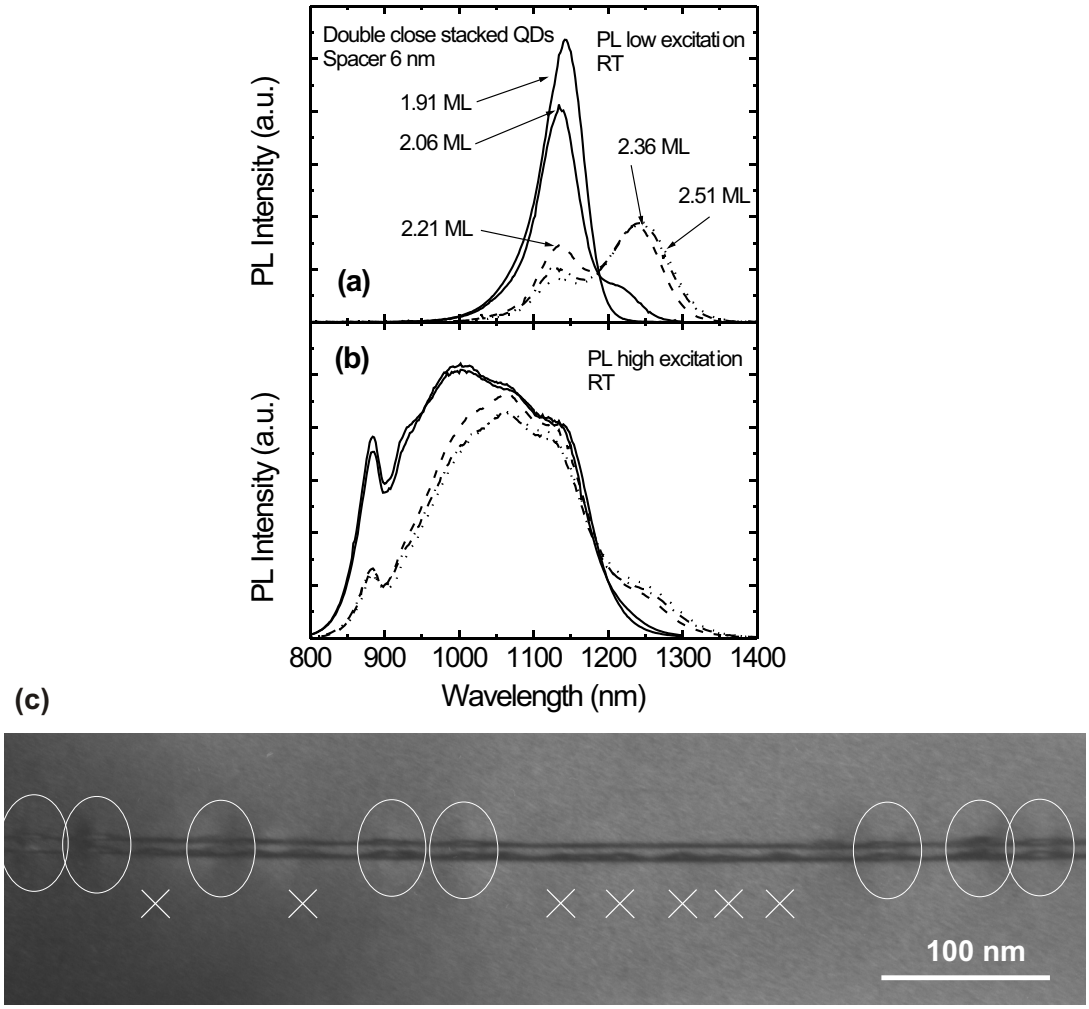

Figure 2.28: Double closely stacked $In_{0.65}Ga_{0.35}As$ QDs. The first layer QDs have a density of $4{\times}10^{10}$ cm^{-2} ($\lambda \approx$1140 nm), the deposition thickness of the second layer is shown in the image (a) ($\lambda \approx$1240 nm). Room temperature PL (a) - excitation density 5 W/cm^2, (b) 5000 W/cm^2, (c) - cross-section TEM.

instead of GaAs underneath the InGaAs QDs was reported for MBE and MOCVD structures to increase the QD area density by a factor of 2 to 4, depending on growth conditions [108, 129, 130]. We found an increase of QD density as well.

The InGaAs template is deposited prior to QDs using a second set of In and Ga sources. The growth rate of the InGaAs template was chosen to be close to the growth rate of the QDs and is 1.15Å/sec. There is no growth interruption between underlayer and QD material deposition. The partial pressure of TBAs during deposition of the underlayer is 0.9 Pa what is a little larger than for QDs, which is 0.6 Pa. A low

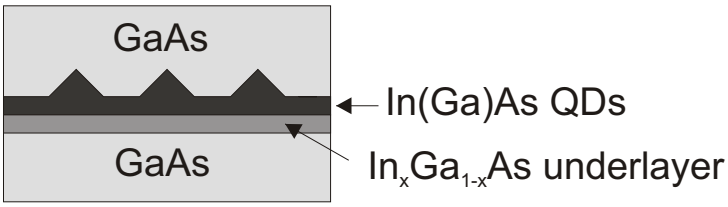

Figure 2.29: Scheme of InGaAs QDs grown on a thin InGaAs underlayer on GaAs substrate.

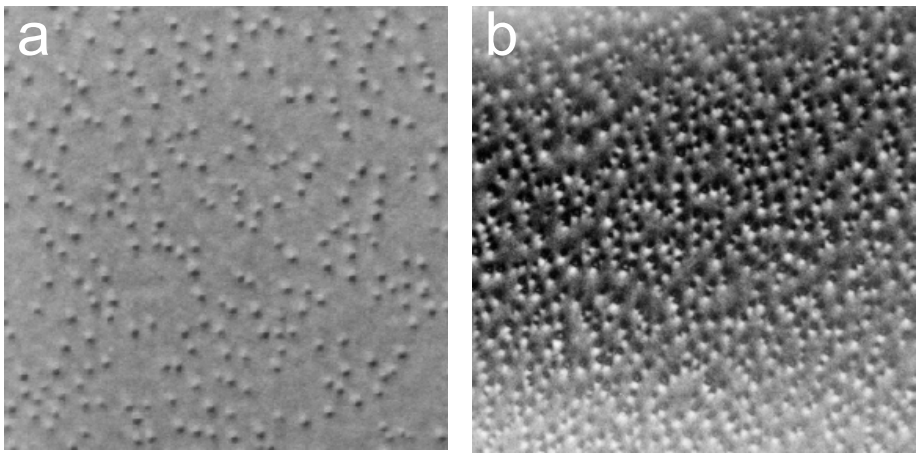

Figure 2.30: Plan view TEM images (1×1 μm^2) of $In_{0.65}Ga_{0.35}As$ QDs on GaAs (a) and on a 1 nm thick $In_{0.3}Ga_{0.7}As$ template (b).

partial pressure of the group V source during growth of the QW was found to cause a degradation of the optical quality. On the other hand larger As pressures which are used for growth of single QWs acts as increased V/III ratio during growth of QDs. The subsequent growth procedure is the same as for QDs on GaAs, namely one minute GRI is applied after the QDs are overgrown with either GaAs or InGaAs.

For our MOCVD samples we correspondingly find a larger density of QDs grown on InGaAs. Figure 2.30 shows TEM images of $In_{0.65}Ga_{0.35}As$ QDs deposited on either GaAs or on 1 nm $In_{0.3}Ga_{0.7}As$ templates, yielding densities of 1.8×10^{10} cm^{-2} and 6.8×10^{10} cm^{-2}, respectively. Based on PL data, the critical thickness for QD formation was found to be smaller on InGaAs templates with respect to deposition on GaAs. The general rule is: the thicker the InGaAs template or higher the In composition the smaller the critical thickness. A summary of QD densities achieved on different templates is collected in table 2.2.

Table 2.2: Density of InGaAs QDs (cm^{-2}) grown at 500℃ on GaAs and on different InGaAs underlayers. The deposition thickness of QD material is optimal.

QD composition	**Underlayers**		
	GaAs	**10Å $In_{0.15}Ga_{0.85}As$**	**10Å $In_{0.3}Ga_{0.7}As$**
$In_{0.65}Ga_{0.35}As$	$1.8{\cdot}10^{10}$	$2.9{\cdot}10^{10}$	$6.8{\cdot}10^{10}$
InAs	$6{\cdot}10^{9}$	$2.4{\cdot}10^{10}$	$4.6{\cdot}10^{10}$

The reduction of the critical layer thickness probably occurs because of In segregation above the InGaAs template. A floating layer of In forms on the top of the growing InGaAs layer, its thickness can reach some monolayers, making a significant contribution into QD formation [131]. The dependence of the critical layer thickness is ploted in figure 2.31. A rise of the In composition in the underlayer accompanied by a monotonic reduction of a critical thickness of QD formation. It becomes even less than one monolayer for InAs QDs on $In_{0.3}Ga_{0.7}As$

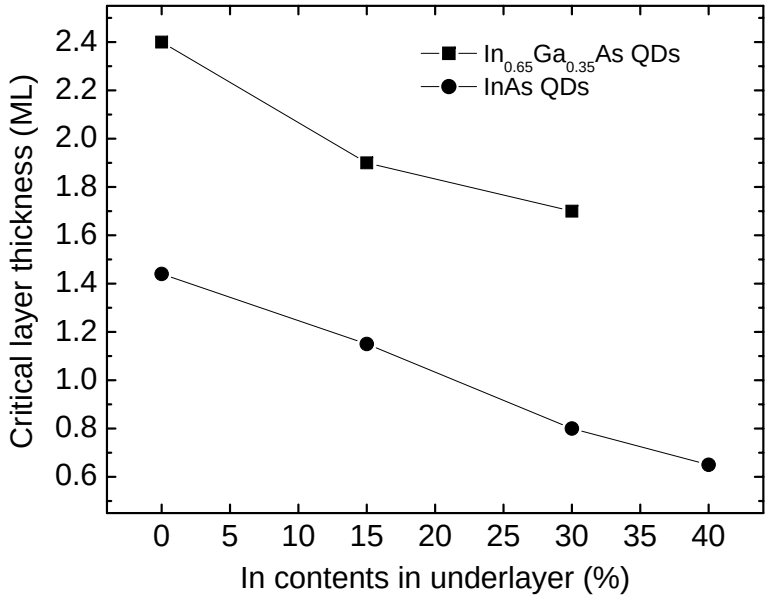

Figure 2.31: Dependence of the critical layer thickness of QD formation on the composition of the InGaAs underlayer. The QDs, namely InAs and $In_{0.65}Ga_{0.35}As$, are deposited either directly on GaAs or on a 10Å thick $In_xGa_{1-x}As$ underlayer. The growth temperature is 500℃, the V/III ratio is 1.5 for all QDs.

Photoluminescence spectra of $In_{0.65}Ga_{0.35}As$ QDs grown on either GaAs or InGaAs

are shown in figure 2.32. The peak emission wavelengths of both kinds of QDs are found to be quite similar, and occur at about 1140 nm. The concept of overgrowth by InGaAs was applied in order to increase the luminescence wavelength. Overgrowth by 5 nm $In_{0.2}Ga_{0.8}As$ leads to a red-shift, with a 50 nm smaller shift for QDs grown on InGaAs templates. The dependence of the peak wavelength on the composition of the cap InGaAs QW for QDs on GaAs and on InGaAs is depicted in figure 2.33. This distinct difference in emission properties is assigned to a smaller size of high density QDs grown on InGaAs with respect to those with a lower density grown on GaAs. It was reported that the height of QDs on InGaAs is smaller than on GaAs [108].

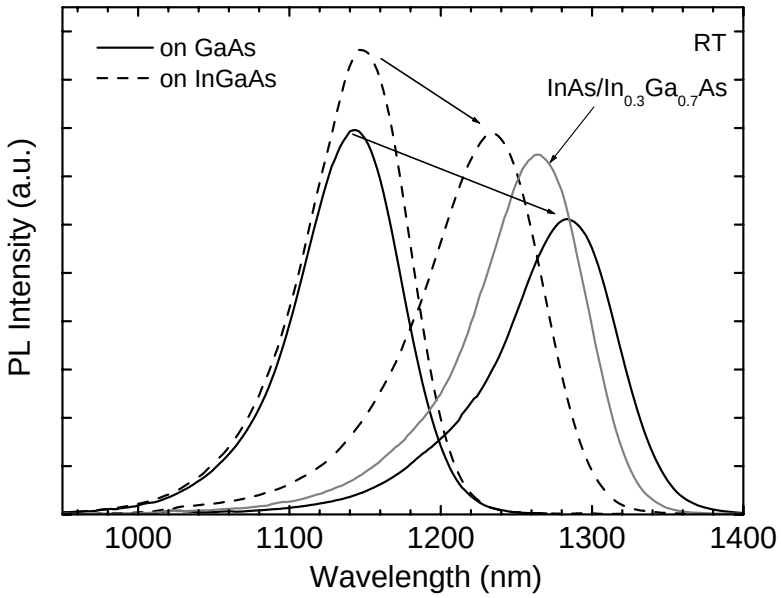

Figure 2.32: PL spectra of $In_{0.65}Ga_{0.35}As$ QDs on GaAs (solid line) and $In_{0.65}Ga_{0.35}As$ QDs on 1nm thick $In_{0.3}Ga_{0.7}As$ templates (dashed line). Arrows denote changes of the respective spectra after overgrowth with 5 nm $In_{0.2}Ga_{0.8}As$. The grey curve represents the PL of binary InAs QDs on 1 nm of $In_{0.3}Ga_{0.7}As$, overgrown with 5 nm $In_{0.2}Ga_{0.8}As$.

QDs grown on the InGaAs underlayer and overgrown with a InGaAs QW are often called dots-in-a-well (DWELL) in literature. These QDs were successfully implemented as active zone of a long wavelength laser. The good performance of lasers based on DWELL QDs was attributed to a larger density, however it was claimed that the composition of the underlayer and QW has a strong impact on the laser performance [132].

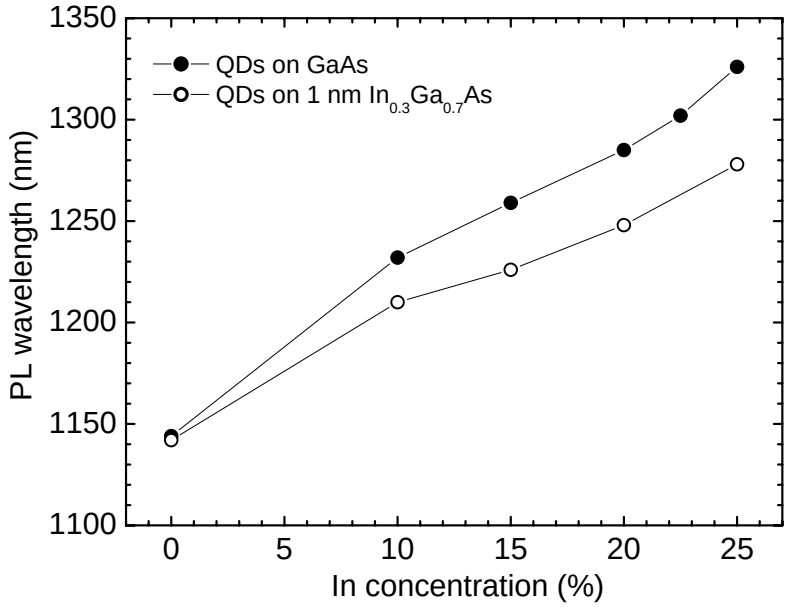

Figure 2.33: Dependence of peak wavelength of $In_{0.65}Ga_{0.35}As$ capped with 5 nm $In_xGa_{1-x}As$ on GaAs and on 1 nm $In_{0.3}Ga_{0.7}As$.

2.7 Growth of InGaAs QDs on an InGaP underlayer

Phosphorus-containing alloys are widely used for the production of optoelectronic devices. The band gap and lattice parameter can be tuned over a wide range. InP and GaAs, two mostly widespread substrates can be used. InGaAsP on GaAs substrates is usually used for red light lasers and light-emitting diodes. QDs grown in InGaP matrix on GaAs emitting in visible red and near infrared spectra region were demonstrated. It was found that thin InGaP layers deposited before QDs can be used to modify properties of long wavelength QDs on GaAs substrates. Long wavelength QDs on InGaP interlayer on GaAs substrate were mostly used for intersublevel photodetectors [133, 134], and a laser based on such QDs emitting near 1.3 μm was also demonstrated [135].

During this work a growth of InGaAs QDs on thin InGaP layer was investigated. The samples were grown using two different growth equipments. The first one is an AIX200/4 4" reactor and infrared heating. Only liquid precursors were used in this growth machine, namely TMGa, TMIn, TBAs and tertiarybutylphosphine (TBP). The second growth machine is an AIX200 2" reactor with radiofrequency heating. It is equipped with both types of group V precursors, liquid TBAs, TBP and gaseous hy-

drides arsine (AsH_3), and phosphine (PH_3). The group III precursors were the same in both reactors, TMGa and TMIn. The calibration of growth rates and surface temperature was performed using the same method, namely epitaxy of an InGaAs/GaAs SL and an Al eutectic. However the nominally identical QDs grown in different reactors do not have the same properties. The deposition thickness, temperature and V/III should be fine tuned for each reactor.

The layer structure is similar to the case of QDs grown on InGaAs interlayer, which is shown in figure 2.29, where an InGaP underlayer is grown instead of InGaAs. Before InGaP growth the group V source was switched from As to P and a phosphor preflow was applied for 2 seconds. Subsequently the In and Ga sources were opened for InGaP layer growth. Hereafter the group V source was switched from P to As for InGaAs QD growth. The growth rate of InGaP and InGaAs was kept as high as 1.15 Å/sec. The growth sequence of QDs is similar as was described earlier. A one-minute growth interruption was applied in order to allow for QD formation with all sources switched off. After the growth interruption the QDs were overgrown with GaAs; the first 5 nm were grown at the same temperature as the QDs, then the temperature was increased to 600℃ during growth of the remaining structure. We investigated the dependence of QD's properties on different growth parameters, such as deposition thickness, growth temperature and V/III ratio, which were varied in wide ranges.

The InGaP interlayer has a strong effect on QD formation. Figure 2.34 shows PL spectra of $In_{0.48}Ga_{0.52}As$ QDs deposited on 15Å of $In_{0.48}Ga_{0.52}P$ at 500℃. The critical layer thickness for QD formation is smaller [134] and the range of coherent QD growth is increased from 3.9 - 4.8 ML to 2 - 4.8 ML of deposition thickness, for growth on lattice-matched InGaP with respect to that on GaAs, respectively. The reduction of critical layer thickness possibly takes place due to In segregation during InGaP growth. A similar phenomenon was observed, when the QDs were deposited on an InGaAs layer. The dependence of the luminescence wavelength of QDs on deposition thickness is opposite to what was observed for QDs on GaAs. The peak wavelength rises with increase of deposition thickness similar reports on InAs QDs grown using MBE, see results presented in section 2.2 to compare.

The QDs grown at 500℃ on GaAs and on 15Å of lattice-matched InGaP have a close emission wavelength near 1.1 μm. However, the samples demonstrate noticeable differences in luminescence intensity. Figure 2.35 shows PL spectra at room temperature and at 10 K of 3.8 ML $In_{0.48}Ga_{0.52}As$ on 15Å of $In_{0.48}Ga_{0.52}P$ and 4.3 ML $In_{0.5}Ga_{0.5}As$ QDs on GaAs, both deposited at 500℃. The room temperature luminescence of QDs grown on InGaP interlayers is typically 3-10 times weaker than the luminescence of comparable QDs deposited on GaAs. However at 10 K the luminescence intensity of

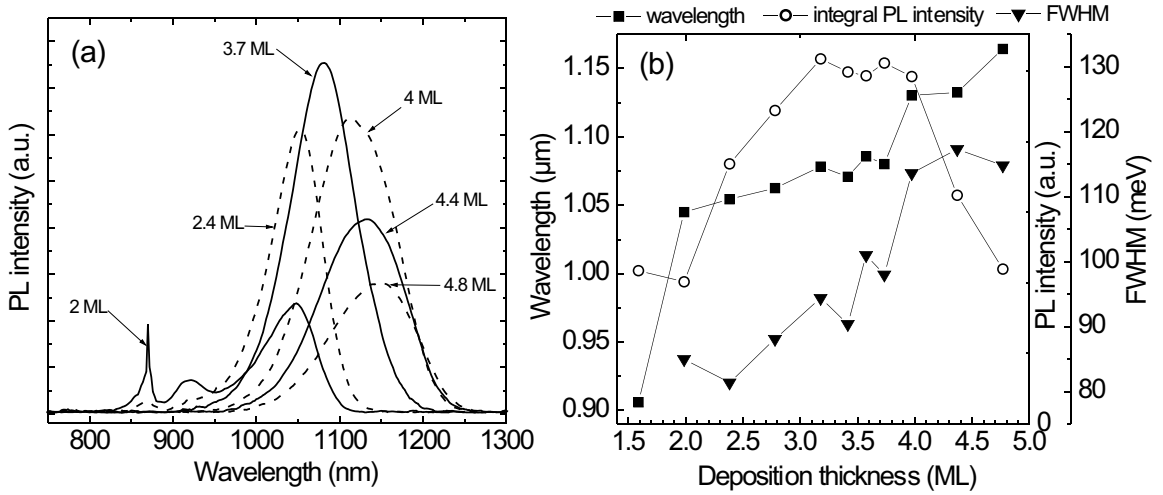

Figure 2.34: (a) Room temperature PL spectra of $In_{0.48}Ga_{0.52}As$ QDs deposited on 15Å of $In_{0.48}Ga_{0.52}P$ at 500℃. The deposition thickness is shown in the image. (b) Dependence of peak wavelength, integral PL intensity, and halfwidth of the spectra on deposition thickness of InGaAs.

both kinds of QDs is comparable, what can be an evidence of strong non-radiative recombination caused by phosphorus.

The emission wavelength of QDs can be easily tuned in a wide range by changing the InGaP layer composition. The wavelength grows with increasing In content in the InGaP layer and drops when the In contents becomes smaller, see fig. 2.36. The luminescence intensity was, however, found to decrease with compositions deviating from lattice-matching.

It was found that the QDs grown on InGaP layers have a bimodal size distribution with large differences in luminescence wavelengths. The small QDs emit near 1.1 μm, whereas the large QDs near 1.25 μm. The growth temperature and the thickness of the InGaP template are crucial for the size distribution. Figure 2.37(a) shows PL spectra of $In_{0.48}Ga_{0.52}As$ QDs deposited on a 15Å thick $In_{0.48}Ga_{0.52}P$ layer at different temperatures. It can be seen that small QDs are present only at low growth temperatures, at 520℃ and above only large QDs can be observed. A bimodal size distribution was often observed in the growth of In(Ga)As QDs using MOCVD [96, 120] but the difference between ground state transitions of different QDs did not exceed 50 meV in all reports known to us. We observe a difference as large as 150 up to 200 meV.

The thickness of The InGaP layer has also a huge impact on the size distribution. Figure 2.37(b) shows PL spectra of $In_{0.48}Ga_{0.52}As$ QDs grown on $In_{0.48}Ga_{0.52}P$ at 520℃.

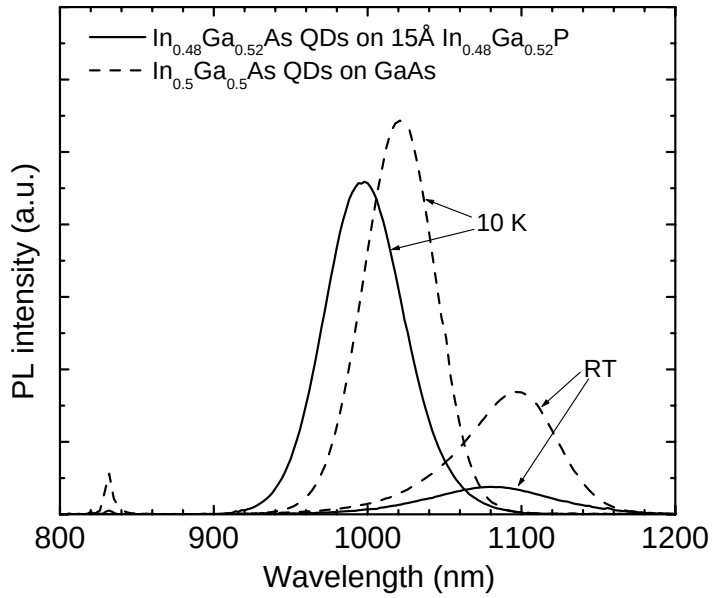

Figure 2.35: A comparison of PL spectra at room temperature and at 10 K of QDs grown on GaAs and on InGaP. Solid line - 3.8 ML $In_{0.48}Ga_{0.52}As$ QDs deposited on 15Å of $In_{0.48}Ga_{0.52}As$, dashed line - 4.3 ML $In_{0.5}Ga_{0.5}As$ QDs deposited on GaAs. The growth temperature is 500℃ in both cases.

The thickness of the InGaP layer was varied from 7.5Å up to 45Å. The large QDs are present only at moderate thicknesses, namely between 15 and 30 Å. If the thickness is out of this range, the small QDs dominate in the spectrum.

By growth of InGaAsP structures an exchange of As and P on the interfaces should be taken into account. Since both As and P have a high partial pressure at growth temperatures a relative easy substitution of one element with another can take place. For example if InP surface is exposured to AsH_3 an InAs layer is formed on the top due to As/P exchange. Since the partial pressure of phosphor is larger than that of arsenic at the same temperature the substitution of P with As is more favourable. Yoon et al. [136] observed strong As/P exchange during growth of InAs QDs on InP substrate, high V/III ratio and high temperature enhance this effect causing an increase of total QD volume by an increase of the AsH_3/III ratio.

In our case if As/P exchange occurs we must expect a significant change of QD properties, since the InGaP layer thickness would be thinner and the InGaAs thicker. Figure 2.38 shows PL spectra of QDs deposited with different AsH_3/III ratio. It can be seen that a large V/III ratio of 360 causes a reduction of the luminescence efficiency. Whereas the increase of V/III from 120 to 240 induces only a red-shift usual for increase

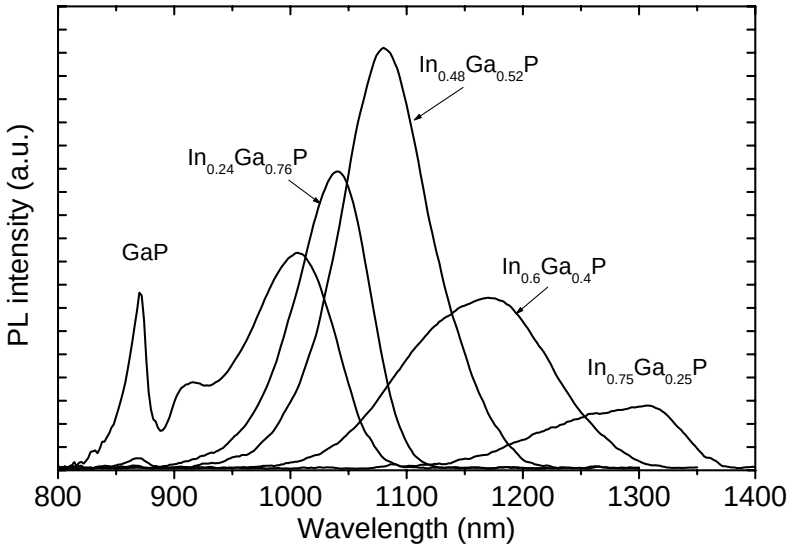

Figure 2.36: Room temperature PL of 3.8 ML $In_{0.48}Ga_{0.52}As$ QDs deposited on 15Å of $In_xGa_{1-x}P$ at 500℃. The composition of the InGaP layer is shown in the figure.

of V/III ratio.

A strong impact on QD properties has a growth interruption between the layers. During a growth of As/P interfaces a growth interruption is usually made in order to flush the precursors of the previous element. Thereby a layers with abrupt As-P transition can be grown. Our growth method described earlier contains a PH_3(TBAs) preflow before InGaP deposition. So InGaP layers should be grown without As contamination. Figure 2.39(a) shows a switching sequence of the sources during growth of QDs. Long wavelength $In_{0.48}Ga_{0.52}As$ QDs deposited at 520℃ on 15Å $In_{0.48}Ga_{0.52}P$ were taken and the growth interruption between InGaP and InGaAs layer implemented as well as the PH_3 preflow were varied. Figure 2.39(b) shows PL spectra of QDs with different preflow durations, namely 2 and 5 seconds. A strong wavelength shift is observed if the duration increased, possibly due to formation of a GaP layer which causes a blue-shift of luminescence wavelength, cf. fig. 2.36. On the other side the growth interruption between InGaP and InGaAs does not shift the luminescence wavelength, but affects the luminescence efficiency if it becomes equal to 10 seconds.

We also investigated the influence of different group V precursors on QD growth. The long wavelength InGaAs QDs grown on 15Å InGaP at 520℃ using AsH_3 and PH_3 were taken as starting point. Then arsine and phosphine were substituted by TBAs and TBP, respectively. Taking into account the higher decomposition efficiency

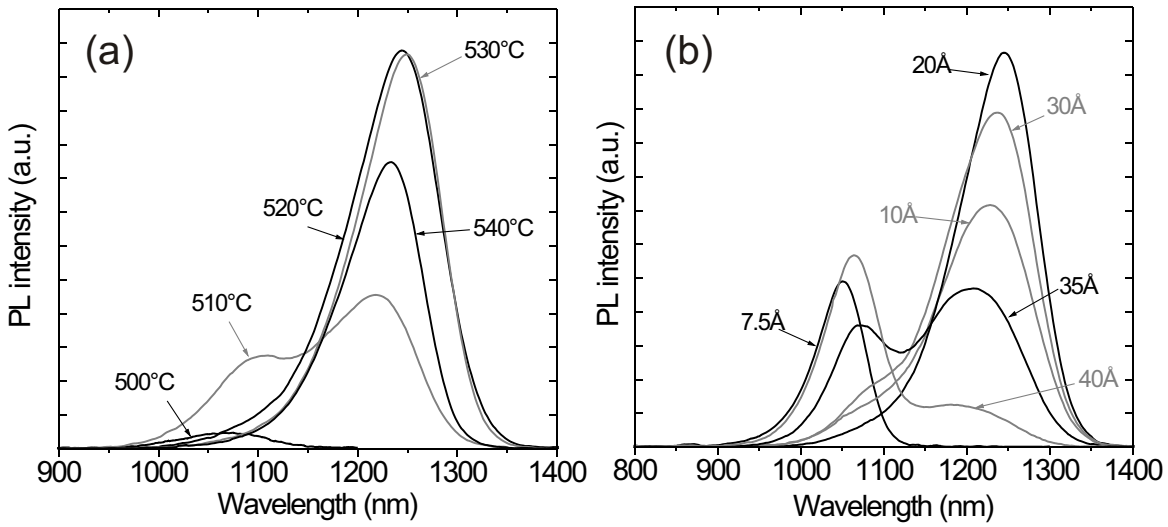

Figure 2.37: Room temperature PL of 3.6 ML $In_{0.48}Ga_{0.52}As$ QDs deposited (a) on 15Å of $In_{0.48}Ga_{0.52}P$ at different temperatures, (b) on $In_{0.48}Ga_{0.52}P$ with varied thickness at 520℃. The thickness of InGaP and growth temperature are shown in the image.

of tertiarybutyl-precursors in comparison with hydride-precursors, the V/III-ratio was adjusted in order to obtain a luminescence similar to that of the samples grown using hydrides. Figure 2.40 shows PL spectra of QDs grown with substitution of one precursor, either of AsH_3 to TBAs fig. 2.40(a) or PH_3 to TBP fig. 2.40(b).

The new optimal V/III ratio was found to be 50 for TBAs instead of 240 with AsH_3 and 2 for TBP instead of 300 with PH_3. The difference between TBP and PH_3 is much larger than between AsH_3 and TBAs, what possibly arises from the fact that phosphine is significantly more stable than arsine, thus at temperatures near 500℃ the decomposition percentage is smaller. In opposite the decomposition of TBAs and TBP is almost complete.

A summary of the samples grown using different combinations of precursors is shown in figure 2.41. It was found that the kind of precursors has a minor influence on the properties of QDs, but the emission wavelength is slightly longer if alternative precursors are used.

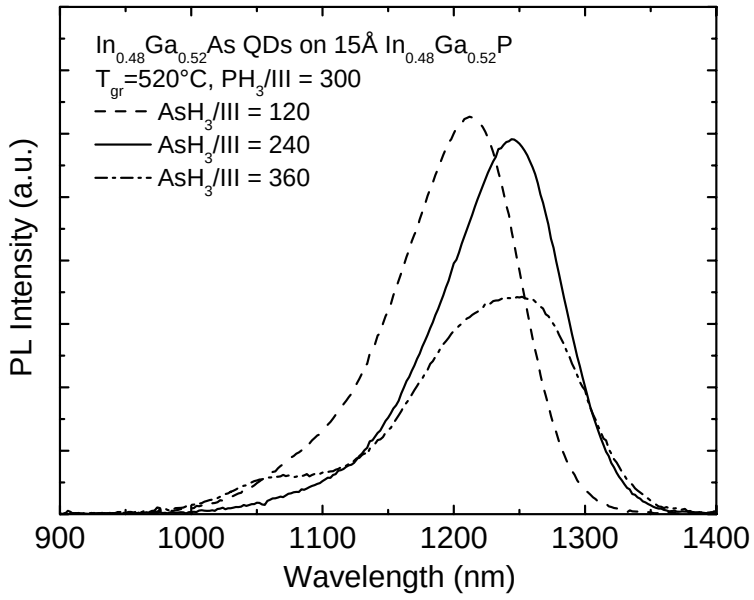

Figure 2.38: Room temperature PL spectra of 3.6 ML $In_{0.48}Ga_{0.52}As$ QDs deposited at 520℃ on 15Å $In_{0.48}Ga_{0.52}P$ with different AsH_3/III ratio.

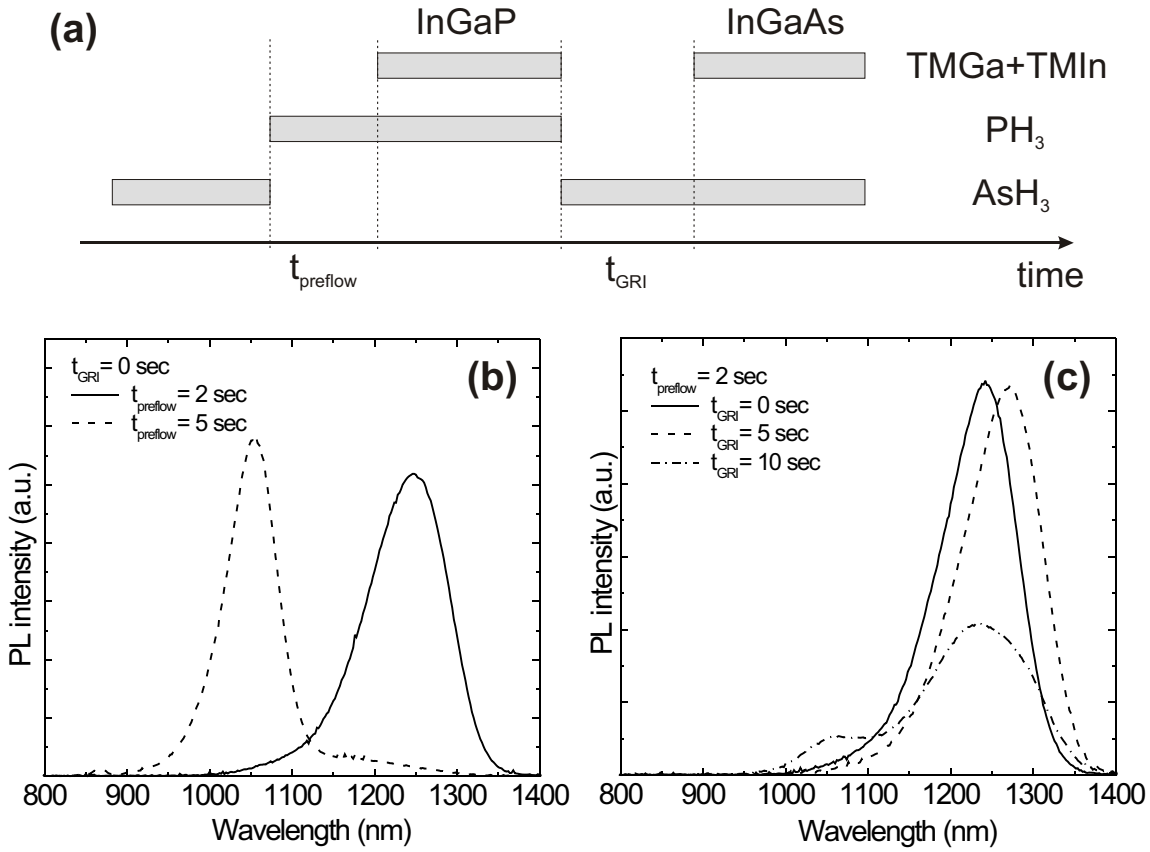

Figure 2.39: (a) Schematic switching sequence of sources used during growth of InGaAs QDs on InGaP interlayers. (b) and (c) room temperature PL spectra of 3.6 ML $In_{0.48}Ga_{0.52}As$ QDs deposited at 520℃ on 15Å $In_{0.48}Ga_{0.52}P$ with different combinations of $t_{preflow}$ and t_{GRI}. (b) t_{GRI}=0 sec, $t_{preflow}$ is varied (c) $t_{preflow}$=2 sec, t_{GRI} is varied.

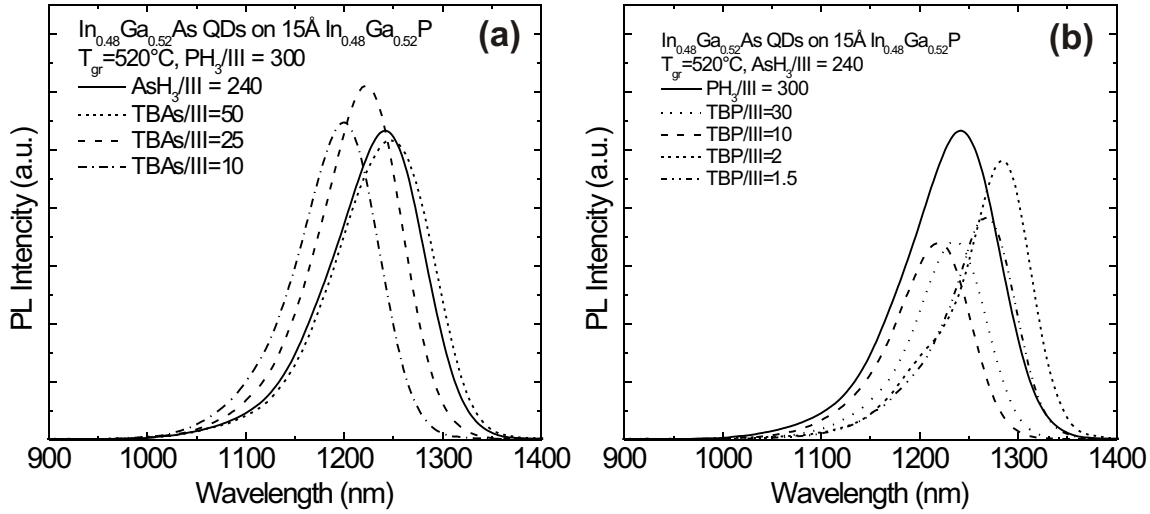

Figure 2.40: PL spectra of 3.6 ML $In_{0.48}Ga_{0.52}As$ QDs grown on 15Å $In_{0.48}Ga_{0.52}P$ at 520°C, using different group V precursors: (a) PH_3 and TBAs, (b) TBP and AsH_3.

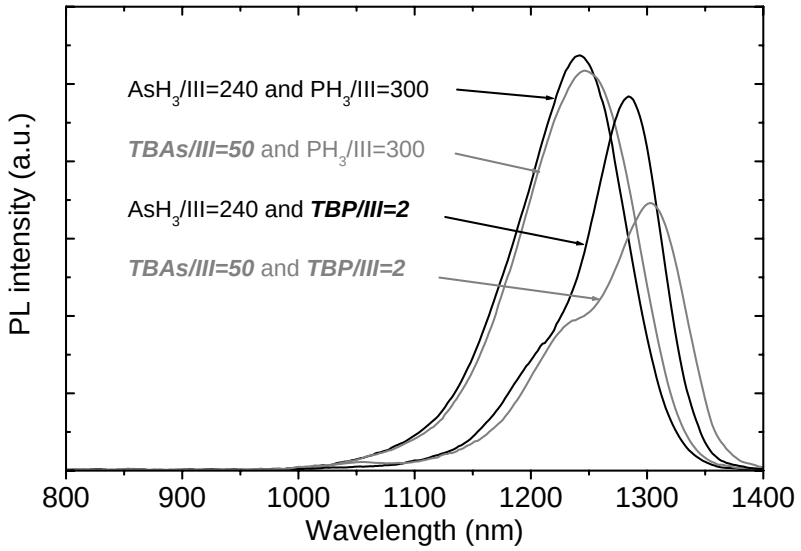

Figure 2.41: Comparison of 3.6 ML $In_{0.48}Ga_{0.52}As$ QDs grown on 15Å $In_{0.48}Ga_{0.52}P$ at 520°C , using different group V precursors.

Chapter 3

In-situ growth control using reflectometry and reflectance anisotropy spectroscopy

Control of growing layers during epitaxy is very important, because it allows a better understanding of the growth process and can help to improve device performance. MOCVD remains always behind MBE with regard to in-situ growth control. Since there is a high vacuum in a MBE growth chamber it was quite easy to implement a lot of test methods, such as optical reflectometry and ellipsometry, X-ray spectroscopy and electron diffractometry. The reflection of high energy electron diffraction (RHEED) is since many years a standard equipment of each MBE setup. It is used to control the reconstruction and morphology of surface during growth, and to estimate the growth rates. MOCVD during long time did not have a comparable useful control method. The gas atmosphere in the MOCVD reactor makes difficult to use anything except optical spectroscopy and reflectometry. In order to guide light to the substrate special windows should be made in the reactor walls. It should be taken into account that changes in the reactor geometry can drastically change the growth. Usually a small hole is made in an inner liner tube, so it should make only minor influence on the growth. On the outer reactor wall is a view port is installed. It is usually supplied with an additional gas purge, which reduces parasitic deposition.

Reflection is the simplest method for growth control. During heteroepitaxy it makes possible to estimate growth rates, temperature and even a composition of ternary materials. There were published some experimental results for optical constants of different semiconductors at high temperatures [137–139]. Knowing optical constants of growing material the growth rate can be estimated using Fabry-Perot oscillations.

Unfortunately there is still a lack of data for many materials, especially ternary and quaternary alloys. A method of simultaneous determination of optical constants and growth rate was suggested by Breiland and Killen [140], however it demands a measurement of absolute reflection. It is much easier to work with relative reflection, the substrate can be used as a reference in this case. Nevertheless optical control in MOCVD is studied further and is implemented for device control [141–144].

The surface temperature of the substrate can be estimated during growth of binary layers using known optical constants. The same method is used to determine the composition of a ternary alloy. However it demands some calibration steps implying a combination of in-situ and ex-situ control, for example X-ray diffractometry. The reflectometry is a powerful method for growth control, unfortunately it is impossible to say anything about the microscopic properties of the growing surface, such as roughness and reconstruction. For example RHEED can easily see the surface reconstruction and a transition from 2D growth to 3D growth. Reflectance is sensitive only to relative large roughnesses of more than 10 nm.

Reflectance anisotropy spectroscopy (RAS) allows to observe microscopic phenomena on the surface. In this method a difference between reflectance of light linearly polarized in two perpendicular directions is measured. The anisotropy of reflectance can originate from surface reconstruction and ordering effects in such materials like InGaP. During growth of materials with zinc-blende lattice on the (100) surface the reconstruction has dimer-like configuration and symmetry axes along [110] axes of the crystal. The reflectance anisotropy is defined as follow [145]

$$\frac{\Delta r}{r} = \frac{r_{[\bar{1}10]} - r_{[110]}}{\frac{1}{2}\left(r_{[\bar{1}10]} + r_{[110]}\right)} \tag{3.1}$$

The surface reconstruction depends mostly on temperature and partial pressures of precursors. It is also different for a growing surface and a stabilized one during growth interruption. RAS can be used to control the material composition, V/III ratio and doping.

A commercially available device from Laytec™ was used. The device could measure both reflectivity and RAS simultaneously at single wavelength. The used wavelength can be tuned in the range from 1.5 up to 4.5 eV. Since an orientation of [110] axis of the substrate is unknown, the data are collected during a whole turnover of the substrate in order to determine the RA, and afterwards a computer calculates the absolute value of the RA. One substrate turnover takes about 1-1.5 seconds, so a control of quick processes, such as QD formation is difficult.

3.1 In-situ determination of composition and growth rate during epitaxy

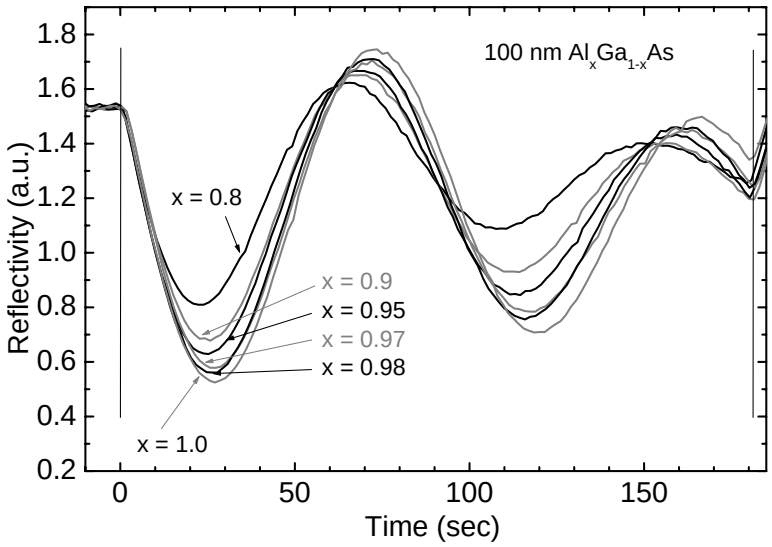

Figure 3.1: Evolution of the reflectivity during deposition of $Al_xGa_{1-x}As$ with different compositions on GaAs. The reflectivity was measured at a single wavelength with a photon energy of 2.6 eV. The growth temperature is 700℃.

In this work growth of different devices was controlled using in-situ reflectometry and RAS with the purpose to improve the reproducibility and performance of lasers and VCSELs. Details of the device structure are discussed in the chapters 4 and 5. In this section the attention is concentrated on the control of growth using optical reflectometry and RAS with application to these devices.

A VCSEL demands a very precise control of thicknesses and composition of all layers. Long growth times increase the influence of the long-term drift of growth rates, which can be caused for example by temperature drift of sources or in electronics. Some AlGaAs layers designed for oxidation during processing of the devices. Since an oxidation rate of AlGaAs is very sensitive to composition it must be very precisely controlled. The deviation of the lasing wavelength from the target has to be below 10 nm, corresponding to a deviation of the thickness less than 1%.

The AlGaAs composition can be estimated using reflectometry. When a material with one refractive index is deposited on a substrate with a different refractive index, the reflectivity begins to oscillate because of an interference of light reflected from the interfaces layer-air and substrate-layer. The shape of the curve depends on the differ-

ence between refractive indices. Since the refractive index is a function of $Al_xGa_{1-x}As$ composition it can be measured. Figure 3.1 shows an evolution of the reflection during growth of $Al_xGa_{1-x}As$ on GaAs with different compositions, collected at a photon energy of 2.6 eV. The depth of the first minima can be used to determine the Al composition at a fixed known temperature. $Al_xGa_{1-x}As$ with a composition difference Δx=0.02 can be still well resolved, for example the curves with x=1 and x=0.98. The curves with Δx=0.01 (x=0.97 and x=0.98) are very close to each other, what corresponds a noise level. Since the refractive index is a function of the temperature it can be also used for precise calibration of the surface temperature. In this case a binary layer is deposited on the substrate. The surface temperature defines the curve depth.

Usually the control of VCSEL structures is based on ex-situ characterisation of grown structures using optical reflectometry. The possible deviations could be corrected and whole structure is repeated with right thicknesses. However this method can work only with processed sample and do not take into account possible drifts during epitaxy. For example, MBE has a monotonic reduction of the growth rate due to source exhaustion, which can reach some percent during VCSEL growth. We tried to combine ex-situ characterisation with in-situ measurements of reflectance during growth and simulation of growth rates. Generally it is possible to perform a correction of growth rates during growth using estimated growth rates and eliminate a drift in such a way.

The measurement of the reflection of Bragg mirrors during growth was found to provide to little information for growth control. Figure 3.2 shows the evolution of the reflection spectra of a VCSEL-like microcavity during growth. A special simplified model structure was chosen to analyse the spectra. The sample consist of two Bragg reflectors with 6 pairs of $\lambda/4$ AlAs/GaAs, between the DBRs a $\lambda/2$ GaAs cavity was grown. The region of measured wavelength corresponds to the stop band of the Bragg mirrors. It can be seen that the characteristic features of the reflection spectra appear only after some DBR pairs are deposited. The cavity dip appears only during growth of the second DBR when any correction is too late. Hence, this method does not have advantages in compare to ex-situ control. The optimal growth control can be possible only when a single DBR pair is needed to estimate the growth rate.

Oscillations due to different refractive indices can be used to determine the growth rate. The precision of the simulation is the higher the more oscillations are involved. The thickness of DBR layers is chosen equal to $\lambda/4$, where λ ~1100-1300 nm, thus to see some oscillations the control wavelength should be chosen near 500 nm. GaAs strongly adsorbs light at this wavelength, what reduces the visible number of oscillations, but helps to see only upper layers. We performed the control using the strongest luminescence line of the Xe lamp, which is about 2.6 eV.

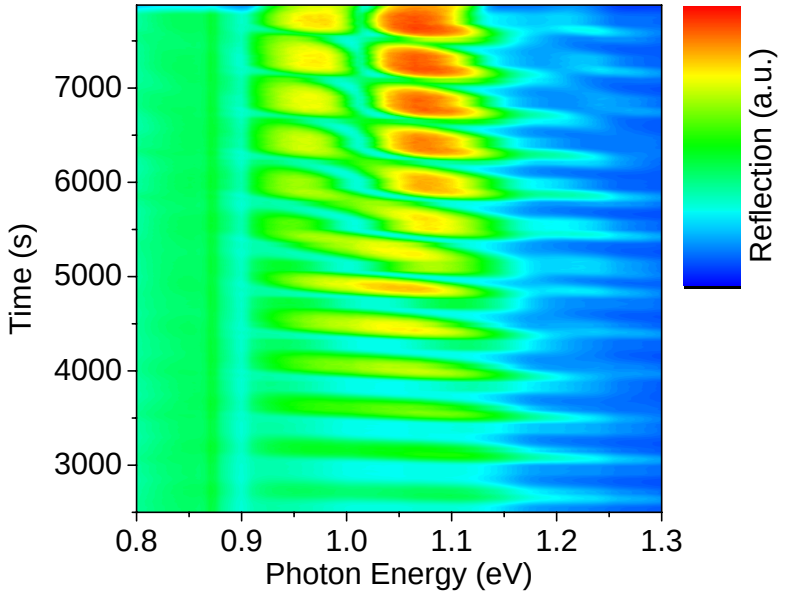

Figure 3.2: Evolution of the reflection spectra of a VCSEL-like structure during growth. The colour depicts the reflection efficiency. The structure consists of two DBRs with six pairs of $\lambda/4$ AlAs/GaAs and a $\lambda/2$ GaAs cavity. The growth temperature is 700℃. The cavity dip wavelength at room temperature is 1080 nm.

Figure 3.3(a) shows the growth rates of GaAs and AlAs, calculated using transient reflectance measurement of bottom AlAs/GaAs DBR. The reflection recorded at 2.6 eV during one DBR pair is shown in figure 3.3(b). A noticeable deviation from one layer to another can be seen. Whereas the deviation for AlAs is about $\pm 0.5\%$, it is almost doubled for GaAs. This result can be explained taking into account the number of Fabry-Perot oscillations, which were taken for simulation and strong damping of oscillations in GaAs. The error should be the smaller the more oscillations is available for a simulation. Breiland et al. [140] performed a Monte-Carlo simulation of the accuracy, which can be reached taking into account a signal noise. He achieve an error of simulated parameters about 0.01% if the signal to noise ratio is 10^{-4}. Since in our case the signal to noise ratio is much larger and is about 1% the deviation of growth rates in the DBR can be attributed to this error. As it is difficult to estimate the error of our simulation, the question if the deviation of the growth rates is real can not be answered definitely. A reduction of the error were possible by simultaneous data collection using several wavelengths, since in case of random noise the data to noise ratio should be proportional to $\sqrt{N}$, where N is the number of channels.

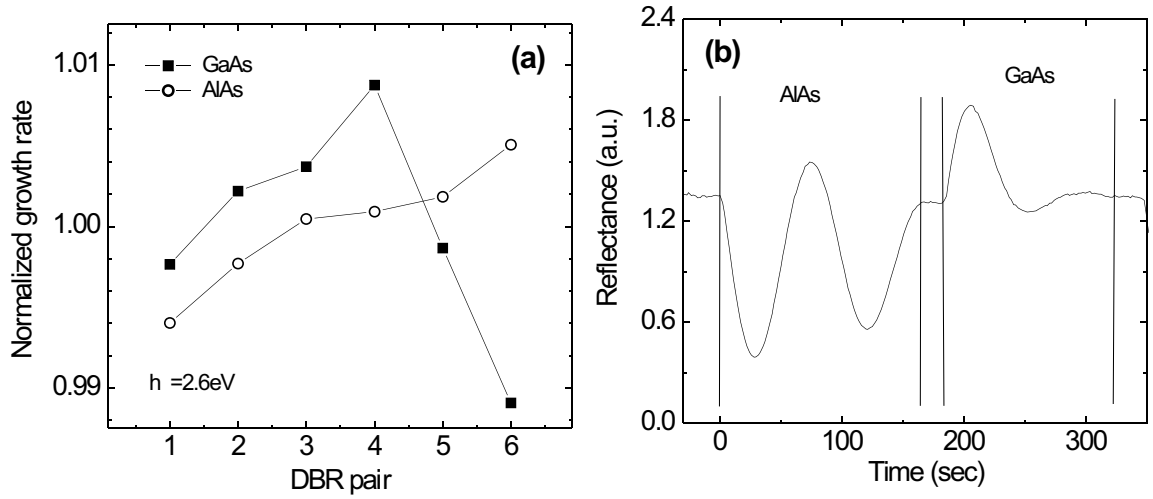

Figure 3.3: (a) Normalized growth rates calculated for each GaAs and AlAs layer of AlAs/GaAs DBR with 6 pairs. (b) Time dependence of the reflectance during growth of a single AlAs/GaAs DBR pair. The measurement was performed using light with a photon energy of 2.6 eV.

3.2 In-situ control of doping level

A doping control can be realized using RAS. The surface reconstruction changes with doping. The origin of the dependence of RAS spectra on doping level was attributed to a modification of a built-in electric field near the surface [143]. Figure 3.4 shows RA spectra of GaAs doped with tellurium. The spectra were recorded during growth at 625℃. The RA spectra are very sensitive to each growth parameter, such as growth rate, temperature and V/III ratio, composition of ternary alloys. Thus in order to provide control first the reference measurements should be made at some specific growth parameters.

The most suitable wavelength for doping control was found to be about 3.9 eV. The response is monotonic in the whole range of n- and p-type doping. Some measurements could be done using photon energy near 3 eV. The relative signal change in this region is maximal, but the dependence of the signal on doping level is not monotonic at some wavelength and the noise to signal ratio is larger than at 3.9 eV. The peak at 2.4 eV is suitable for n-type doping control, but was found to have a very weak response on p-type doping. A summary dependence of RAS response on doping level for both types of doping recorded at 3.9eV is shown in figure 3.5. Each point was calculated by averaging data of a 300 nm thick layer.

The detection limit was found to be about $1{\cdot}10^{18}$ cm^{-3} for n-type doping with Te,

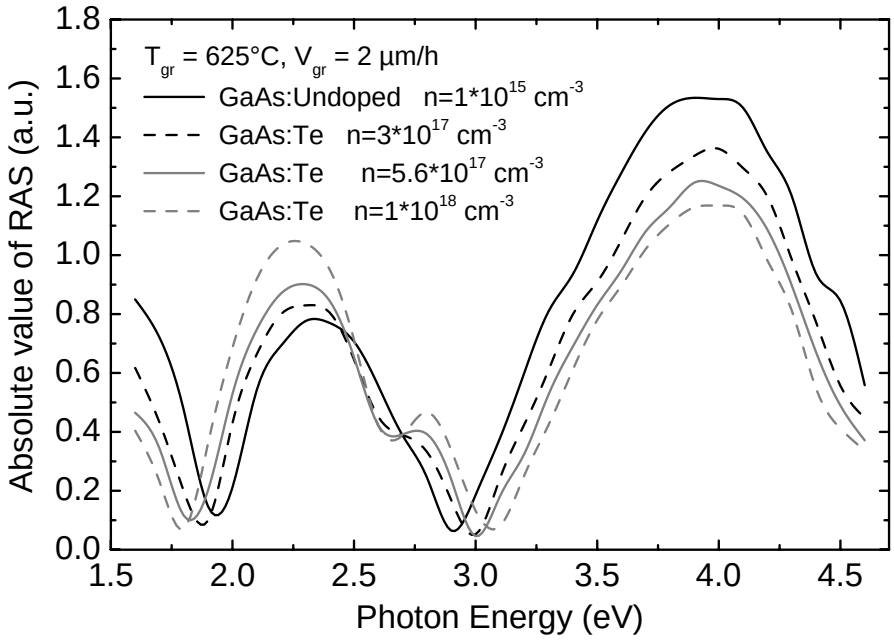

Figure 3.4: Reflectance anisotropy spectra of GaAs doped with Te measured during growth. Different curves correspond to different doping levels as marked in the figure, T_{growth}=625℃.

and about $1{\cdot}10^{18}$ cm^{-3} for p-type doping with C. Wolfram et al. [141] used RAS to control the doping of InGaAsP on InP substrates. A similar behaviour or of RAS response on doping was reported. The sensitivity limit for n-type doping with Si was found to be 10^{17} cm^{-3}, whereas for p-type it depends on the material, the larger the As composition in InGaAsP layers the weaker the RAS response. The detection limit for InGaAs doped with Zn was $4{\cdot}10^{17}$ cm^{-3}. The noise to signal ratio in our case was found to be relative high. The standard deviation is plotted in the figure. In order to estimate the doping level of growing layers it should be at least 100-200 nm thick. It is usually not a problem for edge emitting lasers, but VCSELs contain often layers thinner than 100 nm. So this method can be used for VCSEL control only with some restrictions.

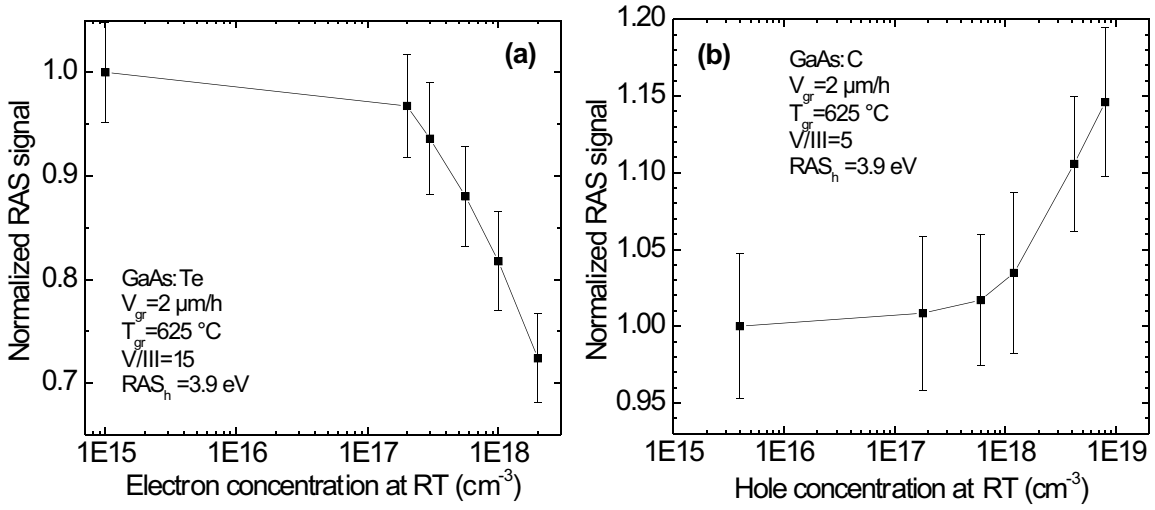

Figure 3.5: Dependence of the RA signal of doped GaAs on doping level. (a) GaAs is doped with tellurium using DETe (n-type), (b) GaAs is doped with carbon using CBr_4 (p-type). The RA signal is measured at 3.9 eV photon energy during growth. The growth rate is 2 μm/h, the growth temperature is 625℃. Each point is an average value of about 200 points, collected during growth. The standard deviation is shown by bars at each point.

Chapter 4

Edge emitting lasers based on InGaAs/GaAs QDs

A typical layer structure of an edge emitting laser is shown in figure 4.1. The growth was performed on Si-doped exactly oriented GaAs (001) substrate. Two $Al_{0.6}Ga_{0.4}As$ cladding layers surround a GaAs waveguide with QDs. The bottom cladding layer is grown at 650-670℃, and is doped with tellurium using diethyltelluride (DETe). Top cladding layer as well as GaAs waveguide and contact layer are grown at 600℃ and are doped with carbon using carbon tetrabromide (CBr_4). The Al concentration on both sides of each cladding layer is linearly ramped on the length of 50 nm in order to avoid potential barriers for charge carriers appearing at a heterojunction.

Laser devices were processed in ridges with shallow mesa, see figure 4.2. Optical lithography was implemented to define the ridge geometry. Outside the ridges a top contact layer and a half of a top emitter are removed using wet etching in order to supress a current spreading. Ohmic contacts are formed by evaporation of Ti/Pt/Au and Ni/AuGe/Au on the top and bottom sides of the wafer respectively and by subsequent rapid thermal annealing at 350℃ during 1 minute. After processing the substrate is cleaved into many bars containing single laser ridges. The mirrors are not covered with any coating. Before processing the substrate is made thinner to about 100 μm in order to achieve an easy and stepless cleavage of the mirrors.

Lasers are characterised in pulse current mode. The pulse length is 400 ns with a repetition rate of 4 kHz. Short pulses allow to avoid the overheating of the active zone due to ohmic resistance. For low temperature measurements laser bars are mounted on a copper heatsink and placed into a cryostat.

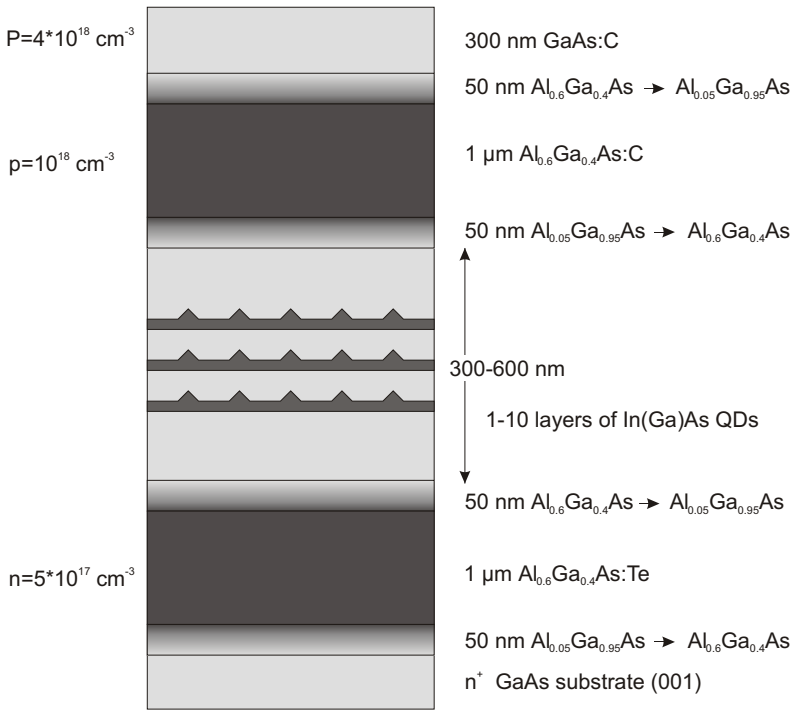

Figure 4.1: Typical layer structure of an edge emitting laser. The number of QD layers in active zone was varied from 1 to 10.

4.1 Growth of edge emitting lasers

Lasers based on QDs should have outstanding properties concerning quality. Since the saturated gain is relative low internal optical losses must be very low in order to achieve laser generation. Heterointerfaces should be perfect to reduce light scattering as well as the doping of structure must be good controlled in order to reduce the losses on free carriers.

The waveguide is usually leaved undoped, and the doping level of some hundreds nm of cladding layers close to waveguide is lower than that of other regions. It reduces the interaction of light wave with charge carries. In our case the GaAs is undoped. However, it was found that a slight p-type doping of waveguide increase the population of hole levels in the QDs and so improves the temperature stability and modulation characteristics of the lasers, keeping the losses on a small level.

Presently the most used n-type dopant for GaAs based MOCVD is silicon, the chemical source is silane (SiH_4). Silicon is a dopand with low diffusion, but in AlGaAs generates deep traps denoted DX-centers [146]. Thus the efficiency of doping can be

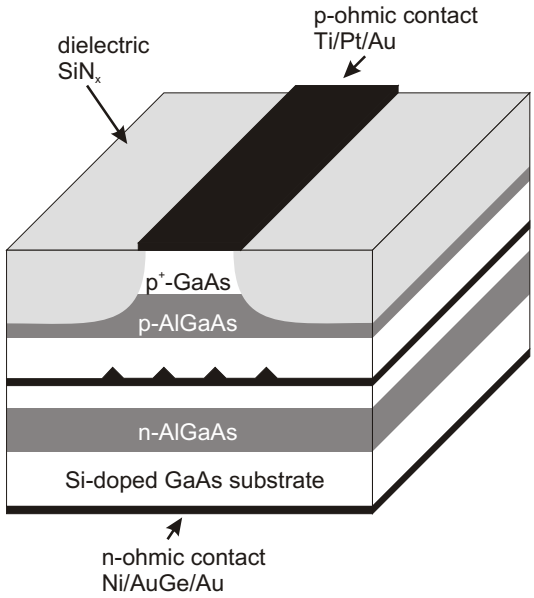

Figure 4.2: Scheme of processed edge emitting laser chip.

very low so that the electron concentration may be only one hundredth of Si atoms concentration. Especially strongly DX-centres are formed in $Al_xGa_{1-x}As$ with x close to 30-50% [147]. Since our MOCVD machine was constructed without gas lines we tried to use the liquid dopant source ditertiarybutyl silane (DTBSi).

Liquid DTBSi is an alternative to silane doping and was successfully implemented for doping of GaAs [148]. We also found that DTBSi can be easily used for doping of GaAs. An electron concentration as high as $1{\cdot}10^{19}$ cm^{-3} was achieved. However it was difficult to achieve a sufficient doping level for AlGaAs. Figure 4.3 shows the electron concentration at room temperature achieved for AlGaAs doped with DTBSi. The samples were grown at 625℃ using two different DTBSi flows, namely $1.1{\cdot}10^{-7}$ and $5.5{\cdot}10^{-7}$ mole/min. The partial pressure of TBAs was kept as high as 20 Pa for GaAs and 45 Pa for AlGaAs. The electron density rapidly drops with increasing of Al content. It was found that a high DTBSi flow causes rough surface morphology so that only GaAs and $Al_{0.3}Ga_{0.7}As$ with moderate doping could be grown with smooth surfaces.

We substituted silicon with tellurium. Tellurium is a group VI element, and is a donor in V-III semiconductors. The diffusion of Te is also neglible. Similar to silicon, tellurium forms DX-centres in $Al_xGa_{1-x}As$, but their density and localization energy was found to be smaller than for Si [149].

The electron density in AlGaAs doped with tellur saturates at a level of

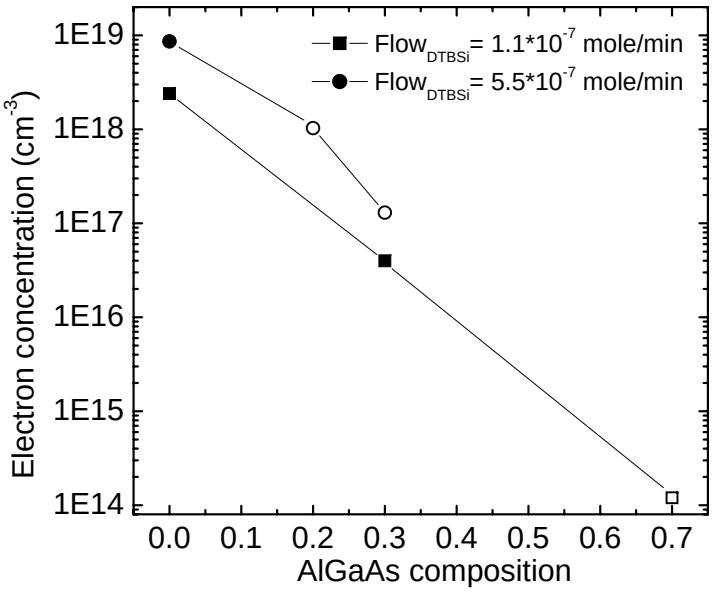

Figure 4.3: Electron density measured at room temperature using the Van-der-Pau method in $Al_xGa_{1-x}As$ doped with ditertiarybutyl silane. The growth temperature is 625℃. The TBAs partial pressure was kept at 20 Pa for GaAs and 45 Pa for AlGaAs. Squares and circles correspond to different DTBSi flows. The solid symbols depict samples with smooth surface morphology, whereas the open symbols depict samples with rough surfaces.

1-4·10^{18} cm^{-3}, depending on Al composition, and does not grow further. However the morphology of AlGaAs becomes worse if too much Te is incorporated in the layer. Figure 4.4 shows microphotographs of the surface of two $Al_{0.6}Ga_{0.4}As$ layers doped with tellurium. The photographs were made using phase contrast microscopy (Nomarski microscopy), which converts a surface relief into a light intensity image, the roughness which can be seen is about 2-3 nm. The two $Al_{0.6}Ga_{0.4}As$ layers are 1.5 μm thick and grown at 650℃. The DETe flow in case of sample (a) is 2.5 times larger than in sample (b), nevertheless the electron density measured using Van-der-Pau method is about 2·10^{18} cm^{-3} for both samples, indicating a saturation. Only sample (b) with low DETe flow has a smooth surface, whereas the surface roughness of sample (a) is about 30 nm.

Another well-known complication appearing by using tellurium is a "memory effect". Tellurium itself or DETe condensate on the reactor walls and supplying tubes, and provide a background flow even after the source is switched off. We found that a memory effect takes place only if the Te flow is very high, at low flows no negative effects

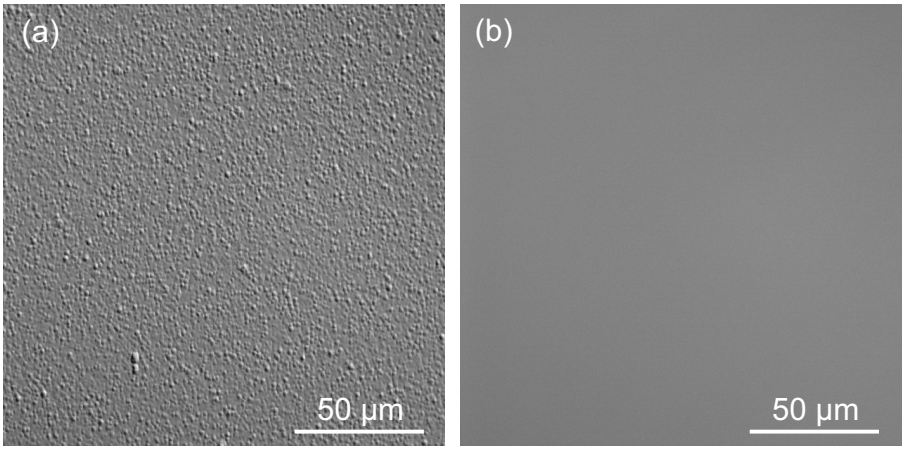

Figure 4.4: Phase-contrast microphotographs of bottom $Al_{0.6}Ga_{0.4}As$ cladding layers doped with Te. The layers are 1.5 μm thick, and are grown at 650℃. Both samples have electron densities at room temperature of about n=$2{\cdot}10^{18}$ cm^{-3}. DETe flows are (a) - $1.33{\cdot}10^{-6}$ mole/min, (b) - $5.27{\cdot}10^{-7}$ mole/min.

was observed. High DETe flow is needed to dope the bottom AlGaAs cladding layer. Since AlGaAs suffers from strong carbon intrinsic doping it must be overcompensated with Te. The doping efficiency of AlGaAs is also lower than that of GaAs. Using RAS we can observe an unintentional doping of undoped GaAs following the growth of a doped AlGaAs layer. Figure 4.5 shows time-dependent RA measurements performed at 3.9 eV during growth. Two structures containing 300 nm thick $Al_{0.9}Ga_{0.1}As$ capped with 300 nm GaAs were compared. The first one is a reference sample, which was grown without doping. An intrinsic doping provides p=10^{17} cm^{-3} for AlGaAs and n≈10^{14} cm^{-3}. In the second structure the $Al_{0.9}Ga_{0.1}As$ layer was doped with Te, the electron density is $5.5{\cdot}10^{17}$ cm^{-3}. A clear difference between the two GaAs responses can be seen. The n-doping of GaAs just after AlGaAs can be estimated to be about $1{\cdot}10^{18}$ cm^{-3}. During growth of the next 200 nm it falls below $1{\cdot}10^{17}$ cm^{-3}, the lowest detection limit of n-type doping by RAS.

Such a strong memory effect could of course disturb QD growth and make a negative impact on laser properties, if the QDs are not placed in an undoped region. It should be mentioned that this experiment was specially constructed, and real laser structures are grown using a little different growth conditions, so that the maximal DETe flow is about 3 times lower. Nevertheless, in order to reduce the unintentional Te doping of the GaAs waveguide, a growth interruption and an annealing at higher temperature is applied after bottom cladding layer growth. The following GaAs is grown with increased V/III ratio, since the incorporation of Te is reduced at high temperatures

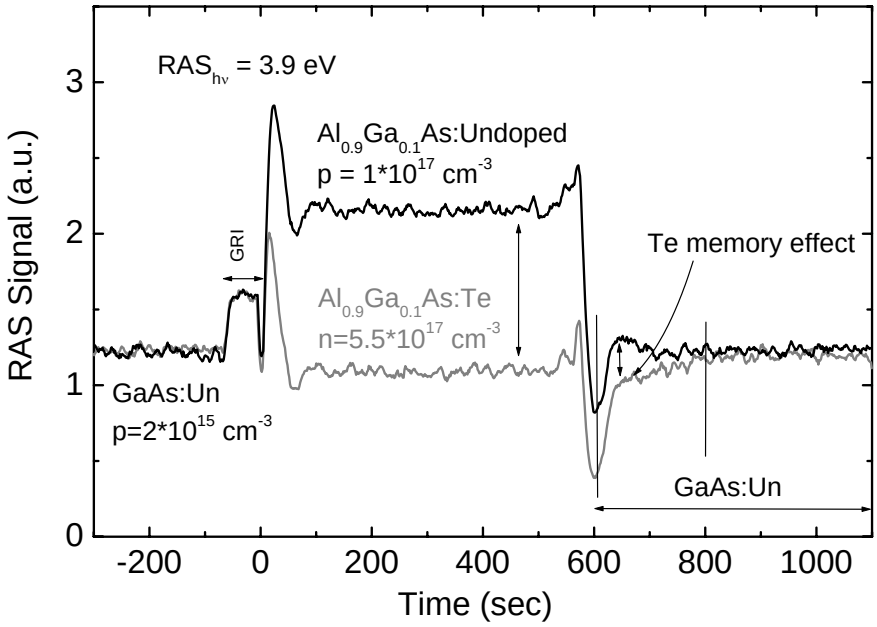

Figure 4.5: Comparison of time-dependent RAS signals during growth of undoped $Al_{0.9}Ga_{0.1}As$ (black curve) and a layer intentionally doped with DETe (grey curve). The AlGaAs layers are 300 nm thick in both cases and capped with thick undoped GaAs layers. The differenses in time evolution of the RAS signals during growth of GaAs is an evidence of unintentional doping with tellurium. The doping level of GaAs can be estimated as high as $1{\cdot}10^{18}$ cm^{-3}.

and high V/III ratio.

P-type doping is performed using carbon. During the last fifteen years carbon became a widely used p-type dopant in GaAs/AlGaAs-based semiconductors. It substitutes the widely used zinc. Carbon has a much lower diffusion coefficient compared with zinc [150], it is about $1\text{-}2{\cdot}10^{-16}$ cm^2/s near 800℃ and is independent on dopant concentration. The diffusion coefficient of zink, on the contrary, depends on concentration and is few orders of magnitude larger than that of carbon (10^{-13} cm^2/s at low doping levels $\leq 10^{18}$ cm^{-3} and up to 10^{-10} cm^2/s at high doping levels $\geq 10^{19}$ cm^{-3} [151]). Thus, layers with abrupt and large δ-doping can be easily grown using carbon. Carbon, like other shallow acceptors, is passivated by hydrogen [152] originating from precursors and the ambient. The hole concentration becomes smaller than the concentration of carbon atoms in the material. However this effect becomes significant only at high C concentrations $>10^{19}$ cm^{-3}. Nevertheless very high hole concentrations in GaAs up to $1\text{-}2{\cdot}10^{20}$ cm^{-3} were achieved [153].

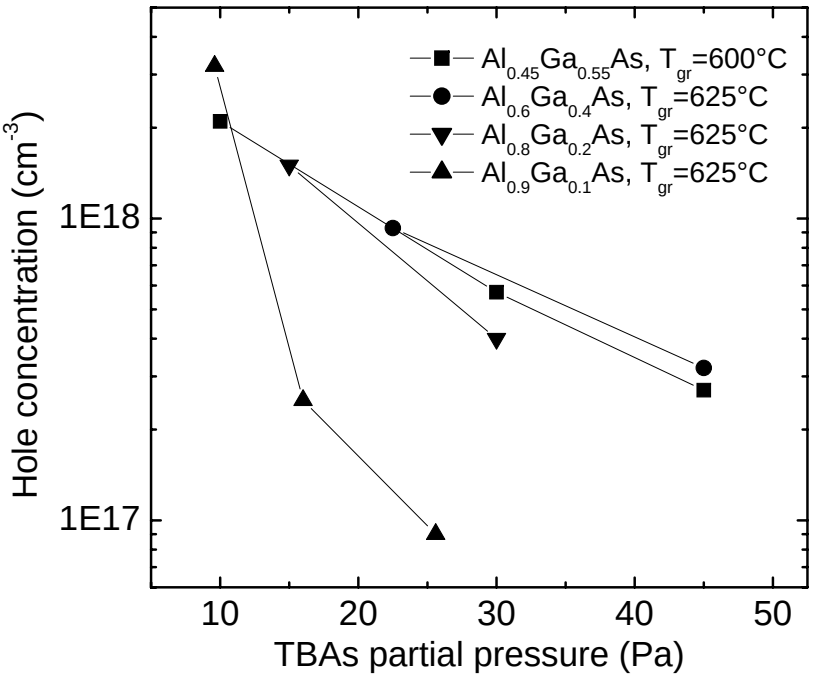

Figure 4.6: The dependence of intrinsic p-type doping of $Al_xGa_{1-x}As$ with different compositions on TBAs partial pressure in the reactor. The Al composition is shown in the figure.

Carbon is one of the main contaminations in AlGaAs grown using MOCVD. Due to the high reactivity of Al a lot of carbon is incorporated in the growing layer. Usually the incorporation take place when highly reactive CH_x (where x=1,2,3) species are adsorbed on the surface. During decomposition of arsine or TBAs atomic hydrogen and large organic radicals are formed. They transform CH_x into inert CH_4 or even larger molecules which are transported out of the reaction zone. So the carbon incorporation can be reduced by increasing the V/III ratio [76]. Figure 4.6 shows the room temperature hole concentration in AlGaAs layers grown with different TBAs partial pressure. A larger intrinsic doping is observed in the $Al_xGa_{1-x}As$ with x close to 0.5. Even at large TBAs flow the hole concentration is about $4{\cdot}10^{17}$ cm^{-3}. The intrinsic hole concentration in GaAs even at low TBAs pressure is lower than 10^{15} cm^{-3}. The large background concentration of carbon makes difficult to reach a high n-doping of AlGaAs, since all acceptors must be overcompensated. The level of contamination depends on the purity of precursors. Following the industry demand, the purification of metalorganic precursors steadily improves. We observed this on the example of the Al source. TMAl from a new batch, which substituted the exhausted source produced

two years earlier, provides an intrinsic carbon doping of AlGaAs of almost one order of magnitude lower than the old one.

Carbon incorporation perturbs the lattice of the growing material, causing a reduction of the lattice parameter [154]. At large C concentration ($>10^{20}$ cm^{-3}) even misfit dislocations form. Figure 4.7(a) shows the XRD $\omega - 2\theta$ rocking curves of AlAs recorded near the (004)-GaAs reflection. The AlAs layers are 1 μm thick and were grown at different temperatures. the growth temperature has an influence on intrinsic carbon doping, which is plotted in figure 4.7(b). It can be seen that the lattice constant of grown layers deviates from the lattice constant of pure AlAs. It is noticeable even at carbon concentration lower than 10^{18} cm^{-3}. The lattice constant deviation is plotted in the inset of figure 4.7(a). This means that a precise determination of a composition of $Al_xGa_{1-x}As$ layers using XRD is almost impossible. An exact control of Al composition, better than 0.5%, is not necessary for edge emitting lasers, but it is crucial for successful realisation of VCSELs. This issue will be discussed in the chapter 5.

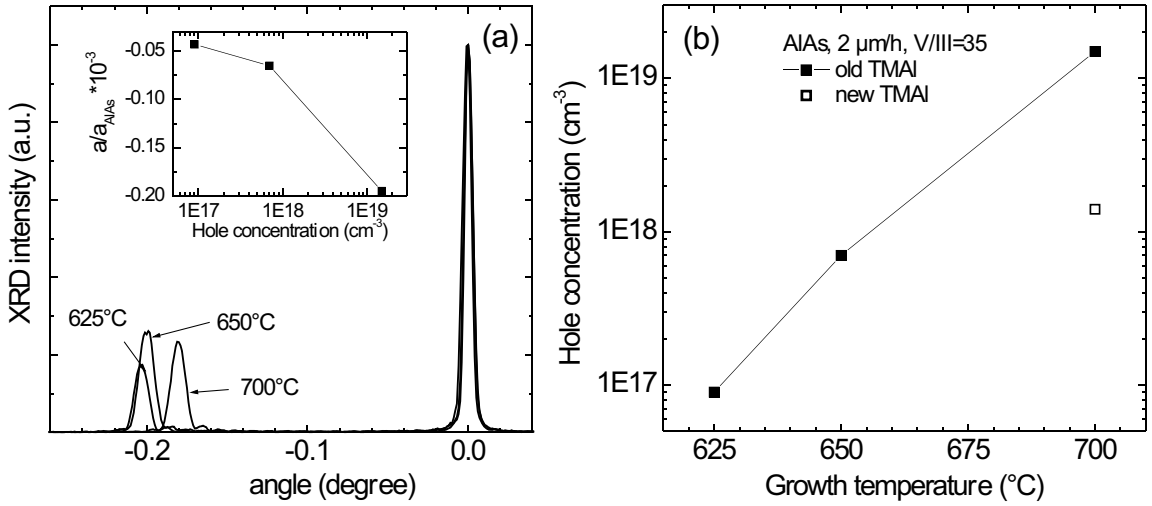

Figure 4.7: (a) Rocking curves of the (004) reflection of 1 μm thick AlAs grown on GaAs substrate at different temperatures. The growth temperature is shown in the image. The origin of the $\omega - 2\theta$ angle corresponds to the position of the GaAs substrate. The inset shows the dependence of the lattice constant deviation caused by carbon doping. (b) Hole density vs. growth temperature. the open square shows the doping achieved with a new TMAl source.

The most used carbon precursors in MOCVD are carbon tetrachloride CCl_4 and carbon tetrabromide CBr_4. Halogen gases Cl_2 and Br_2 have an etching effect on the surface of GaAs, but since bromine is less reactive than chlorine, by now CBr_4 almost

fully replace the CCl_4. Nevertheless the reduction of growth rate during doping using CBr_4 must be taken into account [155], especially at high CBr_4 flow.

The carbon doping efficiency of AlGaAs is up to one order of magnitude larger than that of GaAs at the same growth conditions and CBr_4 flow. The hole concentration was found to be proportional to the CBr_4 flow up to a hole density $5{\cdot}10^{18}$-10^{19} cm^{-3}, when it is saturated due to hydrogen passivation. The incorporation of carbon drops by increase of group V partial pressure, in addition as was mentioned in the section 1.5, TBAs provides lower carbon incorporation in comparison with arsine. Thus, in order to achieve a large carbon doping level, which is necessary for a realisation of low resistivity ohmic contacts, the TBAs partial pressure should be kept low. However low group V pressure has a negative impact on the surface morphology, caused by a transition from As reach to metal reach surface.

A degradation of surface morphology was discovered by high doping of GaAs with CBr_4. Figure 4.8 shows phase-contrast microphotographs of 1 μm thick GaAs doped using CBr_4. The samples were grown with the purpose to achieve high hole concentration. Two different V/III and CBr_4/III ratios were taken, low - V/III=3, CBr_4/III=0.05 and high V/III=10, CBr_4/III=0.2. The samples (a) and (b) contain large defects on the surface with a lateral size from 5 up to 30 μm. AFM measurements show that they are grooves with a deepness of 70 nm. These defects partly induced by an etching effect of CBr_4. The samples (a) and (c) were grown with the same low CBr_4/III ratio, but the sample (c) does not contain defects, since the V/III ratio is high. Larger TBAs partial pressure stabilizes the surface. On the other side, sample (b) was grown with the same V/III ratio as sample (c), but the CBr_4/III ratio was larger, producing again defects with dimensions even larger than in sample (a). The optimal V/III ratio was found to be 5, a hole density up to $6{\cdot}10^{18}$ cm^{-3} could be achieved without surface degradation.

Another task appearing during laser growth was to achieve a good interface morphology. QDs demand low growth temperature in order to avoid QD intermixing, but this is not optimal for GaAs and AlGaAs growth. A rough surface morphology develops during low temperature growth. QDs itself induce a surface corrugation, which can progress further and disturb a growth of upper QD layers. Moreover interface roughness increase a light scattering and optical losses in the waveguide.

One of the method to flatten the surface is to do a growth interruption, was successfully implemented for QD growth using arsine [156]. We found that the growth interruption at 600℃ under TBAs has a neglible impact on a surface roughness. Temperatures higher or equal to 650℃ are needed. Variation of growth parameters such as growth rate and V/III ratio do not significantly improve the situation.

Figure 4.9 shows the investigation on the morphology of the waveguide. The AFM

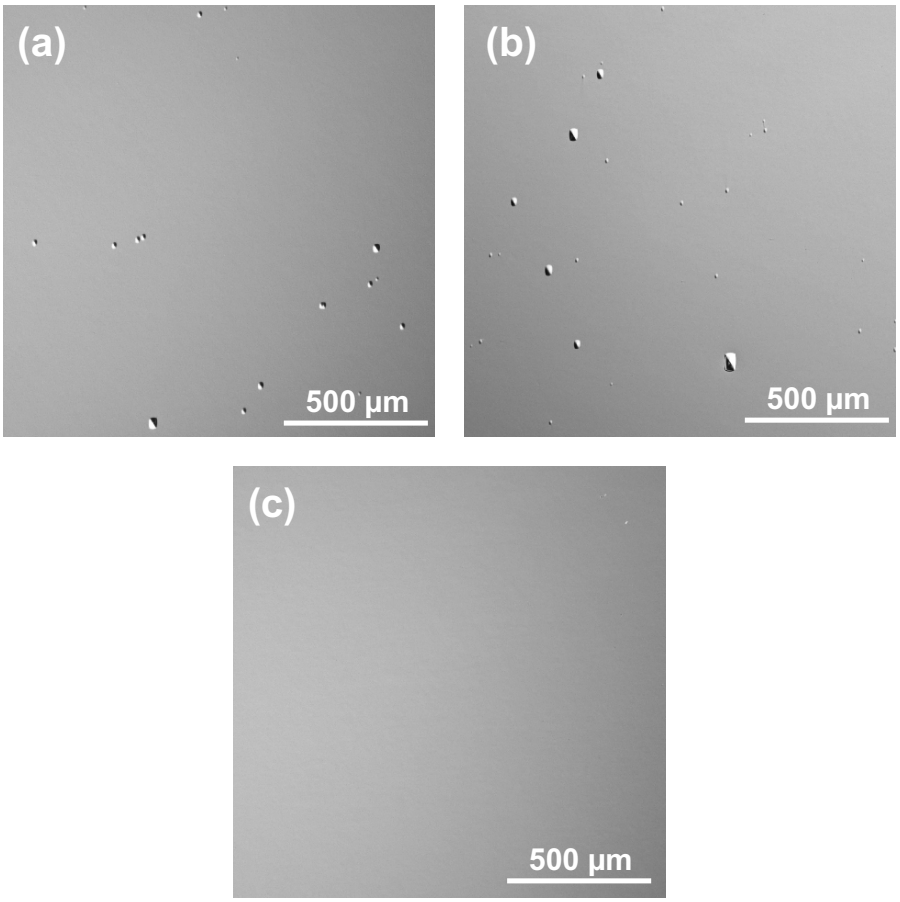

Figure 4.8: Phase-contrast microphotographs of the surface of 1 μm thick GaAs grown at 600℃ and doped with CBr_4. (a) V/III=3, CBr_4/III=0.05, p=$4{\cdot}10^{18}$ cm^{-3}, (b) V/III=10, CBr_4/III=0.2, p=$3.5{\cdot}10^{18}$ cm^{-3}, (a) V/III=10, CBr_4/III=0.05, p=$1{\cdot}10^{18}$ cm^{-3}.

images (a)-(c) depict a GaAs surface grown at 600℃ using different growth conditions. The images (d) and (e) show the surface of the real laser structure interrupted after The GaAs waveguide. In case of (d) the spacers were grown at the same conditions as the GaAs in image (a). The surface morphology becomes worse as a consequence of QD insertion. The flatness can be drastically improved if another Ga precursor is used. We substituted TMGa with TEGa. Now only monoatomic steps can be seen on the surface.

TEGa was found to be ideal to grow smooth GaAs at all temperatures and different V/III ratios. The intrinsic doping is about one order of magnitude lower than in GaAs grown using TMGa. Nevertheless a wide using of TEGa in our case was found to be

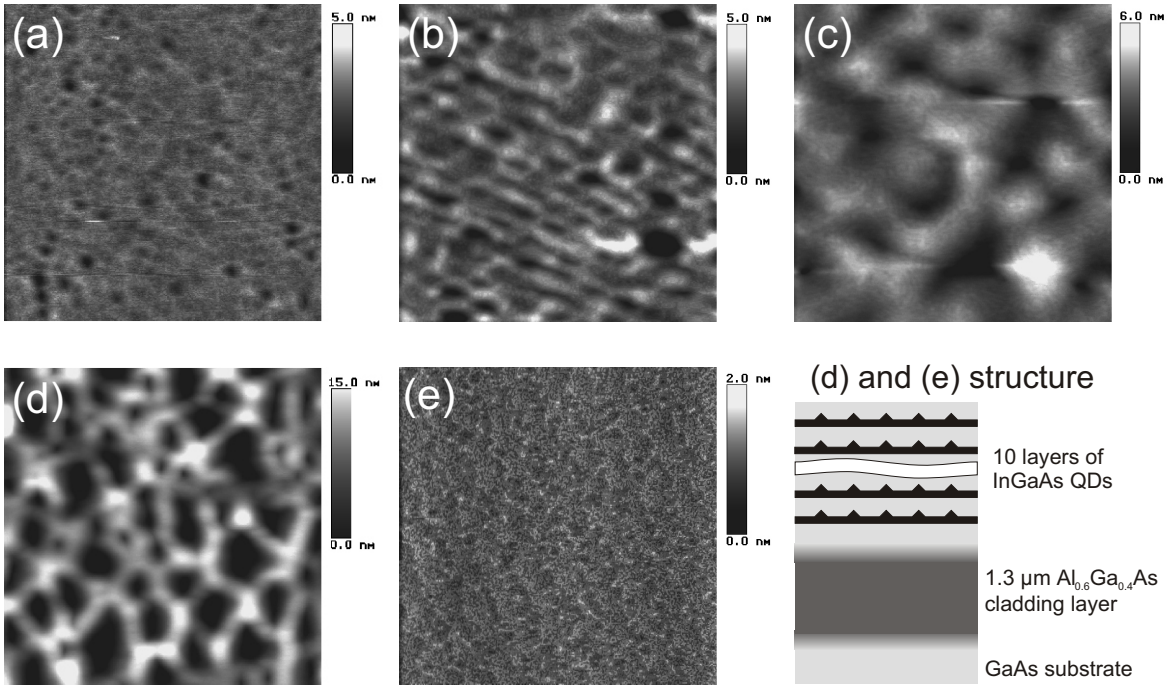

Figure 4.9: AFM images, each covers an area of 10×10 μm^2. (a-c) 1μm of GaAs grown at 600℃ using TMGa and TBAs, (a) 2 μm/h and V/III=15, (b) 2 μm/h and V/III=45, (c) 1 μm/h and V/III=15; (d-e) AFM images of the structure shown on the right, which depicts the interface between the waveguide and the top cladding layer. (d) the spacers between QD layers were grown using TMGa, (e) the spacers were grown using TEGa.

impossible since specific defects appear on the sample surface when TEGa was used. The microphotograph of one such defect is shown in figure 4.10. It looks like a small dust particle. TEGa was found previously reacts in a gas phase with TBAs [157]. There is also a report that TEGa produces adducts with the Al precursor trimethylamine alane [158]. We use TMAl but observe a strong increase of a defect density during growth of AlGaAs using TEGa and TMAl. The use of TEGa was hence limited to thin spacer layers to improve surface flatness. The lasers based on high performance QDs grown using TMGa only and TMGa plus TEGa in spacers do not demonstrate a negative impact of such thin TEGa insertions.

An important issue for production is the uniformity of device parameters fabricated from one substrate. One of the most important parameters of lasers is the wavelength. The emission wavelength can vary from run to run due to drift of growth parameters as well as it deviates among the devices fabricated from the same wafer. For most applications the wavelength should be within a ±5 nm range. It was already mentioned

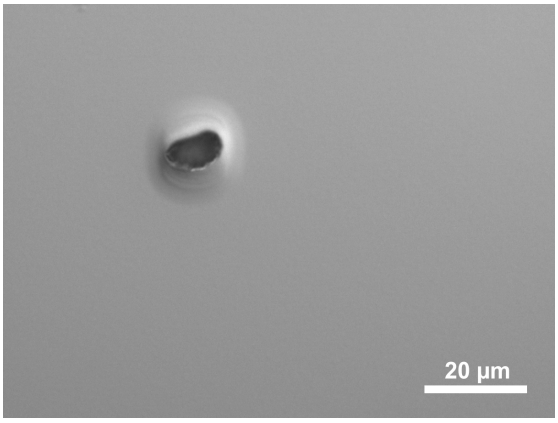

Figure 4.10: Phase contrast microphotograph of a defect on a laser structure caused by using of TEGa.

that in our case the layer thickness deviation of thick AlGaAs and GaAs could be kept within 1% through a 2" substrate. QD growth from this point of view is more complicated. First of all the properties of QDs, as was mentioned earlier, are very sensitive to the thickness of deposited material. Small deviations of the deposited thickness can drastically change the density of QDs, especially if the saturated density is not achieved. The second aspect is the inhomogeneous temperature distribution. Our measurements show that the substrate has the maximal temperature in the middle, and it reduces to the edge. The difference through a 2" substrate is about 4-5℃. The growth rates close to 500℃ are more sensitive to the temperature than that at 600℃ and higher. Figure 4.11 shows PL map measured on whole 2" substrate. The samples (a) and (b) are $In_{0.65}Ga_{0.35}As$ QDs, the deposition thickness of sample (a) is optimal, but it is 0.2 ML smaller than optimal for sample (b). The uniformity of the luminescence wavelength of the sample with optimal deposition thickness is 0.8%, whereas it is 3.6% for sample (b). Sample (c) is a reference $In_{0.31}Ga_{0.69}As$ QW, has a wavelength inhomogeneity of 0.8%.

4.2 Device properties

Lasers based on different types of QDs described in the chapter 2 were produced. Their characteristics are investigated and discussed in this section. High performance $In_{0.5}Ga_{0.5}As$ QDs emitting near 1.1 μm were first implemented as an active zone of lasers. This QDs have the best optical quality and relative high density (4×10^{10} cm^{-2}). Characteristics of laser based on three fold stacked QDs are shown in figure 4.12.

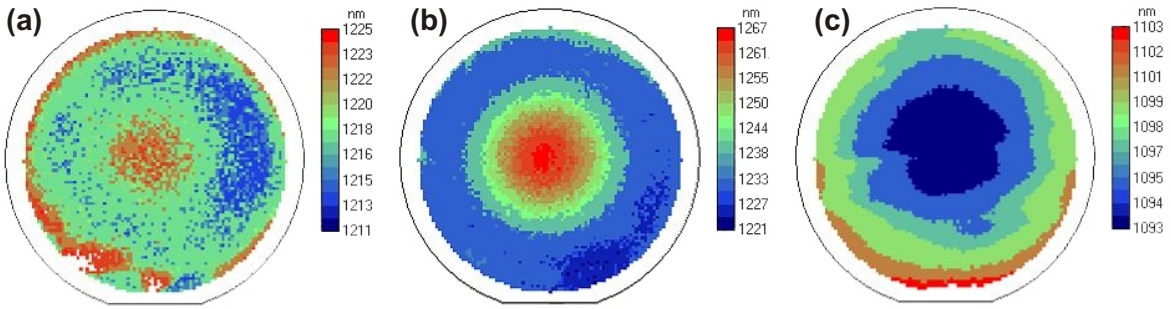

Figure 4.11: Peak wavelength PL map trough a 2" substrate. (a) - 2.1 ML $In_{0.65}Ga_{0.35}As$ QDs on 15Å of $In_{0.3}Ga_{0.7}As$ overgrown with 5 nm of $In_{0.2}Ga_{0.8}As$, (b) - similar QDs as in (a) but the deposition thickness is 1.9 ML, (c) - 7 nm thick $In_{0.31}Ga_{0.69}As$ QW.

The lowest threshold current density of 55 A/cm^2 was achieved for the 2 mm long device. The internal quantum efficiency and optical losses were derived using a linear extrapolation of the reciprocal differential efficiency vs. cavity length (equation (1.8)) are equal 91±3% and 2.2±0.2 cm^{-1}, respectively. The optical losses are a little larger than 1.5 cm^{-1}, the best values achieved by MBE grown QDs. A laser based on a single 7 nm thick $In_{0.31}Ga_{0.69}As$ QW with the same waveguide and cladding layers as in QD-based laser was fabricated in order to control the quality of epitaxy. The emission wavelength is near 1.1 μm close to QD-based laser, but the internal optical losses of the QW-based laser are 4 cm^{-1} what is a factor of two larger than that by the QD-based laser. A magnitude of internal losses is defined not only by a construction of a waveguide but also by the kind of used active zone, namely by absorption.

Despite excellent laser characteristics near 1.1 μm the shift of the wavelength towards 1.3 μm was found to be almost impossible using $In_{0.5}Ga_{0.5}As$. First of all the wavelength shift due to overgrowth is relative small compared to QDs with another composition (see section 2.3). Second, the $In_{0.5}Ga_{0.5}As$ QDs are less stable to temperature treatment than QDs with larger In composition. During laser epitaxy the growth of the top cladding layer and contact layer takes about 1 hour. QDs are annealed at 600℃ all this time. This temperature is not very high but it causes a blue-shift of an emitting wavelength. Figure 4.13 shows a summary data of some laser structures based on $In_{0.5}Ga_{0.5}As$ QDs overgrown with $In_xGa_{1-x}As$ QW of different composition and thickness. The first sample on the left is the $In_{0.5}Ga_{0.5}As$ QDs without overgrowth. It can be seen that a difference of luminescence wavelength between QDs in test structures and lasers grows with increase of wavelength. It reaches 20 nm in some samples. The last laser sample was grown using low growth temperature for top cladding layer,

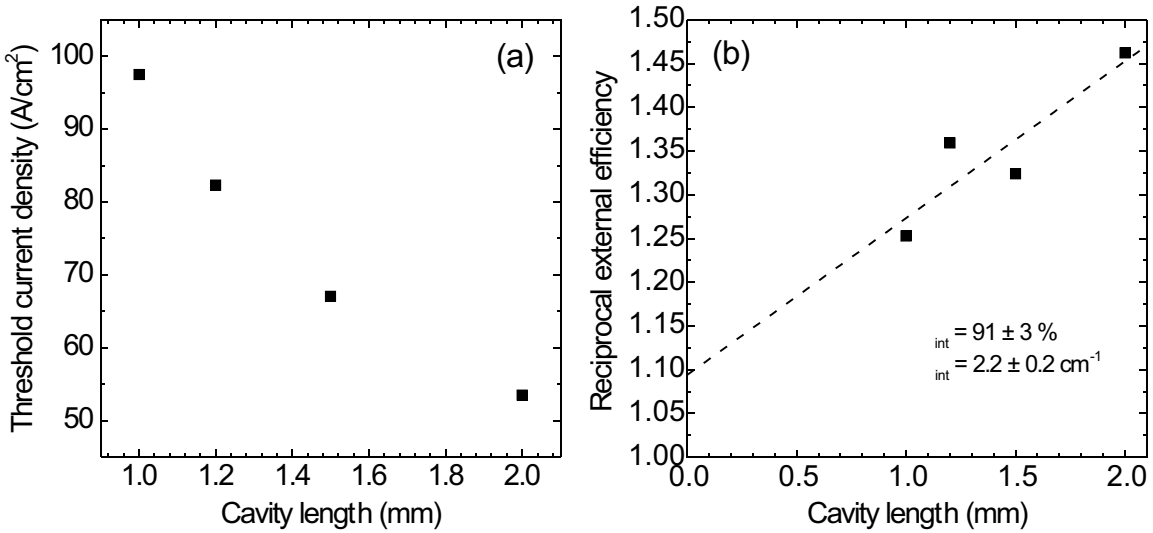

Figure 4.12: Room-temperature pulse-mode characteristics of the laser based on 3 stacks of $In_{0.5}Ga_{0.5}As$ QDs. (a) - threshold current density, (b) - inverse external efficiency.

namely 580℃ instead of 600℃, as a consequence the difference is slightly reduced. In addition the inhomogeneous broadening of the spectra rises causing the difference between the PL wavelength and lasing wavelength of about 15 nm.

One of the difficult tasks during laser growth is to avoid QD intermixing and consequent blue-shift of wavelength. A reduction of growth temperature of the top cladding layer was shown being able to increase the lasing wavelength in MOCVD grown QDs [63]. However, high growth temperature improves the quality of surrounding GaAs. Liu et al. [159] reported a drastically improvement of laser performance when the growth temperature of the spacers between the QDs was increased from 500℃ (growth temperature of QDs) to 600℃ (growth temperature of top cladding layer). We found that the luminescence wavelength of as grown QDs shifts towards shorter wavelength if the QDs are kept long time (1-2 hours) even at 600℃. On the other side the emission wavelength of QDs subjected to in-situ annealing is stable against long time annealing at 600℃, only larger temperature induces a blue-shift.

In order to investigate the influence of the number of QD layers on laser properties high density $In_{0.65}Ga_{0.35}As$ QDs on 10Å of $In_{0.3}Ga_{0.7}As$ were taken. The QDs have a density of 6.8×10^{10} cm^{-2}, what is expected should provide high modal gain so that the lasing operation of samples even with the single QD layer would be possible. The laser samples with 1, 3, 6, and 10 stacks were grown. The claddings layers as well as waveguide thickness are the same in all structures. Threshold current density and

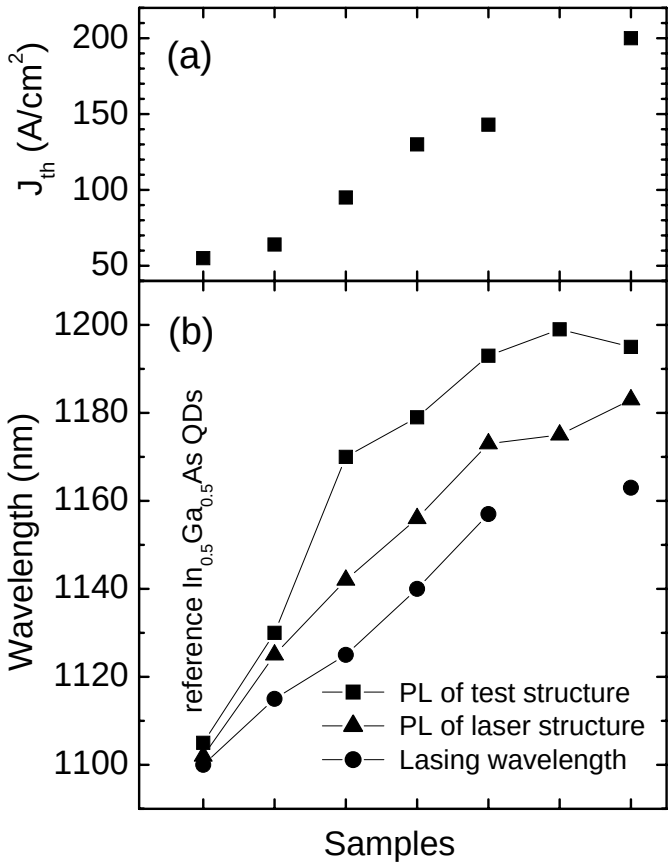

Figure 4.13: Characteristics of lasers based on $In_{0.5}Ga_{0.5}As$ QDs. The horisontal axis corresponds to different samples, which are $In_{0.5}Ga_{0.5}As$ QDs differently overgrown and with an InGaAs QW. All data is collected at room temperature (a) - threshold current density. (b) ■ - PL wavelength of single layer test sample, ▲ - PL wavelength of QDs placed in the laser waveguide, ● - lasing wavelegth.

external efficiency are plotted in figure 4.14.

The modal gain in laser based on single QD layer seems to be insufficient to achieve stable operation. The threshold current and external efficiency strongly deviate for different samples. The lasing wavelength of all lasers is about 1110 nm, except the sample with single QD layer where it is 1090 nm. This wavelength corresponds to a mixture of ground and excited state. Since the halfwidth of ground state transition is about 70 meV it is close to a separation energy between sublevels in the QD, which is about 70 meV. The lasing wavelength shifts smoothly towards shorter wavelength without jumps taking place if the separation between sublevels is larger than the inhomogeneous broadening of the energy levels. Using equation (1.8) the optical losses

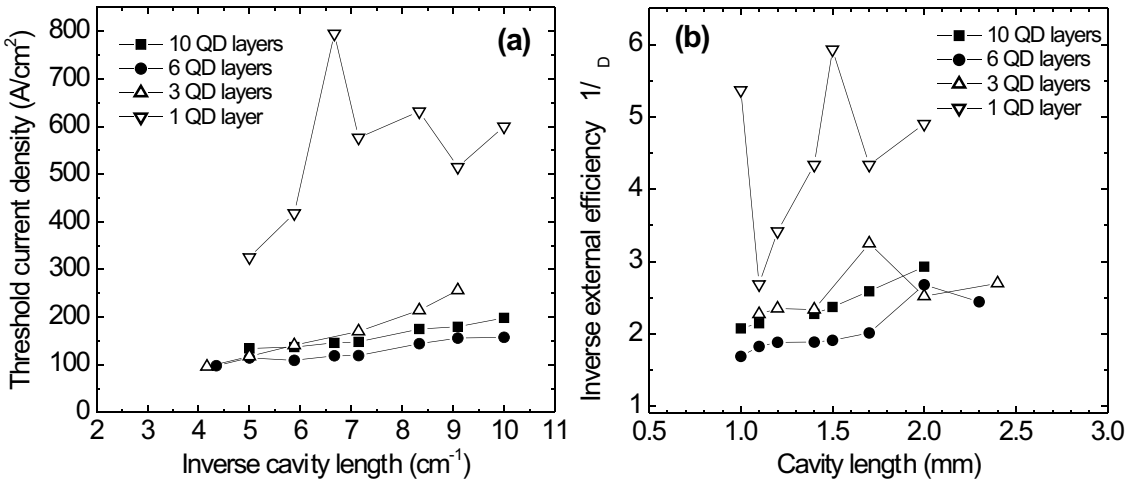

Figure 4.14: Room-temperature laser characteristics of lasers based on $In_{0.65}Ga_{0.35}As$ QDs grown on 10Å of $In_{0.3}Ga_{0.7}As$ with different numbers of layers: 1, 3, 6, and 10. (a) the dependence of threshold current density on the inverse cavity length, (b) the inverse external efficiency on the cavity length.

and internal efficiency were derived and collected in table 4.1. The sample based on the single layer of QDs is excluded from the examination due to improper operation.

Table 4.1: Internal differential efficiency and optical losses of lasers based on diffent numbers of layers of $In_{0.65}Ga_{0.35}As$ QDs grown on 10Å thick $In_{0.3}Ga_{0.7}As$ template at 500℃.

Number of layers	**Internal efficiency** (%)	**Internal losses** (cm^{-1})
10	84%	8.4
6	84%	5.3
3	52%	2

The laser based on 6 QD layers demonstrated the lowest threshold current density as well as the largest external efficiency. Thus we can conclude that the laser based on 3 QD layers operates in the region close to a gain saturation. The optical losses grow with increase of stacking number, this is opposite to the observation made by QDs grown using MBE [160], where the lowest internal losses were achieved for laser based on 10 layers of QDs.

In order to achieve long lasing wavelength a QDs with high In composition overgrown with an InGaAs QW should be implemented. We used two different kinds of

QDs. First are the $In_{0.65}Ga_{0.35}As$ QDs overgrown with 5 nm of $In_{0.2}Ga_{0.8}As$. The QDs have a density of about 2×10^{10} cm^{-2}, and emit near 1280 nm. The in-situ annealing step was implemented for laser structures. As it was shown in section 2.4 the in-situ annealing drastically reduces the rate of non-radiative recombination, especially at high temperatures. After an in-situ annealing the wavelength becomes shorter and is about 1245 nm. $In_{0.65}Ga_{0.35}As$ QDs on $In_{0.3}Ga_{0.7}As$ template have a large density of about 7×10^{10} cm^{-2} but emit only near 1230 nm, after in-situ annealing the wavelength is only about 1200 nm. InAs QDs grown under the same growth conditions allow to reach the luminescence wavelength beyond 1.3 μm, but have a density of only about 6×10^{9} cm^{-2}, hence they are not suitable for laser applications due to an expected too low modal gain. Therefore, we used InAs QDs deposited on a 10Å thick $In_{0.3}Ga_{0.7}As$ template overgrown with a 5 nm $In_{0.2}Ga_{0.8}As$ QW. QDs, having a density of about 4×10^{10} cm^{-2} and a luminescence wavelength of about 1265 nm, cf. black and grey curves in figure 2.32. An in-situ annealing was also implemented for this QDs, inducing a red-shift to 1240 nm.

Laser structures with 10 stacks of QDs were fabricated. Figure 4.15 shows room temperature characteristics of lasers based on InAs QDs on $In_{0.3}Ga_{0.7}As$ and $In_{0.65}Ga_{0.35}As$ QDs on GaAs. The lasing wavelength of both lasers is near 1240 nm. Lasers based on InAs/InGaAs QDs have an almost doubled threshold current density, but are less dependent on cavity length. Using a linear extrapolation of the inverse external efficiency vs. cavity length, we determined the internal quantum efficiency and optical losses. Both lasers have similar internal efficiency of about 75% and 83% for $In_{0.65}Ga_{0.35}As$/GaAs and InAs/$In_{0.3}Ga_{0.7}As$ QDs, respectively. The optical losses are quite different, 4.4 cm^{-1} for $In_{0.65}Ga_{0.35}As$/GaAs QDs, and as large as 15 cm^{-1} for InAs/$In_{0.3}Ga_{0.7}As$ QDs. The exceedingly high internal losses of the latter may be due to residual defects, which were not removed by annealing.

One laser structure was grown with $In_{0.65}Ga_{0.35}As$ QDs without in-situ annealing. Only a few laser devices produced from this wafer showed a lasing with a threshold current of more than a factor of two larger than that of laser with annealing. The in-situ annealing, hence, is crucial for a performance of long wavelength lasers.

The dependence of the threshold current density on temperature for both laser structures is shown in figure 4.16. Both curves show a typical behaviour of threshold current vs. temperature for lasers based on QDs, often observed by other research teams. At low temperature (T<200 K) the threshold current remains constant or even decreases for lasers based on InAs/$In_{0.3}Ga_{0.7}As$ QDs. If the temperature exceeds 225 K and 250 K for $In_{0.3}Ga_{0.7}As$ and $In_{0.65}Ga_{0.35}As$/GaAs QDs, respectively, T_0 becomes about 55 K. This value is quite low for lasers based on QDs, indicating a thermally

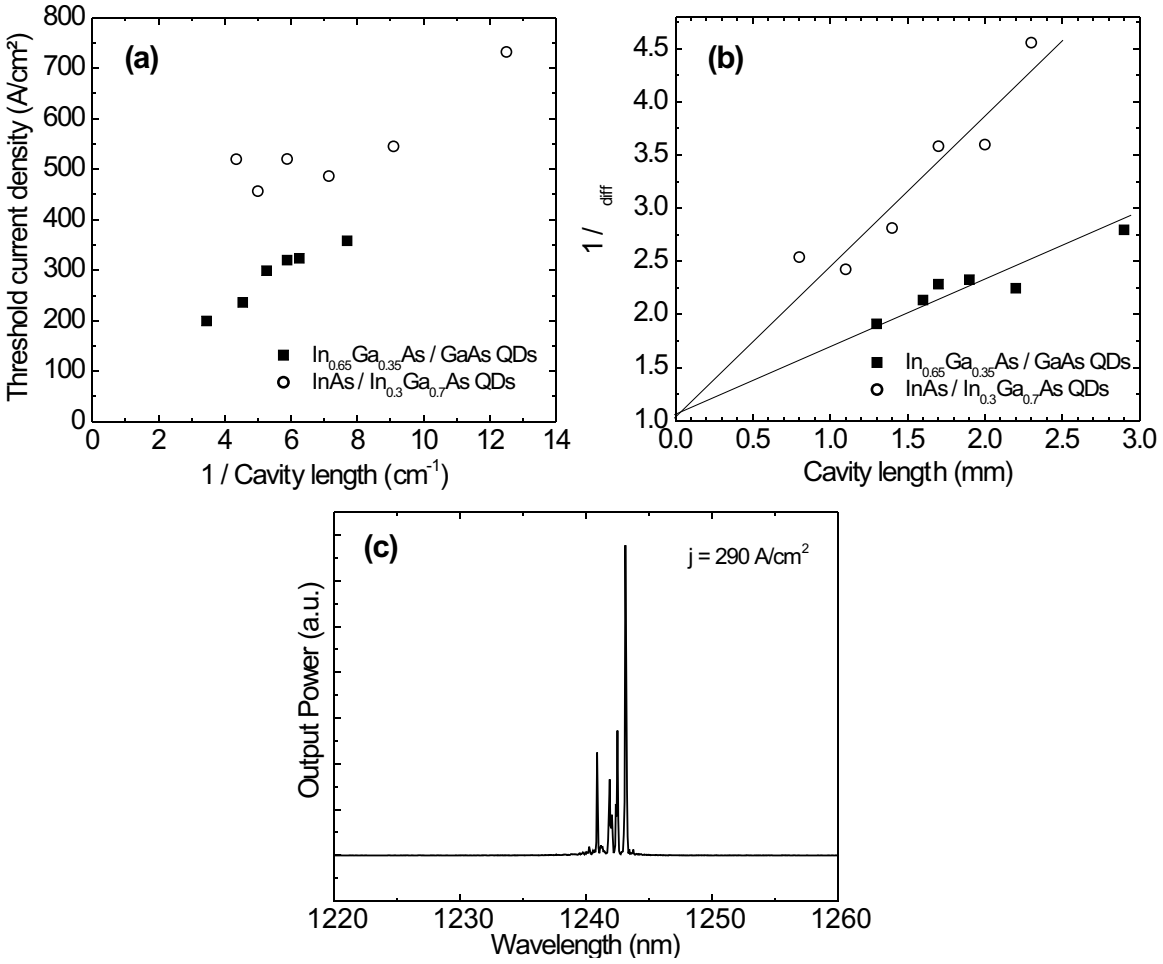

Figure 4.15: Room temperature laser characteristics of lasers based on 10-fold stacked $In_{0.65}Ga_{0.35}As$ QDs on GaAs and on InAs QDs on $In_{0.3}Ga_{0.7}As$ underlayer. (a) threshold current density vs. inverse cavity length, (b) inverse external differential efficiency vs. cavity length, (c) lasing spectra of the laser based on $In_{0.65}Ga_{0.35}As$/GaAs QDs with the cavity length of 2 mm.

induced carrier release from the QDs.

A negative T_0 at low operation temperature was often observed in lasers based on QDs [71]. Such a behaviour is usually related to a non-thermal carrier distribution within the QD ensemble [161]. A thermal escape time of carriers from QDs at low temperature is longer than a radiative recombination, so a uniform distribution instead of Fermi distribution occurs. At high temperature the distribution becomes Fermi-like. This can be easily illustrated by investigation of PL spectra measured at different temperatures. The dependence of halfwidth on temperature is plotted in figure 4.17. The spectra at 10 K have the same FWHM as at 300 K, on the other hand the halfwidth

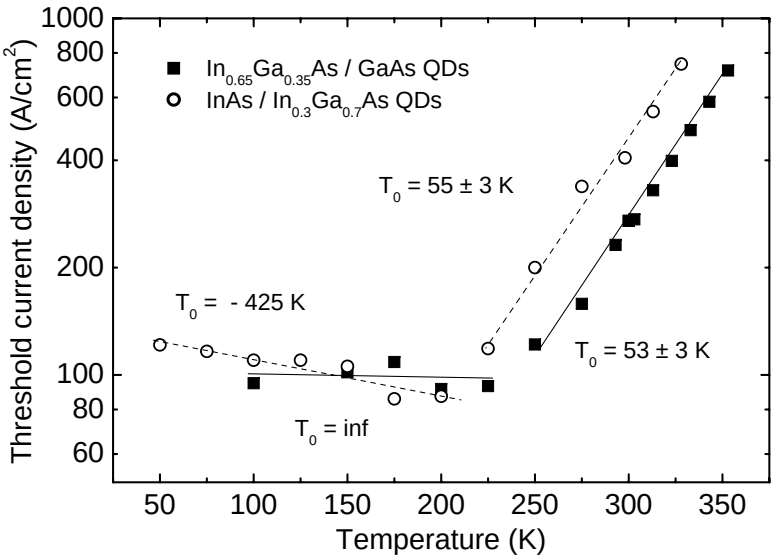

Figure 4.16: Temperature dependence of threshold current densities of edge emitting lasers based on tenfold QD stacks. ■ - $In_{0.65}Ga_{0.35}As$ QDs on GaAs, ◯ - InAs QDs on 10Å $In_{0.3}Ga_{0.7}As$ template.

reach its minima near 200 K, marking a point of the transition from uniform to Fermi-like distribution. An earlier increase of threshold current for InAs/$In_{0.3}Ga_{0.7}As$ QDs can arise from a smaller separation of the energetic sublevels in InAs QDs in compared to InGaAs QDs. The T_0=55 K at room temperature is far away from the best achieved values, but is comparable with that what was published for QDs grown on GaAs. The larger T_0 were usually achieved using special techniques, for example an AlGaAs matrix [69] or p-type doping of the spacers between QDs [162].

The dependence of maximum modal gain on current density for long and short wavelength lasers is given in figure 4.18. The relation was calculated as a sum of internal losses and output losses at lasing threshold, see equation (1.7). The reflection of both mirrors was assumed equal to 0.33. It can be clearly seen that the saturated gain of 10-fold stacked InAs/$In_{0.3}Ga_{0.7}As$ QDs is about 28 cm^{-1}, which is two times larger than for $In_{0.65}Ga_{0.35}As$/GaAs QDs and correlates well with the QDs density. Thus we have the maximal modal gain per QD layer as high as 1.3 cm^{-1} for a QD density $1.8{\cdot}10^{10}$ cm^{-3} and 2.8 cm^{-1} for QD density $4.6{\cdot}10^{10}$ cm^{-3}. The last value is close to those achieved on similar structures with 10 fold stacked InAs QDs grown using MBE [160]. The short wavelength $In_{0.5}Ga_{0.5}As$ QDs demonstrate significantly larger modal gain at the same current and have a maximal modal gain per QD layer about 5.5 cm^{-1}, a factor of two larger comparedg with InAs QDs on $In_{0.3}Ga_{0.7}As$ template

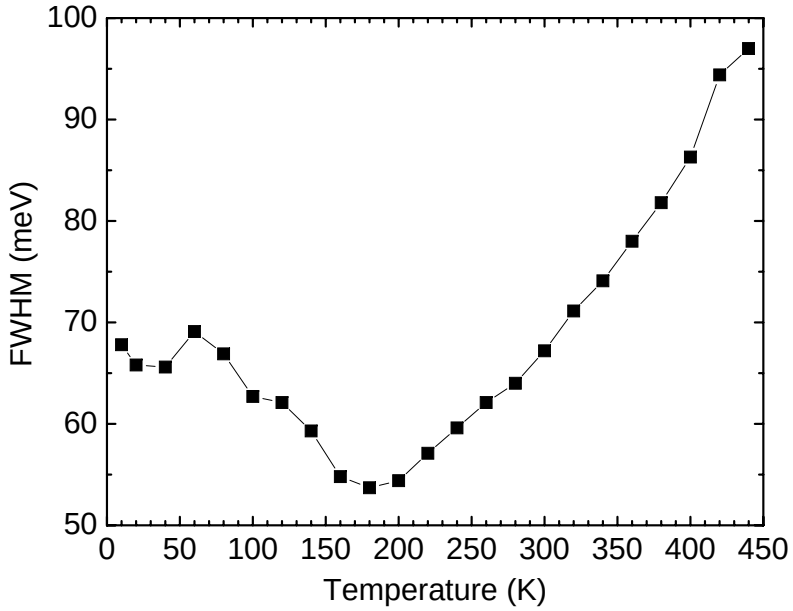

Figure 4.17: Halfwidth of PL spectra measured at different temperatures of $In_{0.65}Ga_{0.35}As$/GaAs QDs overgrown with 5 nm of $In_{0.2}Ga_{0.8}As$ and subjected to defect reduction. P_{ex}=5 W/cm^2

despite the similar QD density.

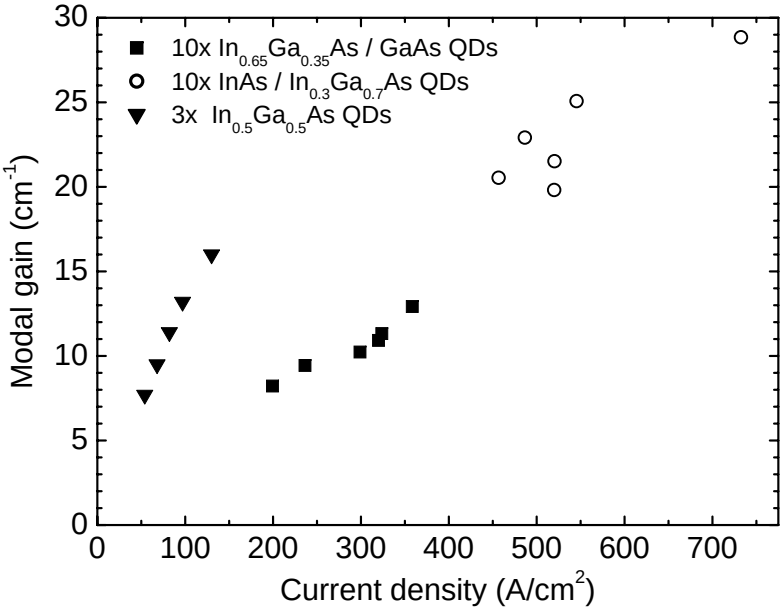

Figure 4.18: Dependence of saturated modal gain on current density for lasers based on tenfold QD stacks of $In_{0.65}Ga_{0.35}As$ QDs on GaAs (■), InAs QDs on 10Å $In_{0.3}Ga_{0.7}As$ template (◯), and three-fold stacked $In_{0.5}Ga_{0.5}As$ QDs (▼)

Chapter 5

Vertical-cavity surface-emitting lasers based on InGaAs/GaAs QDs

Vertical cavity surface emitting lasers (VCSELs) are ideal light sources for optical data communication via fibres. VCSELs have a lot of advantage in comparison to edge emitting lasers. Devices are processed and tested parallel on the wafer reducing the costs per one unit and opening a possibility to fabricate one- and two-dimensional monolithic arrays, what is helpful for applications with parallel data transfer. A symmetric beam with low divergence is desirable for efficient fibre coupling. The fabrication however is a challenge from point of view epitaxy and device processing.

A schematic image of a VSCEL device is shown in figure 5.1. Two Bragg reflectors form a Fabri-Perot resonator perpendicular to the substrate plane. An active zone is placed in the cavity in such way that an optical mode has a maximal overlap with it. Oxide apertures are used in order to confine the current and reduce the current leakage. Electrical contacts can be made either through the mirrors or directly to a cavity, what is shown on the image. The production of VCSELs with extracavity contacts (through mirrors) is less complicate than with intracavity contacts, since less processing steps could be made. There are no demands in high precision etching of mesas for top and bottom contacts, what saves a lot of processing steps and increases the yield. The price for such simplifying is a necessity to dope mirrors. The doped mirrors increase optical losses [163] and resistivity of devices with negative influence on power and speed characteristics. Intracavity contacts allow to achieve low losses with low resistivity [164, 165].

A small cavity length of a VCSEL, only a few λ, provides a low number of longitude modes occuring in the resonator. It demands an exact overlap of gain spectra and cavity mode. A short cavity length and small overlap of optical mode with an active

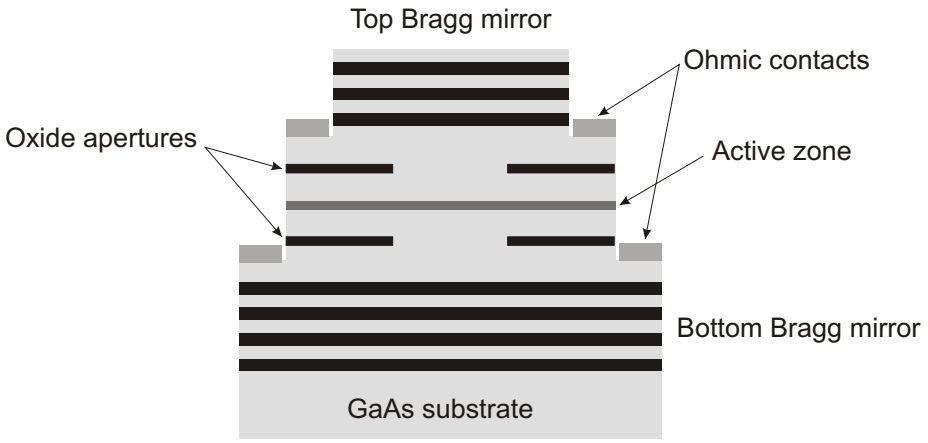

Figure 5.1: Schematic view of a VCSEL device with intracavity electrical contacts and two oxide apertures.

zone increase the demand to a gain of an active media. The lasing generation can be only possible if the mirror reflectivity is close to 100%. The reflectivity of a Bragg mirror depends on the difference of refractive index between layers. The larger this difference the less mirror pairs are needed to achieve given reflectivity. GaAs based VCSELs benefit from the fact that AlAs has the same lattice constant as GaAs, and provides larger refractive index difference, than can be reached on InP substrates. In addition a possibility to use AlO_x, which has even greater index difference, making GaAs/AlO_x mirror very efficient. For example, a reflectivity close to 100% can be reached using 50 pairs of AlInAs/InP, 30 pairs of AlAs/GaAs and only 7 pairs of AlO_x/GaAs. Due to a large stop band of oxide mirrors it increases the tolerance of layer thickness. Difficulties of VCSEL production in InP based systems stimulated the investigation long wavelength VCSELs based on GaAs substrates.

A large inhomogeneous broadening of gain spectra of QDs becomes an advantage in a VCSEL. The operation of a VCSEL is defined by an overlap of the cavity dip and gain spectra of an active zone. The cavity dip shifts very slowly with increase of the environment temperature only about 0.04 nm/K, whereas the semiconductor band gap and emission spectra shifts about 0.4 nm/K. Thus in order to provide operation over larger temperature range, the cavity dip at low temperature is placed at the short-wavelength side of the gain spectra. It shifts towards long wavelength at high temperature, what is depicted in figure 5.2. QDs, having larger width of gain spectra comparing to a QW, provides stable operation over a larger temperature region.

Despite the more complicated processing, VCSELs with intracavity contacts design can potentially reach a larger operation frequency, due to lower resistivity. Another

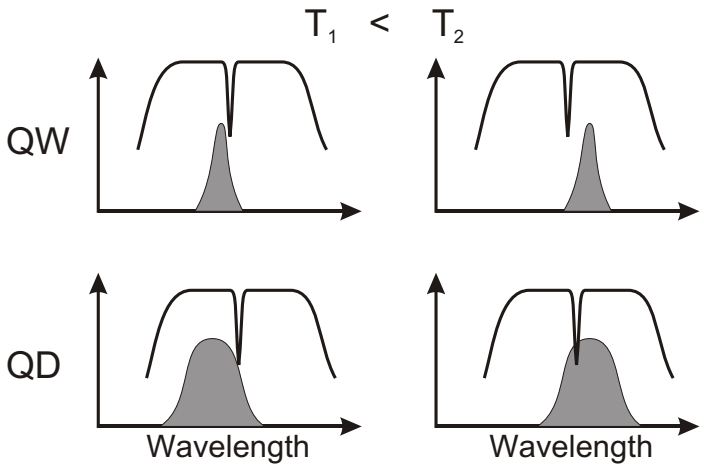

Figure 5.2: Schematic image of a mutual shifts of cavity dip and gain spectra for quantum well and quantum dot upon increase of the temperature.

advantage is the possibility to use oxide Bragg reflectors or dielectric mirrors.

First VCSELs emitting at 1.3 μm were demonstrated in 2000 based on InAs QDs [166] and on InGaAsN QW [167]. Asplund et al. [168] showed a VCSEL device based on InGaAs QW emitting at 1260 nm. He placed a long wavelength InGaAs QW (emitting wavelength 1190 nm) in a cavity with an optical mode at 1260 nm. During operation in continuous mode the active zone was so strong overheated, that the luminescence of the QW was shifted up to cavity mode and a lasing took place.

Due to short cavity lengths of VCSELs, a very high material gain of the active layer is crucial, making high demands on developing such devices based on QDs. In view of the gain limitations of the long wavelength QDs, we decided to use less critical high performance short wavelength QDs. $In_{0.5}Ga_{0.5}As$ QDs emitting at 1100 nm were taken as active zone. The QDs are grown at 500℃ and have a density as high as 4×10^{10} cm^{-2}. The optical quality of these QDs is the best among available structures. The edge emitting laser based on three layers of this QDs has excellent characteristics and high gain. The internal efficiency was close to 100%, the lowest threshold current density was as low as 55 A/cm^2. The modal gain was estimated to be 5.5 cm^{-1} per one QD layer. For more details of QD growth and laser properties see the sections 2.2 and 4.2. A detailed description of VCSEL processing and device properties can be found in the PhD thesis of F. Hopfer [169].

The VCSEL structure consists of two AlO_x/GaAs Bragg mirrors and intracavity contacts. Oxide mirrors were choosen in order to provide high reflection. At the p-side an AlO_x aperture was implemented to confine the current flow. Bragg mirrors and aperture were produced by selectively oxidizing the AlGaAs/GaAs layers in H_20 steam

ambient. The structure was designed in a way to allow the oxidation of both mirrors and the aperture in one step. This enables to reduce the number of high temperature treatments and to increase the yield.

A performance of an oxide mirror strongly depends on how long the sample was subjected to high temperature treatment. It should be the time needed for full oxidation, but not longer, since it decrease the properties and increase the probability that the mirror will fall off during the next processing steps. Since the mirrors and the aperture have a different length to be oxidized, the oxidizing rate must be adjusted in such a way that both mirrors should be fully oxidized at the same time with deviation within 10%. This can be made by small addition of Ga into AlAs layers of the Bragg reflectors. The oxidation rate of AlGaAs strongly depends on Ga composition [170], it drops one order of magnitude of the composition changed from binary AlAs to $Al_{0.96}Ga_{0.04}As$.

5.1 Growth of QD-based VCSEL

High attention was concentrated on interface quality. Rough interfaces increase light scattering and optical losses. The roughness of Bragg mirrors was tested. Typical temperatures used for QD growth were found to be far from optimal for DBR mirrors. As was discussed in section 4.2, the temperature used for growth of the layers above QDs should not exceed 600-625℃, because of QD intermixing. $In_{0.5}Ga_{0.5}As$ QDs was found to be stable against long time annealing at 625℃. However such growth temperature provides slight roughness in edge emitting lasers and VCSELs. Figure 5.3 shows AFM images of 6-pair DBR mirror optimized for 1.1 μm and grown at different temperatures. Top layer roughness of up to 3 nm height is present at 625℃. 700℃ was found to be the optimal growth temperature for a DBR, only monolayer steps can be seen. Such temperature is extremely high for QDs, so it was decided to grow the bottom part until QDs (bottom DBR and n-contact layer) at 700℃ and the other structure at 600℃. The roughness of the whole structure was about 3 nm.

During an oxidation process the Bragg mirror is subjected to strong mechanical and thermal impact. Crystalline AlAs transforms into amorphous AlO_x with a larger volume than AlAs. Strong elastic strain could induce a disintegration of the DBR during oxidation step or during the late processing. It was found that the stability of the mirror improves by an embedding of thin AlGaAs buffer layers between GaAs and AlAs designed to be oxidised. The buffer layers, however, increase the roughness of the whole DBR, especially if the growth temperature is 625℃. In order to improve the flatness a growth interruption was implemented between every layer. Figure 5.4 shows

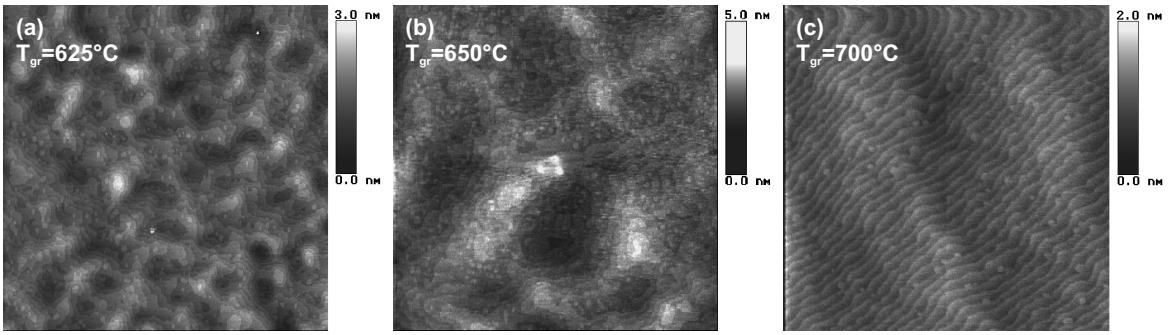

Figure 5.3: AFM images of 6 pair AlAs/GaAs DBR grown at different temperatures. Each image displays an area of 10×10 μm. A height scale is shown on the rigth side of each image.

the AFM images of the as grown oxide DBR optimized for 1.1 μm grown at 625℃ using different combinations of buffer layers and growth interruption. Three different buffers were compared: (a) no buffer layer between AlAs and GaAs, (b) 1 buffer layer 20 nm thick $Al_{0.2}Ga_{0.8}As$, (c) 3 buffer layers with $Al_xGa_{1-x}As$ where x is 0.95/0.65/0.3 and the thickness is 5/5/10 nm respectively. The sample with a single buffer layer was found to have the lowest roughness among tested buffers. The growth interruption is a standard method used to reduce the roughness. In case of our DBR it was found that the sample without GRI, sample (d), has the largest roughness. The smoothest surface is obtained by the GRI equal to 30 seconds between each layer, sample (b). An increase of GRI duration leads to a increase of roughness, sample (e).

5.2 Device properties

A QD-based VCSEL structure was especially optimized for low optical losses. The doping was kept on a moderate level in order to minimize optical losses on free charge carriers. Nevertheless the doping of the aperture makes a strong impact onto the resistivity of devices. Simulations, performed for a device with 5 μm aperture, show the resistivity is almost an inverse function of aperture doping. At p=$1\cdot10^{18}$ cm^{-3} the resistivity is 450Ω, at p=$5\cdot10^{18}$ cm^{-3} is 85Ω. Two series of VCSEL structures were grown with aperture doping of $7\cdot10^{17}$ cm^{-3} and $3\cdot10^{18}$ cm^{-3}. The improvement of a serial resistance was less than awaited according simulations and was 260Ω from 360Ω for devices with 10 μm aperture.

The QDs were combined in a group of 3 layers with 35 nm thick spacers and placed in

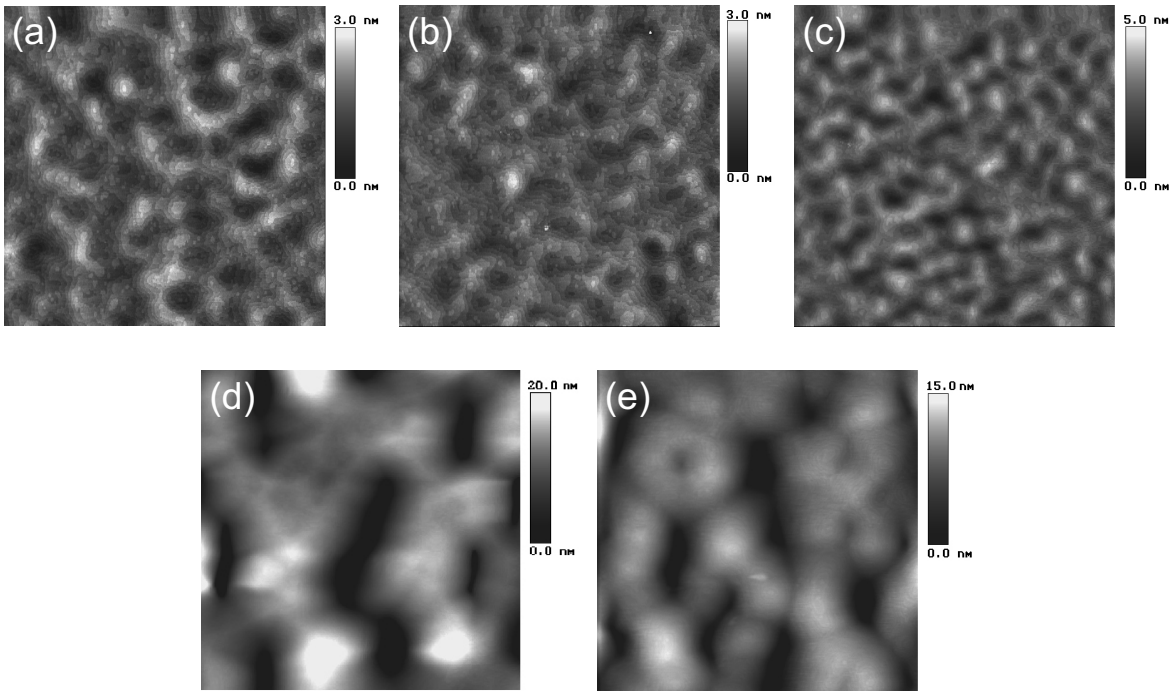

Figure 5.4: AFM images of a 6 pair AlAs/GaAs DBR grown at 625℃ with different buffers and growth interruptions between the layers, see explanation in text. Each image displays an area of 10×10 μm. A height scale is shown on the right side of each image.(a) no buffer, 30s GRI, (b) 1 buffer layer, 30s GRI, (c) 3 buffer layers, 30s GRI, (d) 1 buffer layer, no GRI, (e) 1 buffer layer, 1 min GRI

the central maxima of the optical field. Samples with 1, 2 and 3 groups were grown, i.e. 3, 6, and 9 QD layers. The Bragg mirrors consist of 7 and 6 pairs at bottom and top, respectively. Reflectance spectra of samples before and after oxidation, and respective simulations are shown in Fig. 5.5. The cavity dip of the as grown structure (Fig. 5.5.a) is at 1.5 μm and the reflectivity is about 90%, this happens because the mirrors are designed for oxidation. After oxidation the maximum of reflection is shifted to shorter wavelength. The cavity dip at 1100 nm is not resolved in figure 5.5.b, indicating a very high cavity Q factor. From the emission characteristics Q was estimated to exceed a value of 5000.

The devices were processed simultaneously on one quarter of a substrate. Different aperture and mirror diameters were used. First, using lithography and chemically assisted ion beam etching mirrors and cavity were defined in few steps. Afterwards an oxidation of a whole structure was performed. The side walls of mirrors and cavity were covered by SiN_x in order to protect them from degradation during further treatment.

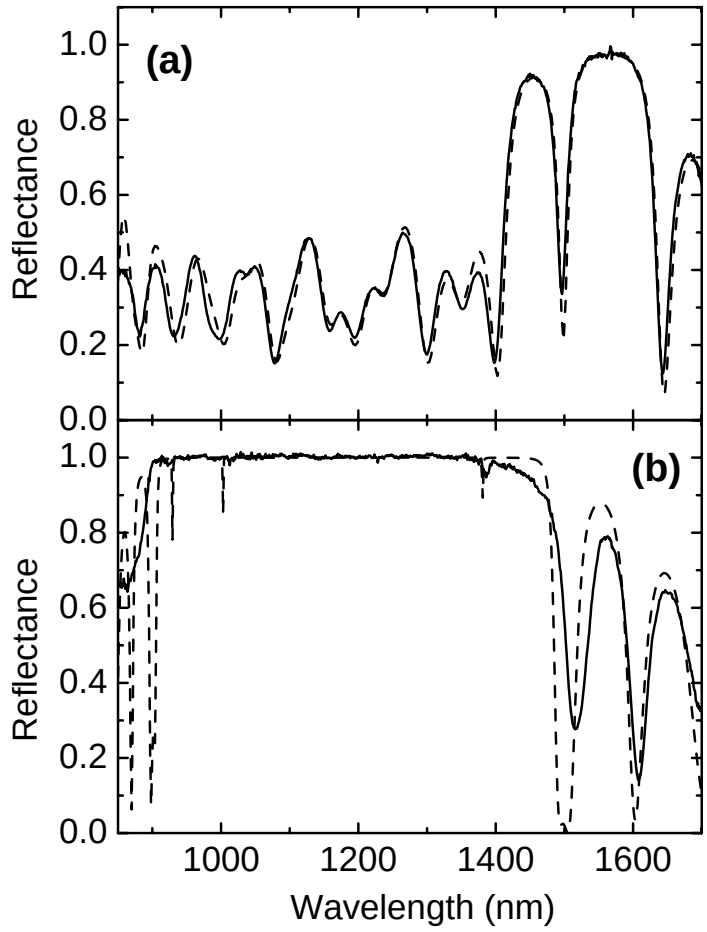

Figure 5.5: Reflectance of a VCSEL structure before selective AlGaAs oxidation (a) and afterwards (b). The measurements are shown with solid lines, and target structure simulation with dashed lines.

At the end the top and the bottom contacts were deposited. A top view photograph of a single device is shown in figure 5.6.

The uniformity of layer thickness over a 2" wafer is better than 1%. The devices were simultaneously fabricated on a quarter substrate and have a very good homogeneity of wavelength and threshold current. A maximal deviation of peak wavelengths as low as $\Delta\lambda/\lambda = 0.005$ over the whole substrate excluding 5 mm from the edge was found.

The device with 3 QD layers does not show lasing at room temperature, indicating insufficient gain. The lasing was observed at low temperatures. Devices with 6 and 9 QD layers showed lasing at room temperature in continuous and pulse current mode.

Normally processed devices have 6 DBR pairs in top mirror, they provide a reflec-

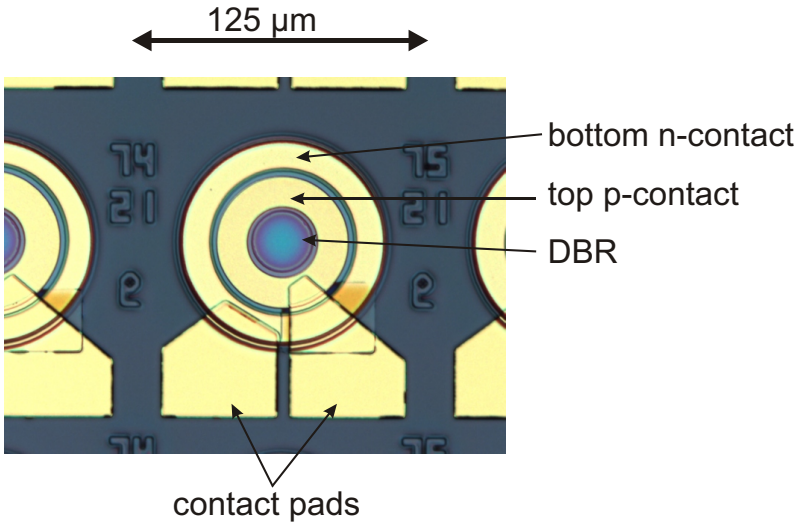

Figure 5.6: A top-view photograph of a single VCSEL device on substrate.

tivity close to 100%. High reflectivity allows to get a low threshold current, but limits the output power since the external efficiency is low (see equation 1.8). The output power can be increased by increasing the output losses due to lower mirror reflectivity. An Efficient method to reduce the mirror reflectivity is a removing of one or more DBR pairs. It was performed using lithography and selective wet etching of GaAs and AlO_x.

According to expectations 6 QD layers provide lower gain than 9 QD layers, limiting the performance of devices. The lasing was observed with 6 and 5 top DBR pairs. The maximal output power in CW mode was achieved as high as 0.23 mW. Devices based on 9 QD layers thanks larger modal gain demonstrated a lasing with a number of top DBR pairs varied from 6 to 3, and has the largest power output. The lowest threshold current was measured as low as 150 μA on device with 6 top pairs.

The power-current and voltage current characteristics are shown in figure 5.7. The measurements were performed at room temperature in CW mode. The devices with 10 μm (a) and 4 μm (b) apertures are presented. The first one demonstrated a multi-mode operation, what can be seen in the lasing spectra given in the inset. A maximum output power as high as 1.42 mW was achieved. The device with 4 μm aperture demonstrated up to 0.68 mW output power in single mode operation with a suppression of side modes about 35 dB.

The output power in CW mode is obviously limited by thermal overheating, what is clearly visible as a saturation and even reduction of light power at large drive current. Since there is almost no overheating in pulse mode, much larger currents can be reached. Similar devices in pulse mode show maximal output power as high as 6.26 mW for

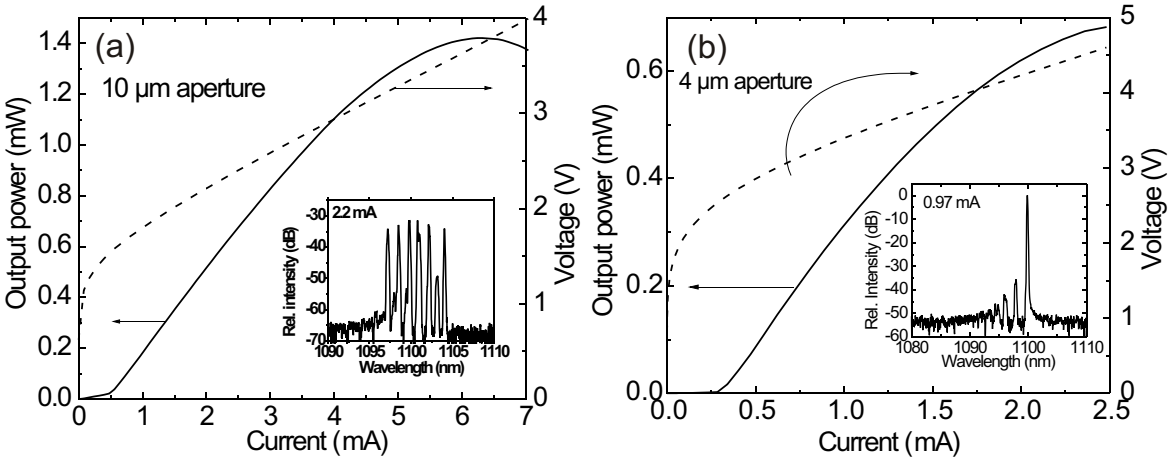

Figure 5.7: P-I and U-I diagrams of a VCSEL with 5 top mirror pairs. An aperture diameter is (a) 10 μm, (b) 4 μm. The insets show the lasing spectra at 2.2 mA injection current (a) and 0.97 mA (b).

10 μm aperture and up to 3.3 mW in single mode operation for 4 μm, what is shown in figure 5.8. An external efficiency as high as 47% was reached.

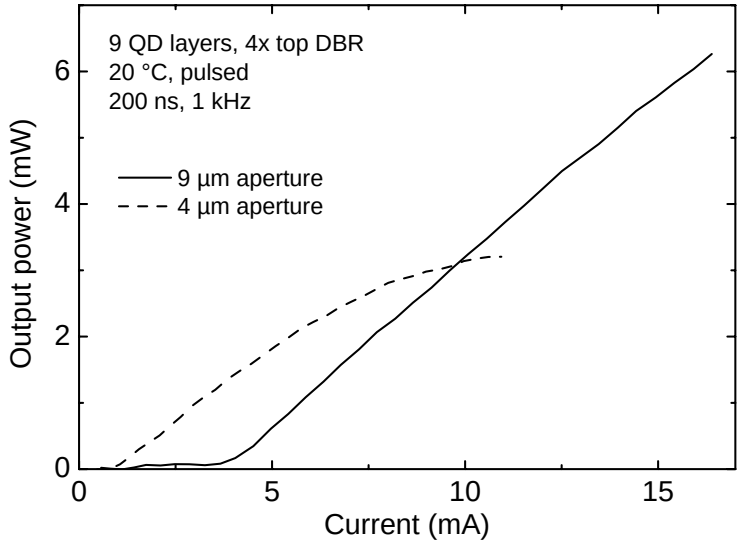

Figure 5.8: P-I and U-I diagrams of a VCSELs with 4 top mirror pairs and 9 μm, and 4 μm aperture in pulse current mode.

Chapter 6

Summary

Within this work a growth of self-assembled InGaAs QDs on GaAs substrates was studied. The growth was performed using metal organic vapour phase epitaxy. QDs formed in the Stranski-Krastanow mode were investigated with the purpose of implementation as an active zone of light emitting devices, namely edge emitting lasers and vertical cavity lasers (VCSEL).

Highly toxic arsine (AsH_3), a typical arsenic precursor in MOCVD of V-III semiconductors, was substituted with an alternative less toxic, liquid precursor tertiarybutylarsine (TBAs). The safety of work is improved, since TBAs has relative low vapour pressure at room temperature in contrast to arsine, which is kept under high pressure. TBAs was proven to be better suitable for low temperature growth, such as growth of QDs, thanks to low decomposition temperature comparing with AsH_3.

The QD growth was investigated from a point of view how different growth parameters, such as growth temperature, V/III ratio, composition and others influence the optical and structural properties of QDs. A significant difference was found between MBE and MOCVD growth concerning the evolution of a QD array by changing the deposition thickness. The composition of QDs was found to have a great impact on QD parameters such as size and density. InGaAs QDs have generally better structural quality and a monomodal size distribution, whereas InAs QDs have a bimodal size distribution and often contain dislocated clusters.

A modification of QD growth was investigated by deposition of QDs on different surfaces, namely InGaAs and InGaP templates. A strong influence of a chemical composition of an underlayer on properties of QDs was found. An InGaAs template increases the density of QDs, what was also observed by other research groups. High QD density allows to reach high modal gain and stable operation of lasers based on QDs. A bimodal size distribution of InGaAs QDs deposited on InGaP template was

observed. The separation of ground state energy levels of QDs with different size was found to be about 150-200 meV being the largest separation to our knowledge reported for multimodal distributed QDs.

An in-situ annealing was developed in order to reduce the density of structural defects in a QD array. TEM images and PL show a disappearance of plastically relaxed clusters in the samples subjected to in-situ annealing.

Lasers based on different types of InGaAs QDs were fabricated. A correlation of structural perfection of QDs and laser performance was observed. Lasers based on InGaAs QDs demonstrate in general better characteristics than lasers based on InAs QDs. A minimal threshold current of 55 A/cm^2 was demonstrated using 3-fold stacked $In_{0.5}Ga_{0.5}As$ QDs. A long wavelength lasing near 1.24 μm at room temperature was demonstrated using 10-fold stacked $In_{0.65}Ga_{0.35}As$ QDs and InAs QDs on $In_{0.3}Ga_{0.7}As$ template both overgrown with strain-reducing 5 nm $In_{0.2}Ga_{0.8}As$ QW. It was found that the defect reduction is crucial for stable operation of long wavelength lasers. Threshold current of both lasers depicts a typical behaviour on temperature for lasers based on QDs. A T_0 is negative or equal to infinity below 225-250 K caused by non-Fermi energy distribution of charge carriers.

Vertical-cavity surface-emitting lasers based on $In_{0.5}Ga_{0.5}As$ QDs were demonstrated. Devices based on 6 and 9 QD-stacks showed a lasing at room temperature. The maximal output power as high as 1.42 mW in multimode operation and up to 0.68 mW in single mode operation in CW mode were achieved with the device based on 9 QD stacks. Pulse current operation eliminates the overheating of the active zone providing the output power up to 6.26 mW and 3.3 mW in multimode and single mode respectively.

The reflectometry and reflectance anisotropy spectroscopy were implemented for in-situ control of edge-emitting lasers and VCSEL growth. It was shown a possibility to control the growth rate of GaAs and AlGaAs with an accuracy of 1% as well as the composition of AlGaAs with an accuracy of 2%. The n- and p- type doping induce a change of RAS response giving a method to estimate the doping level during growth. The doping profile of complicated structures could be analyzed what was shown on an example of an unintentional GaAs doping with Te, caused by memory effect. A doping level from $2{\cdot}10^{17}$ cm^{-3} could be measured. The large noise to signal ratio, however, restricts the implementation of this method to layers thicker than 200 nm.

List of acronyms

AAPS	activated alloy phase separation
AFM	atomic force microscopy
CL	cathode luminescence
CW	continuous wave
DBR	distributed Bragg reflector
DWELL	dots-in-a-well (QDs in InGaAs matrix)
GRI	growth interruption
MBE	molecular beam epitaxy
ML	monolayer
MOCVD	metalorganic chemical vapor deposition
PL	photoluminescence
PLE	photoluminescence excitation spectroscopy
QD	quantum dot
QW	quantum well
RA	reflectance anisotropy
RAS	reflectance anisotropy spectroscopy
RHEED	reflection of high-energy electron diffraction
RT	room temperature
SL	super lattice
STM	scanning tunnelling microscopy
TEM	transmission electron microscopy
VCSEL	vertical-cavity surface-emitting laser
XRD	X-ray diffractometry

Precursors

AsH_3	arsine (arsenic hydride)
CBr_4	carbon tetrabromide
DETe	diethyltellurium
DTBSi	ditertiarybutylsilane
PH_3	phosphine (phosphor hydride)
TBAs	tertiarybutylarsine
TBP	tertiarybutylphosphine
TEGa	triethylgallium
TMAl	trimethylaluminum
TMGa	trimethylgallium
TMIn	trimethylindium

Bibliography

[1] D. Bimberg, M. Grundmann, and N.N. Ledentsov. *Quantum Dot Heterostructures*. John Wiley & Sons, Chichester, 1998.

[2] M. Grundmann, editor. *Nano-Optoelectronics*. Springer, Berlin Heidelberg, 2002.

[3] T.K. Sharma, M. Zorn, F. Bugge, R. Hülsewede, G. Erbert, and M. Weyers, *High-Power Highly Strained InGaAs Quantum-Well Lasers Operating at 1.2 μm*, IEEE Photon. Technol. Lett., **14**, 887 (2002).

[4] N. Tansu, J.-Y. Yeh, and L.J. Mawst, *Extremely low threshold-current-density InGaAs quantum-well lasers with emission wavelength of 1215-1233 nm*, Appl. Phys. Lett., **82**, 4038 (2003).

[5] K.J. Vahala, *Quantum box fabrication tolerance and size limits in semiconductors and their effect on optical gain*, IEEE Journal of Quantum Electronics, **24**, 523 (1988).

[6] M. Grundmann, J. Christen, N.N. Ledentsov, J. Böhrer, D. Bimberg, S.S. Ruvimov, P. Werner, U. Richter, U. Gösele, J. Heydenreich, V.M. Ustinov, A.Y. Egorov, A.E. Zhukov, P.S. Kop'ev, and Z.I. Alferov, *Ultranarrow Luminescence Lines from Single Quantum Dots*, Phys. Rev. Lett., **74**, 4043 (1995).

[7] M. Sugawara, K. Mukai, Y. Nakata, H. Ishikawa, and A. Sakamoto, *Effect of homogeneous broadening of optical gain on lasing spectra in self-assembled $In_xGa_{1-x}As/GaAs$ quantum dot lasers*, Phys. Rev. B, **61**, 7595 (2000).

[8] M.A. Reed, R.T. Bate, K. Bradshaw, W.M. Duncan, W.R. Frensley, J.W. Lee, and H.D. Shih, *Spatial quantization in GaAsAlGaAs multiple quantum dots*, J. Vac. Sci. Technol. B, **4**, 358 (1986).

[9] K. Kash, A. Scherer, J.M. Worlock, H.G. Craighead, and M.C. Tamargo, *Optical spectroscopy of ultrasmall structures etched from quantum wells*, Appl. Phys. Lett., **49**, 1043 (1986).

[10] Y. Miyamoto, M. Cao, Y. Shingai, K. Furuya, Y. Suematsu, K.G. Ravikumar, and S. Arai, *Light Emission from Quantum-Box Structure by Current Injection*, Jpn. J. Appl. Phys., **26**, L225 (1987).

[11] V.A. Shchukin, N.N. Ledentsov, and D. Bimberg. *Epitaxy of Nanostructures*. Springer, 2004.

[12] V.A. Shchukin and D. Bimberg, *Spontaneous ordering of nanostructures on crystal surfaces*, Rev. Mod. Phys., **71**, 1125 (1999).

[13] J.W. Matthews and A.E. Blakeslee, *Defects in epitaxial multilayers: I. Misfit dislocations*, J. Crystal Growth, **27**, 118 (1974).

[14] R. People and J.C. Bean, *Calculation of critical layer thickness versus lattice mismatch for Ge_xSi_{1x}/Si strained-layer heterostructures*, Appl. Phys. Lett., **47**, 322 (1985).

[15] S.M. Wang, T.G. Andersson, and M.J. Ekenstedt, *Temperature-dependent transition from two-dimensional to three-dimensional growth in highly strained $In_xGa_{1-x}As/GaAs$ (0.36<x<1) single quantum wells*, Appl. Phys. Lett., **61**, 3139 (1992).

[16] V.M. Ustinov, A.E. Zhukov, A.Y. Egorov, and N.A. Maleev. *Quantum Dot Lasers*. Oxford University Press, 2003.

[17] M. Sopanen, H. Lipsanen, and J. Ahopelto, *Self-organized InP islands on (100) GaAs by metalorganic vapor phase epitaxy*, Appl. Phys. Lett., **67**, 3768 (1995).

[18] B.R. Bennett, R. Magno, and B.V. Shanabrook, *Molecular beam epitaxial growth of InSb, GaSb, and AlSb nanometer-scale dots on GaAs*, Appl. Phys. Lett., **68**, 505 (1996).

[19] I. Daruka and A.-L. Barabási, *Dislocation-Free Island Formation in Heteroepitaxial Growth: A Study at Equilibrium*, Phys. Rev. Lett., **79**, 3708 (1997).

[20] A.-L. Barabási, *Self-assembled island formation in heteroepitaxial growth*, Appl. Phys. Lett., **70**, 2565 (1997).

[21] N.N. Ledentsov, V.A. Shchukin, D. Bimberg, V.M. Ustinov, N.A. Cherkashin, Y.G. Musikhin, B.V. Volovik, G.E. Cirlin, and Z.I. Alferov, *Reversibility*

of the island shape, volume and density in StranskiKrastanow growth, Semicond. Sci. Technol., **16**, 502 (2001).

[22] K. Pötchke, L. Müller-Kirsch, R. Heitz, R.L. Sellin, U.W. Pohl, D. Bimberg, N. Zakharov, and P. Werner, *Ripening of self-organized InAs quantum dots*, Physica E, **21**, 606 (2004).

[23] L. Goldstein, F. Glas, J.Y. Marzin, M.N. Charasse, and G.L. Roux, *Growth by molecular beam epitaxy and characterization of InAs/GaAs strained-layer superlattices*, Appl. Phys. Lett., **47**, 1099 (1985).

[24] J.P. McCaffrey, M.D. Robertson, S. Fafard, Z.R. Wasilewski, E.M. Griswold, and L.D. Madsen, *Determination of the size, shape, and composition of indium-flushed self-assembled quantum dots by transmission electron microscopy*, J. Appl. Phys., **88**, 2272 (2000).

[25] J. Marquez, L. Geelhaar, and K. Jacobi, *Atomically resolved structure of InAs quantum dots*, Appl. Phys. Lett., **78**, 2309 (2001).

[26] A. Lemaitre, G. Patriarche, and F. Glas, *Composition profiling of InAs/GaAs quantum dots*, Appl. Phys. Lett., **85**, 3717 (2004).

[27] M.V. Maximov, A.F. Tsatsulnikov, B.V. Volovik, D.S. Sizov, Y.M. Shernyakov, I.N. Kaiander, A.E. Zhukov, A.R. Kovsh, S.S. Mikhrin, V.M. Ustinov, Z.I. Alferov, R. Heitz, V.A. Shchukin, N.N. Ledentsov, D. Bimberg, Y.G. Musikhin, and W. Neumann, *Tuning quantum dot properties by activated phase separation of an InGa(Al)As alloy grown on InAs stressors*, Phys. Rev. B, **62**, 16671 (2000).

[28] A. Lenz, R. Timm, H. Eisele, C. Hennig, S.K. Becker, R.L. Sellin, U.W. Pohl, D. Bimberg, and M. Dähne, *Reversed truncated cone composition distribution of $In_{0.8}Ga_{0.2}As$ quantum dots overgrown by an $In_{0.1}Ga_{0.9}As$ layer in a GaAs matrix*, Appl. Phys. Lett., **81**, 5150 (2002).

[29] O. Stier, M. Grundmann, and D. Bimberg, *Electronic and optical properties of strained quantum dots modeled by 8-band k·p theory*, Phys. Rev. B, **59**, 5688 (1999).

[30] O. Stier. *Electronic and Optical Properties of Quantum Dots and Wires*. PhD thesis, Technische Universität Berlin, 2000.

[31] L.-W. Wang, J. Kim, and A. Zunger, *Electronic structures of [110]-faceted self-assembled pyramidal InAs/GaAs quantum dots*, Phys. Rev. B, **59**, 5678 (1998).

[32] J. Kim, L.-W. Wang, and A. Zunger, *Comparison of the electronic structure of InAs/GaAs pyramidal quantum dots with different facet orientations*, Phys. Rev. B, **57**, R9408 (1998).

[33] T. Yang, J. Tatebayashi, S. Tsukamoto, M. Nishioka, and Y. Arakawa, *Narrow photoluminescence linewidth (<17meV) from highly uniform self-assembled InAs/GaAs quantum dots grown by low-pressure metalorganic chemical vapor deposition*, Appl. Phys. Lett., **84**, 2817 (2004).

[34] M.H. Baier, S. Watanabe, E. Pelucchi, and E. Kapon, *High uniformity of site-controlled pyramidal quantum dots grown on prepatterned substrates*, Appl. Phys. Lett., **84**, 1943 (2004).

[35] A. Markus, A. Fiore, J.D. Ganiere, U. Oesterle, J.X. Chen, B. Deveaud, M. Ilegems, and H. Riechert, *Comparison of radiative properties of InAs quantum dots and GaInNAs quantum wells emitting around 1.3 μm*, Appl. Phys. Lett., **80**, 911 (2002).

[36] K. Mukai, N. Ohtsuka, H. Shoji, and M. Sugawara, *Emission from discrete levels in self-formed InGaAs/GaAs quantum dots by electric carrier injection: Influence of phonon bottleneck*, Appl. Phys. Lett., **68**, 3013 (1996).

[37] S. Malik, E.C.L. Ru, D. Childs, and R. Murray, *Time-resolved studies of annealed InAs/GaAs self-assembled quantum dots*, Phys. Rev. B, **63**, 155313 (2001).

[38] Y. Arakawa and H. Sakaki, *Multidimensional quantum well laser and temperature dependence of its threshold current*, Appl. Phys. Lett., **40**, 939 (1982).

[39] M. Asada, Y. Miyamoto, and Y. Suematsu, *Gain and the threshold of three-dimensional quantum-box lasers*, IEEE Journal of Quantum Electronics, **22**, 1915 (1986).

[40] N.N. Ledentsov, V.M. Ustinov, A.Y. Egorov, A.E. Zhukov, M.V. Maximov, I.G. Tabatadze, and P.S. Kop'ev, *Optical properties of heterostructures with InGaAs-GaAs quantum clusters*, Fiz. i Tekn. Poluprovodn., **28**, 1484 (1993).

[41] N. Kirstaedter, N.N. Ledentsov, M. Grundmann, D. Bimberg, V.M. Ustinov, S.S. Ruvimov, M.V. Maximov, P.S. Kop'ev, Z.I. Alferov, U. Richter, P. Werner, U. Gosele, and J. Heydenreich, *Low threshold, large T_0 injection laser emission from (InGa)As quantum dots*, Electron. Lett., **30**, 1416 (1994).

[42] L.V. Asryan and R.A. Suris, *Inhomogeneous line broadening and the threshold current density of a semiconductor quantum dot laser*, Semicond. Sci. Technol., **11**, 554 (1996).

[43] L.V. Asryan, M. Grundmann, N.N. Ledentsov, O. Stier, R.A. Suris, and D. Bimberg, *Maximum modal gain of a self-assembled InAs/GaAs quantum-dot laser*, J. Appl. Phys., **90**, 1666 (2001).

[44] L.V. Asryan, M. Grundmann, N.N. Ledentsov, O. Stier, R.A. Suris, and D. Bimberg, *Effect of Excited-State Transitions on the Threshold Characteristics of a Quantum Dot Laser*, IEEE Journal of Quantum Electronics, **36**, 418 (2001).

[45] M. Grundmann and D. Bimberg, *Theory of random population for quantum dots*, Phys. Rev. B, **55**, 9740 (1997).

[46] M. Grundmann and D. Bimberg, *Gain and Threshold of Quantum Dot Lasers: Theory and Comparison to Experiments*, Jpn. J. Appl. Phys., **36**, 4181 (1997).

[47] N. Kirstaedter, O.G. Schmidt, N.N. Ledentsov, D. Bimberg, V.M. Ustinov, A.Y. Egorov, A.E. Zhukov, M.V. Maximov, P.S. Kop'ev, and Z.I. Alferov, *Gain and differential gain of single layer InAs/GaAs quantum dot injection lasers*, Appl. Phys. Lett., **69**, 1226 (1996).

[48] O.G. Schmidt, N. Kirstaedter, N.N. Ledentsov, M.-H. Mao, D. Bimberg, V.M. Ustinov, A.Y. Egorov, A.E. Zhukov, M.V. Maximov, P.S. Kop'ev, and Z.I. Alferov, *Prevention of gain saturation by multi-layer quantum dot lasers*, Electron. Lett., **32**, 1302 (1996).

[49] A.E. Zhukov, A.R. Kovsh, V.M. Ustinov, A.Y. Egorov, N.N. Ledentsov, A.F. Tsatsul'nikov, M.V. Maksimov, S.V. Zatsev, Y.M. Shernyakov, A.V. Lunev, P.S. Kop'ev, Z.I. Alferov, and D. Bimberg, *Gain characteristics of quantum-dot injection lasers*, Semiconductors, **33**, 1013 (1999).

[50] R.P. Mirin, J.P. Ibbetson, K. Nishi, A.C. Gossard, and J.E. Bowers, *1.3 μm photoluminescence from InGaAs quantum dots on GaAs*, Appl. Phys. Lett., **67**, 3795 (1995).

[51] K. Mukai, N. Ohtsuka, M. Sugawara, and S. Yamazaki, *Self-Formed $In_{0.5}Ga_{0.5}As$ Quantum Dots on GaAs Substrates Emitting at 1.3 μm*, Jpn. J. Appl. Phys., **33**, L1710 (1994).

[52] F. Heinrichsdorff, N. Zakharov, P. Werner, A. Krost, and D. Bimberg. *Electroluminescence of stacked In(Ga)As/GaAs QDs at 1.3 μm - 1.4 μm.* In *41st Electronic Materials Conference, Santa Barbara, USA, Juli 1999*, 1999.

[53] G.T. Liu, A. Stintz, H. Li, K.J. Malloy, and L.F. Lester, *Extremely low room-temperature threshold current density diode lasers using InAs dots in* $In_{0.15}$ $Ga_{0.85}As$ *quantum well*, Electron. Lett., **35**, 1163 (1999).

[54] D.L. Huffaker, G. Park, Z. Zou, O.B. Shchekin, and D.G. Deppe, *1.3 μm room-temperature GaAs-based quantum-dot laser*, Appl. Phys. Lett., **73**, 2564 (1998).

[55] A.E. Zhukov, A.R. Kovsh, N.A. Maleev, S.S. Mikhrin, V.M. Ustinov, A.F. Tsatsul'nikov, M.V. Maximov, B.V. Volovik, D.A. Bedarev, Y.M. Shernyakov, P.S. Kop'ev, Z.I. Alferov, N.N. Ledentsov, and D. Bimberg, *Long-wavelength lasing from multiply stacked InAs/InGaAs quantum dots on GaAs substrates*, Appl. Phys. Lett., **75**, 1926 (1999).

[56] G. Park, O.B. Shchekin, D.L. Huffaker, and D.G. Deppe, *Low-Threshold Oxide-Confined 1.3-μm Quantum-Dot Laser*, IEEE Photon. Technol. Lett., **12**, 230 (2000).

[57] A. Passaseo, M.D. Vittorio, M.T. Todaro, I. Tarantini, M.D. Giorgi, R. Cingolani, A. Taurino, M. Catalano, A. Fiore, A. Markus, J.X. Chen, C. Paranthoen, U. Oesterle, and M. Ilegems, *Comparison of radiative and structural properties of 1.3 μm* $In_xGa_{1-x}As$ *quantum-dot laser structures grown by metalorganic chemical vapor deposition and molecular-beam epitaxy: Effect on the lasing properties*, Appl. Phys. Lett., **82**, 3632 (2003).

[58] P.G. Eliseev, H. Li, G.T. Liu, A. Stintz, T.C. Newell, L.F. Lester, and K.J. Malloy. *Gain in ultra-low-threshold InAs/InGaAs quantum dot lasers.* In *IEEE 17th International Semiconductor Laser Conference*, page 65, 2000.

[59] K. Mukai, Y. Nakata, K. Otsubo, M. Sugawara, N. Yokoyama, and H. Ishikawa, *1.3-μm CW lasing characteristics of self-assembled InGaAs-GaAsquantum dots*, IEEE Journal of Quantum Electronics, **36**, 472 (2000).

[60] M.V. Maximov, Y.M. Shernyakov, I.N. Kaiander, D.A. Bedarev, E.Y. Kondrat'eva, P.S. Kop'ev, A.R. Kovsh, N.A. Maleev, S.S. Mikhrin, A.F. Tsatsul'nikov, V.M. Ustinov, B.V. Volovik, A.E. Zhukov, Z.J. Alferov, N.N. Ledentsov, and D. Bimberg, *Single transverse mode operation of long wavelength (∼1.3 μm) InAsGaAs quantum dot laser*, Electron. Lett., **35**, 2038 (1999).

[61] I.R. Sellers, H.Y. Liu, K.M. Groom, D.T. Childs, D. Robbins, T.J. Badcock, M. Hopkinson, D.J. Mowbray, and M.S. Skolnick, *1.3 μm InAs/GaAs multilayer quantum-dot laser with extremely low room-temperature threshold current density*, Electron. Lett., **40**, 1412 (2004).

[62] J. Tatebayashi, Y. Arakawa, N. Hatori, H. Ebe, M. Sugawara, H. Sudo, and A. Kuramata, *InAs/GaAs self-assembled quantum-dot lasers grown by metal-organic chemical vapor deposition-Effects of postgrowth annealing on stacked InAs quantum dots*, Appl. Phys. Lett., **85**, 1024 (2004).

[63] J. Tatebayashi, N. Hatori, M. Ishida, H. Ebe, M. Sugawara, Y. Arakawa, H. Sudo, and A. Kuramata, *1.28 μm lasing from stacked InAs/GaAs quantum dots with low-temperature-grown AlGaAs cladding layer by metalorganic chemical vapor deposition*, Appl. Phys. Lett., **86**, 053107 (2005).

[64] N. Nuntawong, Y.C. Xin, S. Birudavolu, P.S. Wong, S. Huang, C.P. Hains, and D.L. Huffaker, *Quantum dot lasers based on a stacked and strain-compensated active region grown by metal-organic chemical vapor deposition*, Appl. Phys. Lett., **86**, 193115 (2005).

[65] D.G. Deppe, D.L. Huffaker, Z. Zou, G. Park, and O.B. Shchekin, *Spontaneous emission and threshold characteristics of 1.3-μm InGaAs-GaAs quantum-dot GaAs-based lasers*, IEEE Journal of Quantum Electronics, **35**, 1238 (1999).

[66] O.B. Shchekin, G. Park, D.L. Huffaker, and D.G. Deppe, *Discrete energy level separation and the threshold temperature dependence of quantum dot lasers*, Appl. Phys. Lett., **77**, 466 (2000).

[67] A.E. Zhukov, V.M. Ustinov, A.Y. Egorov, A.R. Kovsh, A.F. Tsatsul'nikov, M.V. Maximov, N.N. Ledentsov, S.V. Zaitsev, N.Y. Gordeev, V.I. Kopchatov, Y.M. Shernyakov, P.S. Kop'ev, D. Bimberg, and Z.I. Alferov, *Injection lasers based on InGaAs quantum dots in an AlGaAs matrix*, Journal of Electronics Materials, **27**, 106 (1998).

[68] H.Y. Liu, I.R. Sellers, M. Hopkinson, C.N. Harrison, D.J. Mowbray, and M.S. Skolnick, *Engineering carrier confinement potentials in 1.3-μm InAs/GaAs quantum dots with InAlAs layers: Enhancement of the high-temperature photoluminescence intensity*, Appl. Phys. Lett., **83**, 3716 (2003).

[69] M.V. Maximov, I.V. Kochnev, Y.M. Shernyakov, S.V. Zaitsev, N.Y. Gordeev, A.F. Tsatsul'nikov, A.V. Sakharov, I.L. Krestnikov, P.S. Kop'ev, Z.I. Alferov,

N.N. Ledentsov, D. Bimberg, A.O. Kosogov, P. Werner, and U. Gsele, *InGaAs/GaAs Quantum Dot Lasers with Ultrahigh Characteristic Temperature (T_0= 385 K) Grown by Metal Organic Chemical Vapour Deposition*, Jpn. J. Appl. Phys., **36**, 4221 (1997).

[70] S. Fathpour, Z. Mi, P. Bhattacharya, A.R. Kovsh, S.S. Mikhrin, I.L. Krestnikov, A.V. Kozhukhov, and N.N. Ledentsov, *The role of Auger recombination in the temperature-dependent output characteristics ($T_0 = \infty$) of p-doped 1.3 μm quantum dot lasers*, Appl. Phys. Lett., **85**, 5164 (2004).

[71] A.E. Zhukov, V.M. Ustinov, A.Y. Egorov, A.R. Kovsh, A.F. Tsatsul'nikov, N.N. Ledentsov, S.V. Zaitsev, N.Y. Gordeev, P.S. Kopv, and Z.I. Alferov, *Negative Characteristic Temperature of InGaAs Quantum Dot Injection Laser*, Jpn. J. Appl. Phys., **36**, 4216 (1997).

[72] Z. Zou, O.B. Shchekin, G. Park, D.L. Huffaker, and D.G. Deppe, *Threshold temperature dependence of lateral-cavity quantum-dot lasers*, IEEE Photon. Technol. Lett., **10**, 1673 (1998).

[73] D. Ouyang, N.N. Ledentsov, S. Bognr, F. Hopfer, R.L. Sellin, I.N. Kaiander, and D. Bimberg, *Impact of the mesa etching profiles on the spectral hole burning effects in quantum dot lasers*, Semicond. Sci. Technol., **19**, L43 (2004).

[74] G.B. Stringfellow. *Organometallic Vapor-Phase Epitaxy.* Academic Press, 1999.

[75] G.B. Stringfellow, *Novel precursors for organometallic vapor phase epitaxy*, J. Crystal Growth, **128**, 503 (1993).

[76] H. Ishikawa, T. Izumiya, and M. Mashita, *Metalorganic Chemical Vapor Deposition of AlGaAs Using Tertiarybuthylarsine*, Jpn. J. Appl. Phys., **34**, 6377 (1995).

[77] S. Leu, F. Hohnsdorf, W. Stolz, R. Becker, A. Salzmann, and A. Greiling, *C- and O-incorporation in (AlGa)As epitaxial layers grown by MOVPE using TBAs*, J. Crystal Growth, **195**, 98 (1998).

[78] T. Takeuchi, Y.-L. Chang, A. Tandon, D. Bour, S. Corzine, R. Twist, M. Tan, and H.-C. Luan, *Low threshold 1.2 μm InGaAs quantum well lasers grown under low As/III ratio*, Appl. Phys. Lett., **80**, 2445 (2002).

[79] R. Beccard, G. Lengeling, D. Schmitz, Y. Gigase, and H. Jürgensen, *Replacements of hydrides by TBAs and TBP for the growth of various III-V materials in production scale MOVPE reactors*, J. Crystal Growth, **170**, 97 (1997).

[80] G. Kirpal, M. Gerhardt, V. Gottschalch, R. Franzheld, H.C. Semmelhack, and B.Xu, *Effects of organic As-precursors on the incorporation of In and Ga into (GaIn)As films grown by metal-organic vapor-phase epitaxy*, Thin Solid Films, **342**, 113 (1999).

[81] D. Leonard, K. Pond, and P.M. Petroff, *Critical layer thickness for self-assembled InAs islands on GaAs*, Phys. Rev. B, **56**, 11687 (1994).

[82] A.Y. Egorov, A.E. Zhukov, P.S. Kop'ev, N.N. Ledentsov, M.V. Maximov, V.M. Ustinov, A.F. Tsatsul'nikov, D.L. Fedorov, D. Bimberg, and Z.I. Alferov, *Optical emission range of strained InAs quantum dots in GaAs matrix*, Semiconductors, **30**, 707 (1996).

[83] P.B. Joyce, T.J. Krzyzewski, G.R. Bell, T.S. Jones, E.C.L. Ru, and R. Murray, *Optimizing the growth of 1.3 μm InAs/GaAs quantum dots*, Phys. Rev. B, **64**, 235317 (2001).

[84] J. Johansson and W. Seifert, *Kinetics of self-assembledislandformation:Part I - Island density*, J. Crystal Growth, **234**, 132 (2002).

[85] J. Johansson and W. Seifert, *Kinetics of self-assembledislandformation:Part II Island size*, J. Crystal Growth, **234**, 139 (2002).

[86] V.G. Dubrovski, Y.G. Musikhin, G.E. Cirlin, V.A. Egorov, N.K. Polyakov, Y.B. Samsonenko, A.A. Tonkikh, N.V. Kryzhanovskaya, N.A. Bert, and V.M. Ustinov, *Dependence of Structural and Optical Properties of QD Arrays in an InAs/GaAs System on Surface Temperature and Growth Rate*, Semiconductors, **38**, 329 (2004).

[87] J. Tatebayashi, M. Nishioka, and Y. Arakawa, *Over 1.5 μm light emission from InAs quantum dots embedded in InGaAs strain-reducing layer grown by metal-organic chemical vapor deposition*, Appl. Phys. Lett., **78**, 3469 (2001).

[88] B.D. Min, Y. Kim, E.K. Kim, S.-K. Min, and M.J. Park, *Suppression of Ostwald ripening in $In_{0.5}Ga_{0.5}As$ quantum dots on a vicinal (100) substrate*, Phys. Rev. B, **57**, 11879 (1998).

[89] M. Berti, A.V. Drigo, G. Rossetto, and G. Torzo, *Experimental evidence of two-dimensional-three-dimensional transition in the Stranski-Krastanow coherent growth*, J. Vac. Sci. Technol. B, **15**, 1794 (1997).

[90] G. Saint-Girons, G. Patriarche, A. Mereuta, and I. Sagnes, *Origin of the bimodal distribution of low-pressure metal-organic-vapor-phase-epitaxy grown InGaAs/GaAs quantum dots*, J. Appl. Phys., **91**, 3859 (2002).

[91] G.X. Qian, R.M. Martin, and D.J. Chadi, *First-principles study of the atomic reconstructions and energies of Ga- and As-stabilized GaAs(100) surfaces*, Phys. Rev. B, **38**, 7649 (1988).

[92] N.N. Ledentsov, M. Grundmann, N. Kirstaedter, O. Schmidt, R. Heitz, J. Böhrer, D. Bimberg, V.M. Ustinov, V.A. Shchukin, A.Y. Egorov, A.E. Zhukov, S. Zaitsev, P.S. Kopev, Z.I. Alferov, S.S. Ruvimov, A.O. Kosogov, P. Werner, U. Gösele, and J. Heydenreich, *Ordered arrays of quantum dots: Formation, electronic spectra, relaxation phenomena, lasing*, Solid State Electronics, **40**, 785 (1996).

[93] R. Leon, C. Lobo, J. Zou, T. Romeo, and D.J.H. Cockayne, *Stable and Metastable InGaAs/GaAs Island Shapes and Surfactantlike Suppression of the Wetting Transformation*, Phys. Rev. Lett., **81**, 2486 (1998).

[94] P.B. Joyce, T.J. Krzyzewski, G.R. Bell, T.S. Jones, S. Malik, D. Childs, and R. Murray, *Growth rate effects on the size, composition and optical properties of InAs/GaAs quantum dots grown by molecular beam epitaxy*, J. Crystal Growth, **227-228**, 1000 (2001).

[95] Y. Nakata, K. Mukai, M. Sugawara, K. Ohtsubo, H. Ishikawa, and N. Yokoyama, *Molecular beam epitaxial growth of InAs self-assembled quantum dots with light-emission at 1.3 μm*, J. Crystal Growth, **208**, 93 (2000).

[96] G. Saint-Girons, G. Patriarche, L. Largeau, J. Coelho, A. Mereuta, J.M. Moison, J.M. Gerard, and I. Sagnes, *Bimodal distribution of Indium composition in arrays of low-pressure metalorganic-vapor-phase-epitaxy grown InGaAs/GaAs quantum dots*, Appl. Phys. Lett., **79**, 2157 (2001).

[97] H. Kissel, U. Müller, C. Walther, W.T. Masselink, Y.I. Mazur, G.G. Tarasov, and M.P. Lisitsa, *Size distribution in self-assembled InAs quantum dots on GaAs (001) for intermediate InAs coverage*, Phys. Rev. B, **62**, 7213 (2000).

[98] R.P. Mirin, K.L. Silverman, D.H. Christensen, and A. Roshko, *Narrow photoluminescence linewidths from ensembles of self-assembled InGaAs quantum dots*, J. Vac. Sci. Technol. B, **18**, 1510 (2000).

[99] R. Heitz, F. Guffarth, K. Pötschke, A. Schliwa, D. Bimberg, N.D. Zakharov, and P. Werner, *Shell-like formation of self-organized InAs/GaAs quantum dots*, Phys. Rev. B, **71**, 045325 (2005).

[100] A.R. Kovsh, A.E. Zhukov, N.A. Maleev, S.S. Mikhrin, A.V. Vasil'ev, Y.M. Shernyakov, D.A. Livshits, M.V. Maximov, D.S. Sizov, N.V. Kryzhanovskaya, N.A. Pikhtin, V.A. Kapitonov, I.S. Tarasov, N.N. Ledentsov, V.M. Ustinov, J.-S. Wang, L.-C. Wei, G. Lin, and J.Y. Chi. *High power lasers based on submonolayer InAs-GaAs quantum dots and InGaAs quantum wells.* In *10th International Symposium on Nanostructures: Physics and Technology*, volume Proceedings of SPIE - Volume 5023, page 353, 2002.

[101] Z. Xu, D. Birkedal, M. Juhl, and J.M. Hvam, *Submonolayer InGaAs/GaAs quantum-dot lasers with high modal gain and zero-linewidth enhancement factor*, Appl. Phys. Lett., **85**, 3259 (2004).

[102] D.L. Huffaker and D.G. Deppe, *Electroluminescence efficiency of 1.3 μm wavelength InGaAs/GaAs quantum dots*, Appl. Phys. Lett., **73**, 520 (1998).

[103] S. Krishna, D. Zhu, J. Xu, K.K. Linder, O. Qasaimeh, P. Bhattacharya, and D.L. Huffaker, *Structural and luminescence characteristics of cycled submonolayer InAs/GaAs quantum dots with room-temperature emission at 1.3 μm*, J. Appl. Phys., **86**, 6135 (1999).

[104] B.V. Volovik, D.S. Sizov, A.F. Tsatsul'nikov, Y.G. Musikhin, N.N. Ledentsov, V.M. Ustinov, V.A. Egorov, V.N. Petrov, N.K. Polyakov, and G.E. Tsyrlin, *The Emission from the Structures with Arrays of Coupled Quantum Dots Grown by the Submonolayer Epitaxy in the Spectral Range of 1.3-1.4 μm*, Semiconductors, **34**, 1316 (2000).

[105] A. Passaseo, G. Maruccio, M.D. Vittorio, R. Rinaldi, R. Cingolani, and M. Lomascolo, *Wavelength control from 1.25 to 1.4 μm in $In_xGa_{1-x}As$ quantum dot structures grown by metal organic chemical vapor deposition*, Appl. Phys. Lett., **78**, 1382 (2001).

[106] F. Guffarth, R. Heitz, A. Schliwa, O. Stier, N.N. Ledentsov, A.R. Kovsh, V.M. Ustinov, and D. Bimberg, *Strain engineering of self-organized InAs quantum dots*, Phys. Rev. B, **64**, 085305 (2001).

[107] G. Balakrishnan, S. Huang, L.R. Dawson, and D.L. Huffaker, *Analysis of atomic structure in InAs quantum dashes grown on AlGaAsSb metamorphic buffers*, J. Vac. Sci. Technol. B, **22**, 1529 (2004).

[108] A.A. El-Emawy, S. Birudavolu, P.S. Wong, Y.-B. Jiang, H. Xu, S. Huang, and D.L. Huffaker, *Formation trends in quantum dot growth using metalorganic chemical vapor deposition*, J. Appl. Phys., **93**, 3529 (2003).

[109] R. Jia, D.S. Jiang, H.Y. Liu, Y.Q. Wei, B. Xu, and Z.G. Wang, *Influence of combinedInAlAs and InGaAs strain-reducing laser on luminescence properties of InAs/GaAs quantum dots*, J. Crystal Growth, **234**, 354 (2002).

[110] S.-K. Park, J. Tatebayashi, and Y. Arakawa, *Formation of ultrahigh-density InAs/AlAs quantum dots by metalorganic chemical vapor deposition*, Appl. Phys. Lett., **84**, 1877 (2004).

[111] S. Shirakata, M. Kondow, and T. Kitatani, *Temperature-dependent photoluminescence of high-quality GaInNAs single quantum wells*, Appl. Phys. Lett., **80**, 2087 (2002).

[112] T. Hakkarainen, J.Toivonen, M.Sopanen, and H.Lipsanen, *GaInNAs quantum well structures for 1.55 μm emission on GaAs by atmospheric pressure metal-organic vapor phase epitaxy*, J. Crystal Growth, **234**, 631 (2002).

[113] A. Babiski, J. Jasiski, R. Boek, A. Szepielow, and J.M. Baranowski, *Rapid thermal annealing of InAs/GaAs quantum dots under a GaAs proximity cap*, Appl. Phys. Lett., **79**, 2576 (2001).

[114] N.N. Ledentsov, M.V. Maximov, D. Bimberg, T. Maka, C.M.S. Torres, I.V. Kochnev, I.L. Krestnikov, V.M. Lantratov, N.A. Cherkashin, Y.M. Musikhin, and Z.I. Alferov, *1.3 μm luminescence and gain from defect-free InGaAsGaAs quantum dots grown by metal-organic chemical vapour deposition*, Semicond. Sci. Technol., **15**, 604 (2000).

[115] D.S. Sizov, M.V. Maksimov, A.F. Tsatsulnikov, N.A. Cherkashin, N.V. Kryzhanovskaya, A.B. Zhukov, N.A. Maleev, S.S. Mikhrin, A.P. Vasilev, R. Sellin, V.M. Ustinov, N.N. Ledentsov, D. Bimberg, and Z.I. Alferov, *The*

Influence of Heat Treatment Conditions on the Evaporation of Defect Regions in Structures with InGaAs Quantum Dots in the GaAs Matrix, Semiconductors, **36**, 1020 (2002).

[116] R.L. Sellin, C. Ribbat, M. Grundmann, N.N. Ledentsov, and D. Bimberg, *Close-to-ideal device characteristics of high-power InGaAs/GaAs quantum dot lasers*, Appl. Phys. Lett., **78**, 1207 (2001).

[117] F. Heinrichsdorff, M. Grundmann, O. Stier, A. Krost, and D. Bimberg, *Influence of In/Ga intermixing on the optical properties of InGaAs/GaAs quantum dots*, J. Crystal Growth, **195**, 540 (1998).

[118] F. Liu, S.E. Davenport, H.M. Evans, and M.G. Lagally, *Self-Organized Replication of 3D Coherent Island Size and Shape in Multilayer Heteroepitaxial Films*, Phys. Rev. Lett., **82**, 2528 (1999).

[119] W. Wu, J.R. Tucker, G.S. Solomon, and J. J. S. Harris, *Atom-resolved scanning tunneling microscopy of vertically ordered InAs quantum dots*, Appl. Phys. Lett., **71**, 1083 (1997).

[120] A. Passaseo, R. Rinaldi, M. Longo, S. Antonaci, A.L. Convertino, R. Cingolani, A. Taurino, and M. Catalano, *Structural study of InGaAs/GaAs quantum dots grown by metalorganic chemical vapor deposition for optoelectronic applications at 1.3 μm*, J. Appl. Phys., **89**, 4341 (2001).

[121] Q. Xie, A. Madhukar, P. Chen, and N.P. Kobayashi, *Vertically Self-Organized InAs Quantum Box Islands on GaAs(100)*, Phys. Rev. Lett., **75**, 2542 (1995).

[122] F. Heinrichsdorff. *MOCVD growth and laser applications of In(Ga)As/GaAs Quantum Dots*. PhD thesis, Technische Universität Berlin, 1998.

[123] X.-D. Wang, N. Liu, C.K. Shih, S. Govindaraju, and J. A. L. Holmes, *Spatial correlation-anticorrelation in strain-driven self-assembled InGaAs quantum dots*, Appl. Phys. Lett., **85**, 1356 (2004).

[124] O.B. Shchekin, G. Park, D.L. Huffaker, and D.G. Deppe. *1.3 μm quantum dot lasers with single and stacked active layers*. In *12th Annual Meeting IEEE Lasers and Electro-Optics Society, LEOS '99.*, volume 2, page 465, San Francisco, CA, 1999.

[125] I. Mukhametzhanov, R. Heitz, J. Zeng, P. Chen, and A. Madhukar, *Independent manipulation of density and size of stress-driven self-assembled quantum dots*, Appl. Phys. Lett., **73**, 1841 (1998).

[126] M.V. Maximov, D.A.Bedarev, A.Yu.Egorov, P.S.Kopev, A.R.Kovsh, A.V.Lunev, Yu.G.Musikhin, Yu.M.Shernyakov, A.F.Tsatsulnikov, V.M.Ustinov, B.V.Volovik, A.E.Zhukov, Zh.I.Alferov, N.N.Ledentsov, and D.Bimberg. *Optimization of quantum dot lasers by seeding of quantum dots.* In *Proc. 24th International Conference on The Physics of Semiconductors (ICPS-24), Jerusalem, Israel, ed. D. Gershoni*, 1998.

[127] A.R. Kovsh, A.E. Zhukov, A.Y. Egorov, V.M. Ustinov, Y.M. Shernyakov, M.V. Maximov, V.V. Volovik, A.F. Tsatsul'nikov, Y.V. Musikhin, N.N. Ledentsov, P.S. Kop'ev, D. Bimberg, and Z.I. Alferov, *Molecular beam epitaxy (MBE) growth of composite (In,Al)As/(In,Ga)As vertically coupled quantum dots and their application in injection lasers*, J. Crystal Growth, **201-202**, 1117 (1999).

[128] S.-K. Park, J. Tatebayashi, T. Nakaoka, T. Sato, Y.J. Park, and Y. Arakawa, *Enhanced Optical Properties of High-Density ($> 10^{11} cm^{-2}$) InAs/AlAs Quantum Dots by Hydrogen Passivation*, Jpn. J. Appl. Phys., **43**, 2118 (2004).

[129] A. Stintz, G.T. Liu, A.L. Gray, R. Spillers, S.M. Delgado, and K.J. Malloy, *Characterization of InAs quantum dots in strained $In_xGa_{1-x}As$ quantum wells*, J. Vac. Sci. Technol. B, **80**, 1496 (2000).

[130] J.X. Chen, U. Oesterle, A. Fiore, R.P. Stanley, M. Ilegems, and T. Todaro, *Matrix effects on the structural and optical properties of InAs quantum dots*, Appl. Phys. Lett., **79**, 3681 (2001).

[131] H. Toyoshima, T. Niwa, J. Yamazaki, and A. Okamoto, *In surface segregation and growth-mode transition during InGaAs growth by molecular-beam epitaxy*, Appl. Phys. Lett., **63**, 821 (1993).

[132] G.T. Liu, A. Stintz, H. Li, T.C. Newell, A.L. Gray, P.M. Varangis, K.J. Malloy, and L.F. Lester, *The influence of quantum-well composition on the performance ofquantum dot lasers using InAs-InGaAs dots-in-a-well (DWELL) structures*, IEEE Journal of Quantum Electronics, **36**, 1272 (2000).

[133] J. Jiang, S. Tsao, T. O'Sullivan, W. Zhang, H. Lim, T. Sills, K. Mi, M. Razeghi, G.J. Brown, and M.Z. Tidrow, *High detectivity InGaAs/InGaP quantum-dot*

infrared photodetectors grown by low pressure metalorganic chemical vapor deposition, Appl. Phys. Lett., **84**, 2166 (2004).

[134] S. Kim and M. Razeghi, *Characteristics of InGaAs/InGaP quantum dot infrared photodetector grown by metal organic chemical vapor deposition*, Mat. Res. Soc. Symp. Proc., **642**, J4.5 (2001).

[135] S.M. Kim, Y. Wang, M. Keever, and J.S. Harris, *High-Frequency Modulation Characteristics of 1.3-μm InGaAs Quantum Dot Lasers*, IEEE Photon. Technol. Lett., **16**, 377 (2004).

[136] S. Yoon, Y. Moon, T.-W. Lee, E. Yoon, and Y.D. Kim, *Effects of As/P exchange reaction on the formation of InAs/InP quantum dots*, Appl. Phys. Lett., **74**, 2029 (1999).

[137] D.E. Aspnes and A.A. Studna, *Dielectric functions and optical parameters of Si, Ge, GaP, GaAs, GaSb, InP, InAs, and InSb from 1.5 to 6.0 eV*, Phys. Rev. B, **27**, 985 (1983).

[138] C.H. Kuo, S. Anand, R. Droopad, K.Y. Choi, and G.N. Maracas, *Measurement of GaAs temperature-dependent optical constants by spectroscopic ellipsometry*, J. Vac. Sci. Technol. B, **12**, 1214 (1994).

[139] C.H. Kuo, S. Anand, H. Fathollahnejad, R. Ramamurti, R. Droopad, and G.N. Maracas, *Measurement of $Al_xGa_{1-x}As$ temperature dependent optical constants by spectroscopic ellipsometry*, J. Vac. Sci. Technol. B, **13**, 681 (1995).

[140] W.G. Breiland and K.P. Killeen, *A virtual interface method for extracting growth rates and high temperature optical constants from thin semiconductor films using in situ normal incidence reflectance*, J. Appl. Phys., **78**, 6726 (1995).

[141] P. Wolfram, E. Steimetz, W. Ebert, B. Henninger, and J.-T. Zettler, *Growth of InGaAsP/InP-laser structures monitored by using RAS techniques*, J. Crystal Growth, **248**, 240 (2003).

[142] J.-T. Zettler, K. Haberland, M. Zorn, M. Pristovsek, W. Richter, P. Kurpas, and M. Weyers, *Real-time monitoring of MOVPE device growth by reflectance anisotropy spectroscopy and related optical techniques*, J. Crystal Growth, **195**, 151 (1998).

[143] K. Haberland. *Optical in-situ studies during metal-organic vapor phase epitaxy with respect to III-V device production.* PhD thesis, Technische Universität Berlin, 2002.

[144] K. Haberland, A. Bhattacharya, M. Zorn, M. Weyers, J.T. Zettler, and W. Richter, *MOVPE Growth of (Al,Ga)InP-Based Laser Structures Monitored by Real-Time Reflectance Anisotropy Spectroscopy*, Journal of Electronics Materials, **29**, 468 (2000).

[145] I. Kamiya, D.E. Aspnes, L.T. Florez, and J.P. Harbison, *Reflectance-difference spectroscopy of (001) GaAs surfaces in ultrahigh vacuum*, Phys. Rev. B, **46**, 15894 (1992).

[146] D.K. Maude. *DX centres in GaAs.* In Michael R. Brozel, editor, *Properties of Gallium Arsenide*, volume XXVII, page 250. INSPEC, London, 1996.

[147] L.G. Salmon and I.J. D'Haenens, *The effect of aluminum composition on silicon donor behavior in* $Al_xGa_{1x}As$, J. Vac. Sci. Technol. B, **2**, 197 (1984).

[148] S. Leu, H. Protzmann, F.Hohnsdorf, W. Stolz, J. Steinkirchner, and E. Hufgard, *Si-doping of MOVPE grown InP and GaAs by using the liquid Si source ditertiarybutyl silane*, J. Crystal Growth, **195**, 91 (1998).

[149] Y.-M. Houng and T.S. Low, *Te doping of GaAs and AlGaAs using diethyltellurium in low pressure OMVPE*, J. Crystal Growth, **77**, 272 (1986).

[150] B.T. Cunningham, L.J. Guido, J.E. Baker, J. J. S. Major, J. N. Holonyak, and G.E. Stillman, *Carbon diffusion in undoped, n-type, and p-type GaAs*, Appl. Phys. Lett., **55**, 687 (1989).

[151] S. Tiwari, J. Hintzman, and A. Callegari, *Rapid thermal diffusion and ohmic contacts using zinc in GaAs and GaAlAs*, Appl. Phys. Lett., **51**, 2118 (1987).

[152] N.M. Johnson, R.D. Burnham, R.A. Street, and R.L. Thornton, *Hydrogen passivation of shallow-acceptor impurities in p-type GaAs*, Phys. Rev. B, **33**, 1102 (1986).

[153] S.A. Stockman, G.E. Hfler, J.N. Baillargeon, K.C. Hsieh, K.Y. Cheng, and G.E. Stillman, *Characterization of heavily carbon-doped GaAs grown by metal-organic chemical vapor deposition and metalorganic molecular beam epitaxy*, J. Appl. Phys., **72**, 981 (1992).

[154] W. Li and M. Pessa, *Lattice contraction in carbon-doped GaAs epilayers*, Phys. Rev. B, **57**, 1462714629 (1998).

[155] K. Tateno, Y. Kohama, and C. Amano, *Carbon doping and etching effects of CBr4 during metalorganic chemical vapor deposition of GaAs and AlAs*, J. Crystal Growth, **172**, 5 (1997).

[156] R. Sellin, F. Heinrichsdorff, C. Ribbat, M. Grundmann, U.W. Pohl, and D. Bimberg, *Surface flattening during MOCVD of thin GaAs layers covering InGaAs quantum dots*, J. Crystal Growth, **221**, 581 (2000).

[157] T.R. Omstead, P.M.V. Sickle, P.W. Lee, and K.F. Jensen, *Gas phase and surface reactions in the MOCVD of GaAs from triethylgallium, trimethylgallium, and tertiarybutylarsine*, J. Crystal Growth, **93**, 20 (1988).

[158] B.L. Pitts, D.T. Emerson, and J.R. Shealy, *Gas phase reactions of trimethylamine alane in low pressure organometallic vapor phase epitaxy of AlGaAs*, Appl. Phys. Lett., **62**, 1821 (1993).

[159] H.Y. Liu, I.R. Sellers, T.J. Badcock, D.J. Mowbray, M.S. Skolnick, K.M. Groom, M. Gutirrez, M. Hopkinson, J.S. Ng, J.P.R. David, and R. Beanland, *Improved performance of 1.3 μm multilayer InAs quantum-dot lasers using a high-growth-temperature GaAs spacer layer*, Appl. Phys. Lett., **85**, 704 (2004).

[160] A.R. Kovsh, N.A. Maleev, A.E. Zhukov, S.S. Mikhrin, A.R. Vasil'ev, Y.M. Shernyakov, M.V. Maximov, D.A. Livshits, V. Ustinov, Z.I. Alferov, N.N. Ledentsov, and D. Bimberg, *InAs/InGaAs/GaAs quantum dot lasers of 1.3 μm range with high (88%) differential efficiency*, Electron. Lett., **38**, 1104 (2002).

[161] H. Jiang and J. Singh, *Nonequilibrium distribution in quantum dots lasers and influence on laser spectral output*, J. Appl. Phys., **85**, 7438 (1999).

[162] O.B. Shchekin, J. Ahn, and D.G. Deppe, *High temperature performance of self-organised quantum dot laserwith stacked p-doped active region*, Electron. Lett., **38**, 712 (2002).

[163] C. Asplund, S. Mogg, G. Plaine, F. Salomonsson, N. Chitica, and M. Hammar, *Doping-induced losses in AlAs/GaAs distributed Bragg reflectors*, J. Appl. Phys., **90**, 794 (2001).

[164] D.L. Huffaker and D.G. Deppe, *Intracavity contacts for low-threshold oxide-confined vertical-cavity surface-emitting lasers*, IEEE Photon. Technol. Lett., **11**, 934 (1999).

[165] D.L. Huffaker, Z. Zou, and D.G. Deppe. *Reduced cavity loss for ultra-low threshold vertical cavity surface emitting lasers.* In *12th Annual Meeting IEEE Lasers and Electro-Optics Society, LEOS '99.*, volume 2, page 391, 1999.

[166] J.A. Lott, N.N. Ledentsov, V.M. Ustinov, N.A. Maleev, A.E. Zhukov, A.R. Kovsh, M.V. Maximov, B.V. Volovik, Z.I. Alferov, and D. Bimberg, *InAs-InGaAs quantum dot VCSELs on GaAs substrates emitting at 1.3 μm*, Electron. Lett., **36**, 1384 (2000).

[167] K.D. Choquette, J.F. Klem, A.J. Fischer, O. Blum, A.A. Allerman, I.J. Fritz, S.R. Kurtz, W.G. Breiland, R. Sieg, K.M. Geib, J.W. Scott, and R.L. Naone, *Room temperature continuous wave InGaAsN quantum well vertical-cavity lasers emitting at 1.3 μm*, Electron. Lett., **36**, 1388 (2000).

[168] C. Asplund, P. Sundgren, S. Mogg, M. Hammar, U. Christiansson, V. Oscarsson, C. Runnstrm, E. Odling, and J. Malmquist, *1260 nm InGaAs vertical-cavity lasers*, Electron. Lett., **38**, 635 (2002).

[169] F. Hopfer. *Oberflächenemittierende Quantenpunktlaser: Design, Technologie und Charakterisierung.* PhD thesis, Technische Universität Berlin, 2004.

[170] K.D. Choquette, K.M. Geib, C.I.H. Ashby, R.D. Twesten, O. Blum, H.Q. Hou, D.M. Follstaedt, B.E. Hammons, D. Mathes, and R. Hull, *Advances in selective wet oxidation of AlGaAs alloys*, IEEE J. Sel. Top. Quantum Electron., **3**, 916 (1997).

Acknowledgements

I would like to thank Prof. Dr. Dieter Bimberg who gave me the opportunity to work in his workgroup on a very interesting topic of QD epitaxy. I am very grateful to Prof. Nikolai Ledentsov for his support of my work.

I highly appreciate a help of many people making the creation of this work possible. Dr. Roman Sellin for an introduction in the topic of a gas phase epitaxy. Dr. Udo Pohl for many discussions and a careful reading of my thesis. I am very grateful to Konstantin Pötschke and Kathrin Schatke for steady help by an epitaxy and equipment maintenance.

I am also deeply indebted to

Dr. Florian Guffarth and Till Warming for help in PL and PLE measurements.

Natalia Kryzhanovskaya and Andrei Gladyshev from A.F. Ioffe Physico-Technical Institute, St-Petersburg, Russia for some PL measurements.

Christian Ribbat, Oliver Schulz, Thorsten Kettler, Dongxun Ouyang, Kristijan Posilovic for laser processing and characterisation.

Friedhelm Hopfer and Vladimir Heisler for VCSEL processing and characterisation.

Dr. Nikolai Zakharov and Dr. Peter Werner form the Max-Plank Institut of Microstructure Physics, Halle, Germany for TEM investigations of my samples.

Sven Rodt for quick and competent help with computers.

Dr. Vitali Shchukin and Andrei Schliwa for discussions of theoretical aspects of QDs.

and to all other members of AG Bimberg.